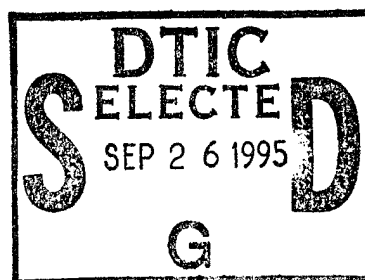


NAVAL POSTGRADUATE SCHOOL

Monterey, California



THESIS

**ELECTRICAL CHARACTERISTICS AND
THERMAL ANALYSIS OF A TOPAZ-II
SINGLE-CELL THERMIONIC FUEL ELEMENT
TEST STAND**

by

J. Richard Venable

March 1995

Thesis Advisor:

Oscar Biblarz

Approved for public release; distribution is unlimited.

19950922 055

QUALITY INSPECTED 1

REPORT DOCUMENTATION PAGE			Form Approved OMB No. 0704	
Public reporting burden for this collection of information is estimated to average 1 hour per response, including the time for reviewing instruction, searching existing data sources, gathering and maintaining the data needed, and completing and reviewing the collection of information. Send comments regarding this burden estimate or any other aspect of this collection of information, including suggestions for reducing this burden, to Washington headquarters Services, Directorate for Information Operations and Reports, 1215 Jefferson Davis Highway, Suite 1204, Arlington, VA 22202-4302, and to the Office of Management and Budget, Paperwork Reduction Project (0704-0188) Washington DC 20503.				
1. AGENCY USE ONLY (Leave blank)		2. REPORT DATE March, 1995		3. REPORT TYPE AND DATES COVERED Master's Thesis
4. TITLE AND SUBTITLE ELECTRICAL CHARACTERISTICS AND THERMAL ANALYSIS OF A TOPAZ-II SINGLE-CELL THERMIONIC FUEL ELEMENT TEST STAND			5. FUNDING NUMBERS	
6. AUTHOR(S) Venable, J. Richard				
7. PERFORMING ORGANIZATION NAME(S) AND ADDRESS(ES) Naval Postgraduate School Monterey CA 93943-5000			8. PERFORMING ORGANIZATION REPORT NUMBER	
9. SPONSORING/MONITORING AGENCY NAME(S) AND ADDRESS(ES)			10. SPONSORING/MONITORING AGENCY REPORT NUMBER	
11. SUPPLEMENTARY NOTES The views expressed in this thesis are those of the author and do not reflect the official policy or position of the Department of Defense or the U.S. Government.				
12a. DISTRIBUTION/AVAILABILITY STATEMENT Approved for public release; distribution is unlimited.			12b. DISTRIBUTION CODE	
13. ABSTRACT (maximum 200 words) The general objectives of this research are to investigate the electrical and thermal characteristics of the TOPAZ-II thermionic fuel element (TFE) test stand which allows testing of a single TFE. Detailed cross-sectional drawings have been developed and a one-dimensional network has been created for use in a thermal model of the TFE test stand. Critical resistances in the network are identified as the regulated helium gap, the cesium-filled interelectrode gap and the cooling water channel. Experimental data show the TFE operational dependence upon cesium pressure in the interelectrode gap. Thermionic performance at varying thermal input power levels has been analyzed based on the determined optimal cesium pressures which range from 0.4 torr at about 1000 Watts to 1 torr at about 3000 Watts input. Thermionic efficiencies can be as high as 7 %, but the low thermal inputs have efficiencies of about 1.5 %. Results provided by the TFE test stand are compared to the TOPAZ-II reactor system performance. Operation of the reactor at much lower thermal power (not previously analyzed) may produce useful electrical output (1 kilowatt-electric) for "housekeeping" purposes.				
14. SUBJECT TERMS Thermionics, TOPAZ-II, Electrical Characteristics			15. NUMBER OF PAGES 119	
			16. PRICE CODE	
17. SECURITY CLASSIFICATION OF REPORT Unclassified	18. SECURITY CLASSIFICATION OF THIS PAGE Unclassified	19. SECURITY CLASSIFICATION OF ABSTRACT Unclassified	20. LIMITATION OF ABSTRACT UL	

Approved for public release; distribution is unlimited.

**ELECTRICAL CHARACTERISTICS AND THERMAL
ANALYSIS OF A TOPAZ-II SINGLE-CELL
THERMIONIC FUEL ELEMENT TEST STAND**

by

J. Richard Venable
Lieutenant, United States Navy
B.S., United States Naval Academy, 1985

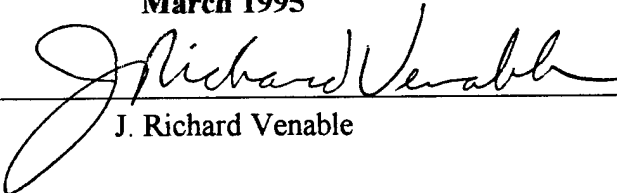
Submitted in partial fulfillment
of the requirements for the degree of

MASTER OF SCIENCE IN ASTRONAUTICAL ENGINEERING

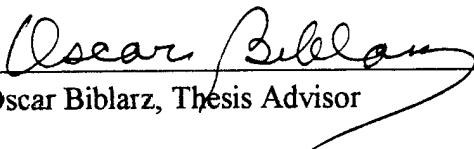
from the

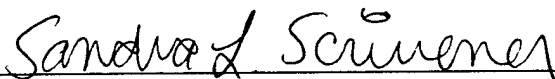
NAVAL POSTGRADUATE SCHOOL
March 1995

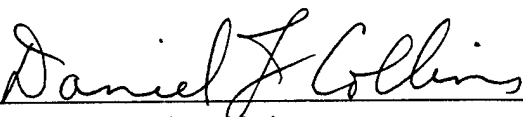
Author:


J. Richard Venable

Approved by:


Oscar Biblarz, Thesis Advisor


Sandra L. Scrivener, Second Reader


Daniel J. Collins, Chairman,
Department of Aeronautics and Astronautics

ABSTRACT

The general objectives of this research are to investigate the electrical and thermal characteristics of the TOPAZ-II thermionic fuel element (TFE) test stand which allows testing of a single TFE. Detailed cross-sectional drawings have been developed and a one-dimensional network has been created for use in a thermal model of the TFE test stand. Critical resistances in the network are identified as the regulated helium gap, the cesium-filled interelectrode gap and the cooling water channel.

Experimental data show the TFE operational dependence upon cesium pressure in the interelectrode gap. Thermionic performance at varying thermal input power levels has been analyzed based on the determined optimal cesium pressures which range from 0.4 torr at about 1000 Watts to 1 torr at about 3000 Watts input. Thermionic efficiencies can be as high as 7 %, but the low thermal inputs have efficiencies of about 1.5 %.

Results provided by the TFE test stand are compared to the TOPAZ-II reactor system performance. Operation of the reactor at much lower thermal power (not previously analyzed) may produce useful electrical output (1 kilowatt-electric) for "housekeeping" purposes.

Accession For	
NTIS CRA&I	<input checked="checked" type="checkbox"/>
DTIC TAB	<input type="checkbox"/>
Unannounced	<input type="checkbox"/>
Justification _____	
By _____	
Distribution /	
Availability Codes	
Dist	Avail and/or Special
A-1	

TABLE OF CONTENTS

I. INTRODUCTION	1
II. BACKGROUND	3
A. TOPAZ INTERNATIONAL PROGRAM	3
B. DIRECT ENERGY CONVERSION	5
1. Direct Energy Conversion Methods	5
a. Thermoelectric Generators	5
b. Photovoltaic Generators	7
c. Magnetohydrodynamic (MHD) Generators	7
d. Fuel Cells	8
2. Terrestrial Applications	8
3. Space Applications	9
III. THERMIONIC ENERGY CONVERSION	11
A. IDEAL VACUUM DIODE	12
B. PLASMA DIODES	16
C. CESIUM VAPOR DIODE OPERATION	18
a. Ignited Mode	18

b. Unignited Mode	20
IV. TOPAZ-II SPACE NUCLEAR POWER SYSTEMS	23
A. TOPAZ-II REACTOR SYSTEM	23
B. TOPAZ-II THERMIONIC FUEL ELEMENT	26
C. TOPAZ-II TFE TEST STAND	28
V. TEST STAND THERMAL ANALYSIS	37
A. THERMAL MODEL DESCRIPTION	37
B. CRITICAL RESISTANCES	42
1. Regulated Helium Gap	42
2. Cooling Water Channel	43
3. Cesium Interelectrode Gap	45
C. TITAM COMPARISON	45
VI. SINGLE TFE ELECTRICAL CHARACTERISTICS	49
A. EXPERIMENT DESCRIPTION	49
B. CESIUM PRESSURE OPTIMIZATION	51
C. CURRENT-VOLTAGE CHARACTERISTICS	53
D. TFE OPERATING POINT	60
E. TEST STAND RESULTS APPLIED TO THE REACTOR SYSTEM	65

VII. SUMMARY CONCLUSIONS AND RECOMMENDATIONS	71
APPENDIX A. TEST STAND RUSSIAN CROSS-SECTION	77
APPENDIX B. CURRENT-VOLTAGE SWEEPS	79
LIST OF REFERENCES	101
INITIAL DISTRIBUTION LIST	105

ACKNOWLEDGMENT

Resources for this project were provided by the Naval Postgraduate School in Monterey, CA and by the Air Force Phillips Laboratory in Albuquerque, NM. All experimental work was performed at the New Mexico Engineering Research Institute in Albuquerque, NM by the Topaz International Program (TIP) personnel.

The author wants to thank Professor Oscar Biblarz of the Naval Postgraduate School for his continual support and guidance throughout this effort. His knowledge of the subject area, experience and resourceful problem solving techniques enhanced this thesis greatly. He made this process an excellent educational experience.

Thanks to Dr. Mohamed S. El-Genk of the University of New Mexico for providing direction in the choice of this thesis subject and his constant willingness to help toward the completion of this work. The sharing of his knowledge of all aspects of heat transfer analysis and experimental procedure was invaluable. Thanks also go to Dimitry Paramonov of the University of New Mexico for his basic instruction in thermionic energy conversion.

A special thanks to all the TIP personnel. Their positive attitude and willingness to help during all phases of this research are greatly appreciated. Through the difficulties of collecting the great deal of data used in this project, many lasting friendships were developed. The author would like to especially thank Frank Wyant, Oleg Izhvanov and all the shift work operators at TIP.

Greatest appreciation goes to my close friend and colleague Steve Benke. Without his diligent work ethic and determination, the completion of this research would not have been achieved.

I. INTRODUCTION

The TOPAZ-II thermionic fuel element (TFE) test stand was originally built and tested at the Scientific Industrial Association "LUTCH", Podolsk, Russia. In December 1992, the stand was reassembled at the New Mexico Engineering Research Institute (NMERI) in Albuquerque, New Mexico. Acceptance and demonstration testing were conducted throughout 1993 by personnel of the Topaz International Program (TIP) at NMERI (Luchau, *et al.* 1993). The TFE test stand was designed to conduct single TFE non-nuclear testing by replacing the nuclear fuel with a tungsten heating element (TISA heater). The test stand provides the means to test a single TFE so that its performance can be better observed without the interference of the integrated TOPAZ-II system. This removes the direct coupling of the TOPAZ-II in-core TFE with the coolant loop, radiator and the other TFEs that are electrically connected in series. (Benke and Venable, 1995)

Production of electrical power in the TOPAZ-II space nuclear power system is provided by thermionic energy conversion. Thermionic energy conversion is a process by which thermal energy is transformed into electrical energy directly without the intermediate steps of more traditional methods like steam-powered turbine electric generators. Thermionic energy conversion is a subset of direct energy conversion. Direct energy conversion is the means by which a primary energy source is converted into electricity directly without moving mechanical parts, and is discussed in depth by Angrist (1965). Forms of direct energy conversion covered in this thesis include thermoelectric generators, photovoltaic generators, magnetohydrodynamic (MHD) generators and fuel cells. Detailed emphasis is directed toward explanation of thermionic energy conversion and follows the tenets delineated by Rasor (1971). Ned Rasor is the founder of Rasor Associates Incorporated (RAI) and continues to be a greatly respected authority in the field of thermionic energy conversion.

To better understand and predict the performance of a single TFE, a thermal model of the TFE test stand is provided in a companion thesis written by Benke (1994).

Establishment of a one-dimensional heat transfer network method for the test stand and detailed cross-sectional drawings, not previously available at TIP, were developed to support Benke's thermal model and are presented in this thesis.

The experimental data for this work were collected in March 1994, with follow-on experimental data taken in August 1994 to aid in evaluation of the thermal network critical resistances. Along with verifying the thermal model, the collected experimental data are used to investigate the low-power operating characteristics of the TFE during ignited and unignited converter operation. These low power levels have not yet been analyzed by TIP. (Benke and Venable, 1995)

The unignited mode is particularly interesting because mission profiles for space nuclear power systems could include long periods at reduced power requirements. Exploiting these reduced power situations would be limited by providing electrical power for "housekeeping" purposes. "Housekeeping" loads could include the reactors' electromagnetic coolant pump which maintains coolant temperatures high enough to prevent freezing of the coolant, the reactor control unit, command and communications for the satellite and other vital spacecraft system loads (Taylor, 1995). Lowering core thermal power to accomplish these requirements removes the need for an auxiliary power source. Thermionic converters can produce DC (direct current) power at emitter temperatures below the temperatures required for presently used ignited mode operations. These lower emitter temperatures are compatible with minimum reactor power levels. (Benke and Venable, 1995)

Results gathered from the extensive testing of a single TFE in the test stand are provided to TIP for reference in future operations of the TFE test stand. An analysis is made to indicate how data gathered in the test stand can be better applied to the overall reactor power system. This analysis is then compared with the data reported by Taylor (1995) concerning operation of the TOPAZ-II reactor system at low power levels.

II. BACKGROUND

Increased electrical power generation will be needed to support future space missions. These missions could include deep space exploration, manned missions to Mars, manufacturing capabilities on the moon, reusable space tugs and planetary colonization. Solar energy will not be sufficient or readily available for many of these missions and may be subject to harsh environmental conditions. Requirements for larger power generation capabilities, non-reliance on the Sun's energy, durability despite extreme radiation environments and long mission duration lead to nuclear energy as a likely power source.

Direct energy conversion is a means by which the primary energy source is converted into electricity directly without moving mechanical parts. In thermionic energy conversion, a heated refractory metal emits electrons that are collected by another section of the converter and applied to a load. Nuclear fuel is ideal in this application due to the high temperatures and high energy densities required for the thermionic process. Higher temperature energy conversion is appealing for space power systems because they must rely upon radiation heat transfer for excess heat removal. Radiation heat transfer is directly proportional to the surface area of the radiator and proportional to temperature raised to the fourth power. Therefore, increased heat rejection temperatures can significantly reduce the size of the space radiator and reduce the size and weight of the spacecraft. The TOPAZ-II Space Power System bought from the former Soviet Union by the U.S. uses the thermionic method of energy conversion with a nuclear fuel heating source. The TOPAZ-II system also allows for the simulation of fission heating by electrical heaters thereby removing the requirement of testing the system with nuclear fuels.

A. TOPAZ INTERNATIONAL PROGRAM

In the early 1960's, the then U.S.S.R began development of single-cell and multi-cell thermionic systems for use in space nuclear reactors. The Central Design Bureau for

Machine Building (CDBMB) in Leningrad was the lead for single-cell thermionic fuel element (TFE) design. The program was named ENISY. Krasnaya Zvezda (Red Star) in Moscow was the system developer of the multi-cell TFE system that was named TOPAZ. TOPAZ is a Russian language acronym for Thermionic Experiment with Conversion in Active Zone. At the end of the 1980's, the Soviets approached a private U.S. company (International Scientific Products, San Jose, CA) about the purchase of Russian space reactor systems. In the preliminary negotiations the U.S. company inadvertently renamed ENISY to TOPAZ-II and TOPAZ to TOPAZ-I. (Voss, 1994)

Two TOPAZ-II reactor systems along with all the supporting equipment including data acquisition systems, turbomolecular vacuum pumps, a vacuum chamber suitable for the entire reactor system, shipping containers and a single TFE test stand were purchased by the U.S. Government in 1992. Funding was provided by the Strategic Defense Initiative Office (SDIO) to investigate the use of TOPAZ-II in support of the Nuclear Electric Propulsion (NEP) Space Mission. (Wyant, 1994)

Despite cancellation of the flight program in 1993, four more TOPAZ-II units were purchased in 1994 allowing further research in thermionic energy conversion and space nuclear reactor operations. The systems are currently under funding by the Ballistic Missile Defense Organization (BMDO, successor to SDIO) and are maintained by contractors, Air Force personnel, and a team of international scientists. The project is currently named the Topaz International Program (TIP) and includes U.S., British, French, and Russian personnel. TIP is physically located at the New Mexico Engineering Research Institute (NMERI) which is owned by the University of New Mexico.

Cost is many times the motivator in the procurement process. The first two TOPAZ-II systems and other support equipment cost 13.1 million dollars. The high bay built to house the vacuum chamber for testing TOPAZ-II had a one million dollar price tag. The additional four units purchased in 1994 were 20.4 million dollars. To date cumulative procurement costs amount to approximately 34.5 million dollars. The Soviets spent 25 years working on this technology at a cost of 20 billion dollars. (Wyant, 1994)

Clearly the apparent savings in engineering, manufacturing and development times are enormous. Non-developmental item (NDI) purchase removes the cost of manufacturing and developing a product and is a method by which the U.S. Government is attempting to reduce spending. TIP can be considered as a modern acquisition success considering NDI purchase and international cooperation. Furthermore, it was accomplished during a unique period of East-West cooperation.

B. DIRECT ENERGY CONVERSION

The interest in producing electricity directly from an energy source is not a new concept. In 1802, Thomas Johann Seebeck discovered that a junction of dissimilar metals upon which a temperature difference had been imposed could deliver an electric current. He did not realize that an electric current did flow, but fortunately some of his contemporaries did. Common electrical generation techniques include burning fossil fuel to make steam which, upon expansion through a turbine, powers an electrical generator. Alternate methods to produce electricity from thermal, radiant, and mechanical energies are essential as the finite resources are depleted. The primary advantage of direct energy conversion methods is the bypassing of intermediate steps. Among the disadvantages is the fact that only a few direct conversion devices have achieved efficiencies that approach the more conventional methods. (Angrist, 1965)

1. Direct Energy Conversion Methods

There are numerous conversion methods that fall into this category. A few of the more prevalent ones are described here to illustrate the breadth of this field. Thermionic generation is not covered because it will be addressed in depth later in the thesis.

a. Thermoelectric Generators

A combination of famous discoveries is used to describe thermoelectric generator design. The above-mentioned Seebeck effect was the starting point. Jean Charles Peltier discovered that passing current through a junction formed by dissimilar conductors caused

absorption and liberation of heat. Not unlike Seebeck, Peltier also misunderstood his discovery and thought it showed only that Ohm's law may not be followed by weak currents. Emil Lenz clarified Peltier's findings in 1838 by demonstrating that water could be frozen when placed on a bismuth-antimony junction with an electric current applied. He found reversing the current caused the ice to melt. Lord Kelvin (William Thomson) derived a relation between the Peltier and Seebeck effects using thermodynamic arguments. He found a lateral heating or cooling effect that takes place in a homogeneous conductor when an electric current is applied in the direction of a temperature gradient. (Angrist, 1965).

The basic theory for thermoelectric generators was derived adequately in 1911 by Altenkirch. He showed that for this application materials were needed with high Seebeck coefficients, high electrical conductivities to minimize joule heating and low thermal conductivities to reduce heat transfer through the devices. Fifty years passed before these desirable materials became known and widely available. The significant material discovery for use in direct conversion of heat or light to electricity was the semiconductor. (Angrist, 1965)

The generator uses a hot junction electrode, p-type semiconductor material on one side of the generator and n-type on the other with a common cold junction electrode completing a circuit. The temperature induces a current from the p-type to the n-type material. These principles are also used to create thermoelectric coolers that transfer heat from a low temperature to a high temperature by passing an electric current through the junction of dissimilar materials. Varied heat sources can be used in thermoelectrics. A radioisotope thermoelectric generator (RTG) uses heat liberated in the decay of a radioisotope such as Plutonium 238.

The Department of Energy (DOE) has completed the conceptual design of a twenty-kilowatt space reactor thermoelectric power system using near-term technology. This system was designated as the SP-100 Space Reactor Power System Program. Despite close-out of the SP-100 Program during FY 94, most of the key components

required for a space reactor power system were fabricated by the end of FY 93. The DOE is documenting the progress made in the SP-100 Program so that the technology can be retrieved for future use. (Mondt, et al. 1994)

b. Photovoltaic Generators

In 1839 Edmond Becquerel discovered that incident light on one of the electrodes in an electrolyte solution produced a voltage. This effect was observed in a solid (selenium) in 1877 by W. G. Adams and R. E. Day. Schottky, Lange, and Grondahl also did pioneering work in photovoltaic cells with selenium and cuprous oxide. (Angrist, 1965).

Solar cells are the most common type of photovoltaic generators. Semiconductor material in a solar cell converts radiant energy from the sun into electrical energy through the semiconductor's p-n junction. Extensive work and considerable gains have been realized in the area of solar cell designs. The most common types of solar cells are silicon-germanium, but cells that are less susceptible to radiation damage such as gallium-arsenide and indium-phosphide are now available. Efficiencies of solar cells have been demonstrated up to 19 %.

c. Magnetohydrodynamic (MHD) Generators

In an MHD generator a stream of hot ionized gas replaces the rotating armature in a conventional turbogenerator. The plasma has good electrical conductivity and moves through a magnetic field, thus inducing an electric field in the generators' stationary conductor. The kinetic energy of the gas stream is converted directly into electrical energy and that makes it simpler than a conventional turbogenerator. It does not have any hot highly stressed moving parts so it can operate in conditions that would quickly destroy a conventional turbine. (Angrist, 1965)

Significant technology challenges remain to be surmounted before MHD generators become practical machines. One of these challenges is an ionization instability that causes plasma nonuniformities and loss of MHD performance. Another is the electrodes' ability to withstand the thermal stress imposed by heat transfer rates which are

very high compared to those that ceramics usually are called upon to withstand and the Hall effect that magnifies the effect of nonuniform volume properties and the consequences of a nonuniform boundary condition. The Hall effect is the deflection of electrons perpendicular to the plasma flow path when in the presence of a magnetic field. A complete discussion of recent technological challenges facing MHD generator production is contained in Rosa, et al. (1991). (Rosa, et al. 1991)

d. Fuel Cells

A fuel cell is an electrochemical device in which the chemical energy of the fuel is converted directly and efficiently to electrical energy. These cells are also known as primary batteries and undergo oxidation-reduction reactions. In the fuel cell, the oxidizer and fuel are kept separate and electrons are transferred via a metallic path that may contain a load. (Angrist, 1965)

Hydrogen-oxygen fuel cells are the most extensively developed. These cells use hydrogen as fuel and oxygen or oxygen in air as the oxidant. Some of these systems incorporate their own fuel-generation devices by using a metal hydride, such as calcium hydride pellets or sodium aluminum hydride pellets, and water. Electrolyte soluble fuels have also been considered, including ammonia, hydrazine and methanol. (Angrist, 1965)

2. Terrestrial Applications

There are many terrestrial applications for direct conversion devices. The U. S. Weather Bureau has placed sensors in harsh environments north of the Arctic Circle and in Antarctica to enhance their long range prediction techniques. These environments are not practical for the stationing of personnel due to the expense and hardship. The devices are radioisotope thermoelectric generators that maintain a trickle charge to a 32-volt sealed nickel-cadmium battery. These units require infrequent maintenance, about once every ten years. The U. S. Navy uses a 4270-watt hybrid thermoelectric environmental control unit on its deep submergence search vehicles. The thermoelectric unit design was compared rigorously and favorably with vapor compression and absorption refrigeration systems.

Small self-contained water pumping units have been designed to raise the standard of living in underdeveloped areas of the world. The 50-watt units use solar energy and a set of thermoelectric cells to drive a pump that can be used for irrigation as well as household needs. Solar arrays are utilized in many applications from large farms to small arrays for household heating. Very large terrestrial power systems can potentially be built using MHD electrical generators. (Angrist, 1965)

3. Space Applications

Direct energy conversion is predominant in spacecraft. Radioisotope thermoelectric generators are used for deep space missions due to their high reliability and long lifetime. Solar cells are used in practically all present day satellites. Most satellites also rely on batteries for power generation when the satellite is in eclipse.

Hydrogen-oxygen fuel cell power plants supplied electricity for the Apollo vehicle on all the flights to the moon. The water produced as a byproduct of the chemical reaction provided all of the drinking water for the astronauts. (Angrist, 1965)

Thermionic generators are ideal for use in reactor cores since they operate in high temperature regimes and are not affected by the radiation. Having the generators in the core is a great space saving technique. Space nuclear reactors are the basis for new designs in the so-called bimodal systems. Bimodal concepts include using in-core thermionic units for electrical power generation and using the reactor for satellite propulsion. The reactor core could provide propulsion through a variety of schemes such as passing hydrogen through the core around the thermionic units then expanding the heated gas through a nozzle to generate thrust or through electric propulsion using the generated electric power across an arc jet or ion engine.

III. THERMIONIC ENERGY CONVERSION

It is difficult to determine precisely when the study of thermionic energy conversion began. Du Fay was first to note that the space near a "red-hot body" is a conductor of electricity over two hundred years ago. Published material by Edmond Becquerel in 1853 expanded on the subject of thermionics. One of his observations was that a potential of only a few volts could drive measurable current across a gap between two platinum electrodes heated to a temperature corresponding to "red-hot". Credit for discovery of thermionic emission is given to Thomas Edison who requested a patent in 1883 that described the phenomenon. The electron was discovered by J. J. Thomson in 1897 and in 1899, Thomson found that the negative charge carriers emitted in the thermionic process correspond to electrons based on their charge to mass ratio. (Angrist, 1965)

The physical quantitative description of thermionic emission was reported by Richardson in 1902. Advances in the areas of nuclear fuel heat sources, high-temperature materials technology and the need for compact and efficient electrical power sources in space led to the first demonstration of thermionic power generation at practical levels by Marchuk of the USSR in 1956. Wilson demonstrated thermionic converter operation in the U. S. in 1957 and Grover *et al.* in 1959 showed thermionic operation in the core of a nuclear reactor. By 1965, technology advances were sufficient to start development of in-core thermionic nuclear power systems in the U. S., USSR, France and West Germany. (Rasor, 1991)

Figure 3-1 illustrates a simplified flat-plate thermionic element. The emitter (commonly called the cathode) and collector (commonly called the anode) are typically composed of refractory metals to withstand the high temperatures required for the thermionic process. Because thermionics deals with power generation, the emitter is not negative as far as the load is concerned. In this simplest form of converter, electrons are discharged from the emitter and travel across the gap to the collector which is at a lower potential than the emitter. The potential difference between the emitter and collector

drives a current that can be connected to an external load. The electrodes are separated by a vacuum or by a plasma. The space between the electrodes is termed the interelectrode gap (IEG). Improved understanding of the physical processes of vacuum and plasma filled converters have driven the technological development of thermionic energy converters.

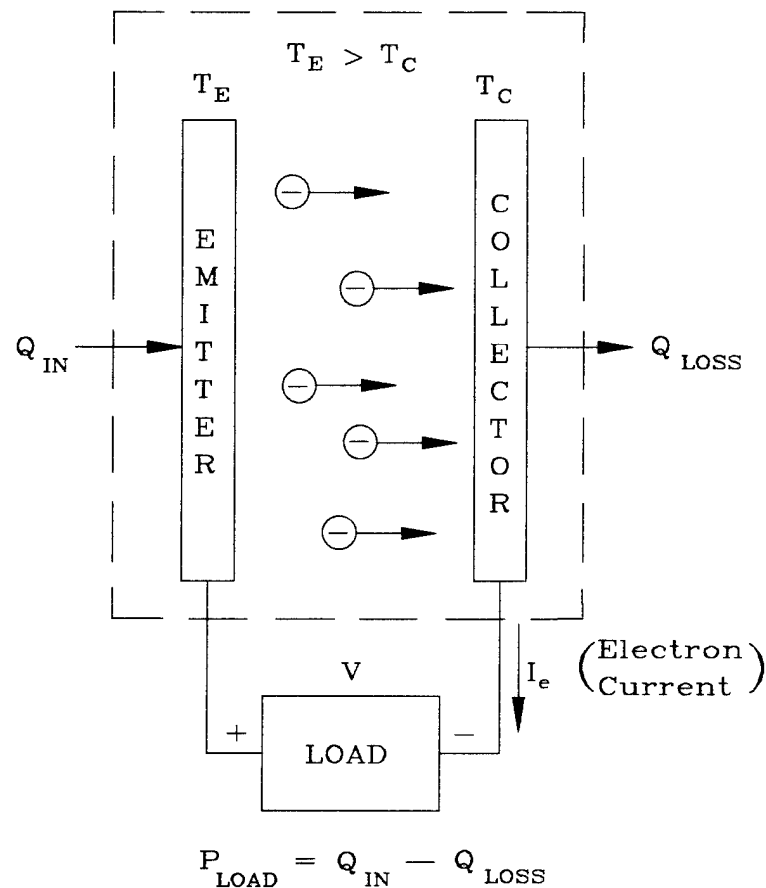


Figure 3-1. Simplified flat-plate thermionic. From (Rasor, 1991).

A. IDEAL VACUUM DIODE

Prior to any discussion of the plasma effects on thermionic energy conversion, it is useful to quantify operation of an ideal converter with only a vacuum in the IEG. Before entering the IEG, an electron must overcome a potential energy barrier called the emitter

work function. The emitter work function is designated as ϕ_E and is shown in Figure 3-2. Similarly, the collector work function ϕ_C exists at the collector. (Rasor, 1991)

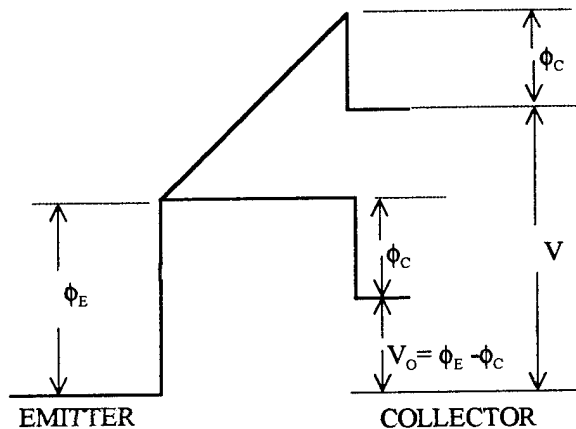


Figure 3-2. Motive diagram for an ideal thermionic converter. From (Rasor, 1991).

The term "motive" describing Figure 3-2 above is a substitute for electric potential in the thermionic community.

Space-charge effects occur in the IEG since electrons, which are charged particles, act as the working fluid for the thermionic converter. Buildup of electrons causes an overall negative charge in the gap that tends to inhibit further electron flow. This is a space-charge which can be reduced either by narrowing the distance between electrodes or by introducing positive ions in the IEG to neutralize the charge. (Angrist, 1965)

The ideal diode ignores collisional effects encountered by the electrons in the IEG and space-charge effects that reduce electron flow. As can be seen in Figure 3-2, electrons must surmount the potential barrier $V + \phi_C$ to cross the gap when the output voltage V is greater than the potential energy difference of the electrodes $V_0 = \phi_E - \phi_C$. With V less than V_0 the emitter work function barrier must be overcome. (Rasor, 1991)

Although the collector is at a relatively lower temperature than the emitter it will emit electrons. This back emission of electrons into the IEG reduces the thermionic efficiency of the converter. Richardson first and then Dushman, doing work in the field of

thermionics, determined an equation for the output current density of a thermionic converter. The equation can be applied to the collector as well as the emitter.

The Richardson-Dushman equations applied to the ideal diode are,

$$J = AT_E^2 \exp[-e(V + \phi_C)/kT_E] \text{ for } V > V_o \quad (3.1)$$

$$J = AT_E^2 \exp[-e\phi_E/kT_E] \text{ for } V < V_o \quad (3.2)$$

where $A = 120 \text{ A/cm}^2\text{-K}^2$, $e/k = 11,600 \text{ eV/K}$ (k is Boltzmann's constant), T_E is the emitter temperature, and J is the output current density in A/cm^2 . (Rasor, 1991)

The thin lines in Figure 3-3 shows the current-voltage characteristics of an ideal vacuum diode. The thick line represents the characteristics of a cesium vapor diode which will be addressed in detail in a subsequent section of this chapter.

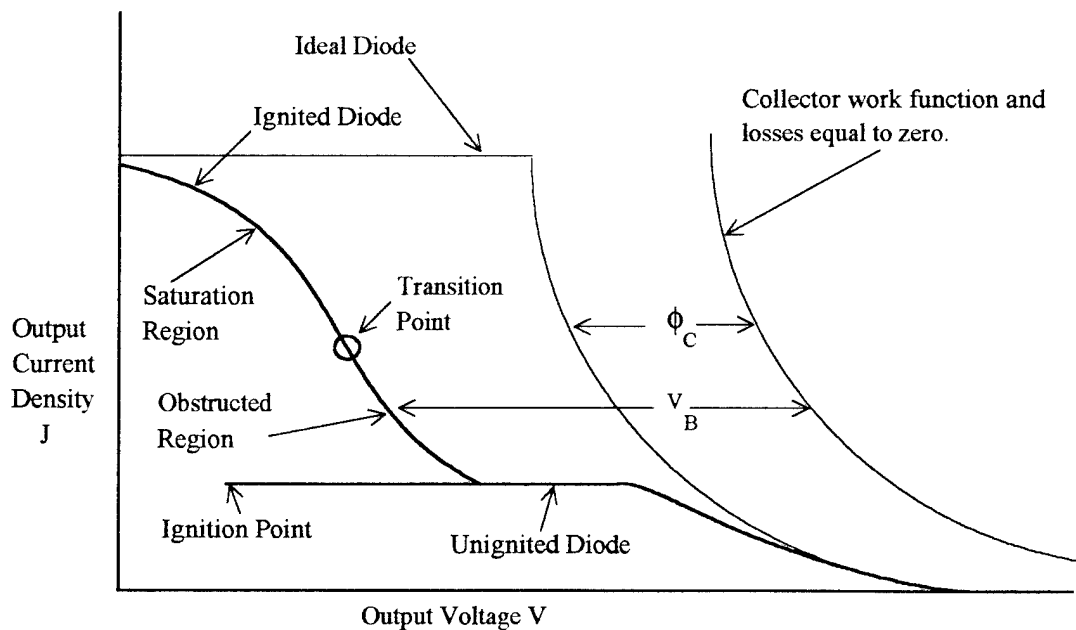


Figure 3-3. Ideal and cesium vapor diode electrical output characteristics. From (Rasor, 1991).

The efficiency of the ideal converter can be found based on the electrical output versus the thermal input required for operation. The output emission current density times the voltage difference between the voltage drop across the electrodes V and the lead loss voltage V_L is a measure of the electrical output.

Equations 3.3 through 3.5 show the thermal input that must be supplied to the emitter for thermionic conversion.

$$q_E = q_e + q_r + q_L \quad (3.3)$$

$$q_e = J(\phi_E + 2kT_E) \quad (3.4)$$

$$q_L = \sigma \epsilon (T_E^4 - T_C^4) \quad (3.5)$$

Where q_E is the total heat supplied by the emitter; q_e is the heat removed from the emitter by electron emission, q_r is the heat removed from the emitter by thermal radiation and q_L is the heat conducted down the emitter lead. ϵ is the net thermal emissivity of the electrode system, $\sigma = 5.67E-12 \text{ W/cm}^2\text{-K}^4$ is the Stefan-Boltzmann constant and T_C is the collector temperature (Rasor, 1991).

Ideal converter efficiency can now be represented as

$$\eta = J(V - V_L)/q_E \quad (3.6)$$

Equation 3.6 shows that there is a tradeoff between emission current density and heat input to the emitter since they are both functions of temperature, emitter and collector work functions.

In real thermionic converters, energy losses occur due to scattering reactions of the electrons back to the emitter and electron collisions in the interelectrode gap. Back emission of electrons from the collector to the IEG is another loss term and it increases with increasing collector temperature (Angrist, 1965). This results in a reduction of the output voltage compared to that of an ideal diode at the same current density. The quantity V_B shown in Figure 3-3 is used to account for these energy losses in a real converter. Substituting V_B for ϕ_C in Equation 3.1 results in Equation 3.7 and an ideal diode equivalent for the same T_E , J and V .

$$J = AT_E^2 \exp[-(V + V_B)/kT_E] \quad (3.7)$$

In this way, V_B can characterize a real thermionic diodes' performance. (Rasor, 1991)

B. PLASMA DIODES

The ideal diode case gives an upper limit for thermionic converter performance. The space charge effect described earlier as well as other losses listed above significantly lower thermionic conversion efficiency. Reducing the gap size of a vacuum converter can reduce space charge effects. This gap size is close to the electrons' Debye length which is approximately $1\mu\text{m}$ (Rasor, 1991). It is difficult to manufacture and operate converters with such small tolerances without shorting the collector to the emitter. Use of nuclear fuel for the heating source in this arrangement is prohibitive due to the expected fuel swelling throughout the life of the fission process that could force the gap closed.

Using a plasma in the IEG allows for considerably larger gap sizes. These gaps range from 100 to 1000 μm (Rasor, 1991). The solid line in Figure 3-3 depicts the electrical output characteristics of a cesium vapor diode thermionic converter. Notice that the cesium vapor diode performance is below the ideal diode performance, but it is better than any practical vacuum diode. Cesium vapor is used because it has the lowest ionization potential of the chemical elements.

A plasma is necessary to transport the electron current efficiently. It is near equipotential within a tenth of a volt, only a few electron mean free paths thick and highly energy and charge conservative. For these reasons, the plasma is predominantly one dimensional and its features and state is mostly due to interaction with the electrode surfaces bounding it. (Rasor, 1991)

The interaction of cesium vapor with the electrode surface gives rise to another appealing property. Immersion of the electrodes in cesium vapor leads to adsorption of cesium as ions to the electrode surface that lowers the electrode work function. A monoatomic layer of cesium on a metal oxide can produce a polarized atomic layer at the surface (Angrist, 1965). This polarized layer creates an electric field that lowers the energy required by an electron to escape the surface thereby reducing the work function.

The work function or surface work is the energy required for an electron to escape the attractive force of a metal surface (Angrist, 1965). Recall that having a lower emitter work function ϕ_E , as shown on the motive diagram Figure 3-2, reduces the potential that the electrons need to overcome for thermionic emission. Although Figure 3-2 is not the motive diagram for a cesium vapor diode, the emitter work function is the initial potential for motive diagrams used with thermionic diodes. The work functions obtainable using cesium plasmas makes cesium the present choice for plasma type thermionic conversion devices.

Cesium vapor adsorption effects on electrode surfaces are not uniform between different surface types. For example, the crystal lattice of the surface may be preferentially oriented for cesium adsorption or a surface may be etched to expose preferred orientations for cesium adsorption (Angrist, 1965). Additionally, for the same surface type thermionic efficiency is strongly dependent upon the cesium vapor operating pressure. Considering the adsorbed layer of cesium to be in thermal equilibrium, a formula is obtained that correlates the work function ϕ of a surface immersed in cesium at pressure with the "bare" work function ϕ_0 of the surface (Rasor and Warner, 1964). Equation 3.8 shows this relationship

$$p = p_0 \exp(-h/kT_R) \quad (3.8)$$

with p being the cesium vapor pressure, T_R is the cesium liquid reservoir temperature, k is the Boltzmann constant, $p_0 = 7.5E-6$ torr and $h = 0.75$ eV. This relationship can characterize the work function of the emitter quite well in the significant operational regions for thermionic emission. Understanding of the collector work function is inadequate, however and relies upon entirely empirical data. (Rasor, 1991)

Figure 3-3 also shows different operating regimes for the cesium diode. There is a low current unignited mode that is relatively insensitive to current changes and an ignited mode that is relatively insensitive to voltage changes. The ignited mode depicts two areas of concern - the obstructed region and the saturation region. Each of these regions has

significant physical differences in the IEG that changes the output characteristics as Figure 3-3 illustrates. A discussion of these areas of thermionic energy production follows.

C. CESIUM VAPOR DIODE OPERATION

a. Ignited Mode

The ignited or arc mode of thermionic energy conversion occurs spontaneously between two heated electrodes immersed in a cesium vapor. Ignition into the ignited mode refers to going from ionization only at the surface of the electrode to volume ionization of the gas. It is the most efficient region of thermionic conversion and therefore, the region of operation most often employed for useful thermionic converters. In general, for this mode, energy dissipated in the IEG by collisional processes heats up the electrons in the gas to a temperature sufficient to ionize the gas and maintain a neutral plasma. (Rasor, 1991)

Collisions governing the ionization process in the gap are probably well represented by the four equations below:



Cs is the cesium element, Cs* is cesium at its first excitation energy level, Cs⁺ is a cesium ion and e is an electron with the asterisk representing a higher excitation energy. The first excitation energy level for cesium is 1.40 electron-volts (eV). These equations show that volume ionization of the cesium plasma can occur at 1.4 eV which is significantly below the 3.89 eV ionization potential of cesium in a non-excited state. (Biblarz, 1995)

A reduction in thermionic efficiency of ignited converters occurs due to charge sheaths that buildup adjacent to the collector and emitter. The difference between negative electron and positive ion concentrations in the plasmas and sheaths forms electric

fields that hold electrons in the plasma. This phenomenon causes an energy potential that electrons must overcome, thereby reducing the converters electrical output and efficiency. (Hatsopoulos and Gyftopoulos, 1973)

The transition point shown in Figure 3-3 is the point at which the ignited mode of operation changes from the "obstructed" region to the "saturated" region. This point is significant because it is near the points of maximum power and converter efficiency. At the transition point there is zero electric field at the emitter. The zero field occurs because the positive ions generated in the plasma are adequate to neutralize the space charge without excess ions present. The obstructed and saturation regions have considerably different properties. (Rasor, 1991)

Voltage drop between the electrodes is insufficient to sustain the plasma ignited in the obstructed region. This inability to maintain the plasma ignited is the explanation for the term "obstructed." Why then is this region part of the ignited mode? The reason is that emitted electrons are accelerated across the emitter sheath and heat the electrons at the edge of the plasma to a substantially higher temperature than is found at the electrodes. The temperature these electrons reach must be high enough to produce positive ions by impact ionization to maintain the plasma ignited. Typically the plasma is only 1% ionized at the emitter and 0.1% ionized at the collector in the obstructed region. Yet ignited operation is sustained and practical converter operating points fall in this region. (Rasor, 1991)

The so-called "saturation" region is that region where the emission current is saturated, meaning changes in voltage no longer cause changes in current. Figure 3.3 shows that the region would better be called the "quasi-saturation" region since constant current is not quite reached. In the field of thermionics, these two terms are sometimes used synonymously since the physics involved for both regions is essentially equivalent.

In the saturation region of the ignited mode there is an excess voltage drop across the plasma. The excess voltage is ΔV above that required to maintain the plasma neutral. The excess ΔV energy is not absorbed by the plasma electrons because increased electron temperatures would cause greater impact ionization producing positive ions and

the plasma would no longer be neutral, which is a physical constraint on the system. The ΔV energy is used in ion production in the emitter sheath as determined experimentally. These ions are attracted to the emitter immediately rather than entering the plasma. This process results in a loss in efficiency for the converter. The approximately linear increase in output current density in the saturation region (refer to Figure 3-3) is mostly due to increased ion current associated with the excess voltage drop. (Rasor, 1991)

b. Unignited Mode

In unignited plasma operation, the ions are retained in the plasma by the collector and emitter sheaths. Electrons readily diffuse to the electrodes, which is the opposite of the ignited mode condition. The absence of the large retaining electron sheath at the emitter makes the unignited converter more susceptible to attenuation by electron scattering. This greater susceptibility also causes the unignited plasma to be more sensitive to Coulomb scattering (electron-ion) at high output current. Self-generated magnetic fields can be present in unignited plasmas because they have a higher collision path length and absence of electron-reflecting sheaths (Baksht, et al. 1973). These magnetic fields act transversely to the output current flow through the plasma. (Rasor, 1991)

The Coulomb scattering and magnetic effects cause losses that make the unignited mode impractical due to low efficiencies. Although the unignited mode is inefficient compared to the ignited mode there are applications that can take advantage of several regimes in the unignited mode. For example, the diffusion regime of unignited operation is uniquely dependent on plasma properties and is used for converter diagnostics because it is modeled more easily than the ignited mode and can be compared to an ideal diode. The Knudsen regime is an essentially collisionless plasma because the gap is much less than the mean free path for collisions. Operation at very high temperatures and extremely small gap sizes are needed to operate in this regime. Also, the high current densities resulting from the high temperatures cause unacceptable Coulomb scattering. There is however, application for the Knudsen arc. The Knudsen arc results in a Knudsen

plasma at sufficiently high output currents and voltage drop across the IEG. This arc has been used as a plasma switch and injection plasma for advanced types of thermionic converters. (Rasor, 1991)

IV. TOPAZ-II SPACE NUCLEAR POWER SYSTEMS

The TOPAZ-II space nuclear power systems located at the Topaz International Program facility in Albuquerque, New Mexico include a complete space reactor system and testing equipment. The electrical power generating component for the reactor system is the thermionic fuel element (TFE). A vacuum chamber test stand is provided for testing of the entire power system. Additionally, a TOPAZ-II TFE test stand is provided for testing of individual TFEs.

A. TOPAZ-II REACTOR SYSTEM

The TOPAZ-II Space Nuclear Power System is shown in Figure 4-1. Major subsystems that form the power system include the nuclear reactor, liquid metal coolant system, radiation shield, cesium supply system for the thermionic converters, structure and radiator and the control drive unit. The system was designed to provide five to six kilowatts of electrical power for a lifetime of one to three years. (Schmidt, et al. 1994)

A cross-sectional view of the TOPAZ-II reactor is shown in Figure 4-2. The reactor incorporates thirty-seven single-cell TFEs. Each TFE is individually fueled with uranium dioxide (UO_2) pellets that contain 96% enriched uranium 235. The reactor core is 37.5 centimeters high and has a diameter of 26.0 cm. The converters are cylindrical in design and fit into channels in the zirconium-hydride (ZrH) moderator blocks. TFE design allows fueling from the top of the reactor and can be done at the launch site. Electrical heating is available for testing the system thereby removing the need for nuclear fuel. Thirty-four of the TFEs are connected in series and provide electrical power generation. The other three are connected in parallel and drive an electromagnetic pump used to circulate liquid metal sodium-potassium (NaK) coolant. Each of the TFEs has a channel for coolant flow and is supplied cesium from a single reservoir manifold. (Schmidt, et al. 1994)

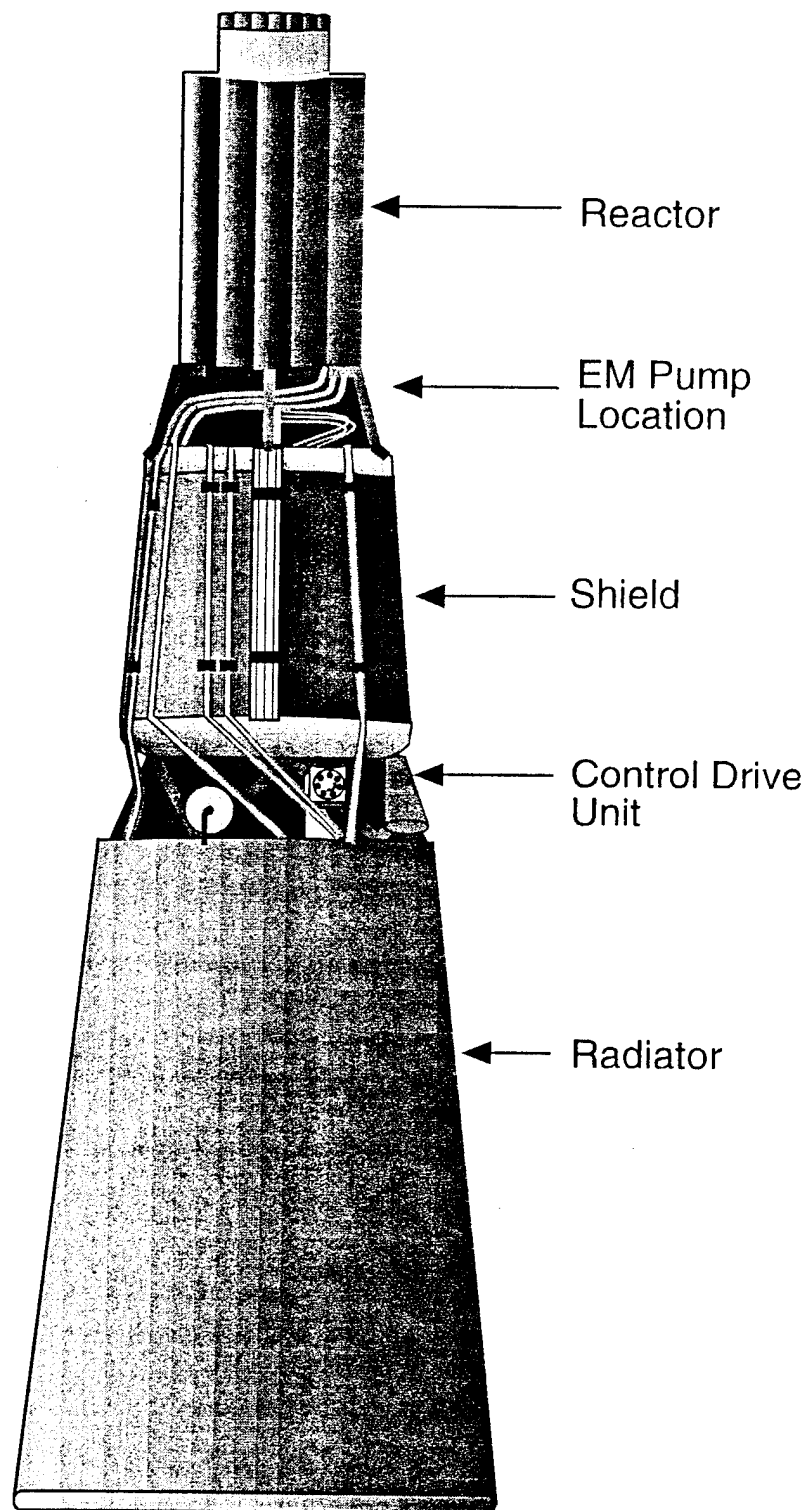


Figure 4-1. TOPAZ-II Space Nuclear Power System. From (Schmidt, et al. 1994).

The NaK coolant removes excess heat from the TFEs and then flows through the conical radiator where waste heat is rejected to space. Thermionic emitter temperatures range from 1800 K to 2100 K during normal operation with nuclear heating. The NaK loop maintains collector temperatures in the range of 743 K to 843 K. (Schmidt, et al. 1994)

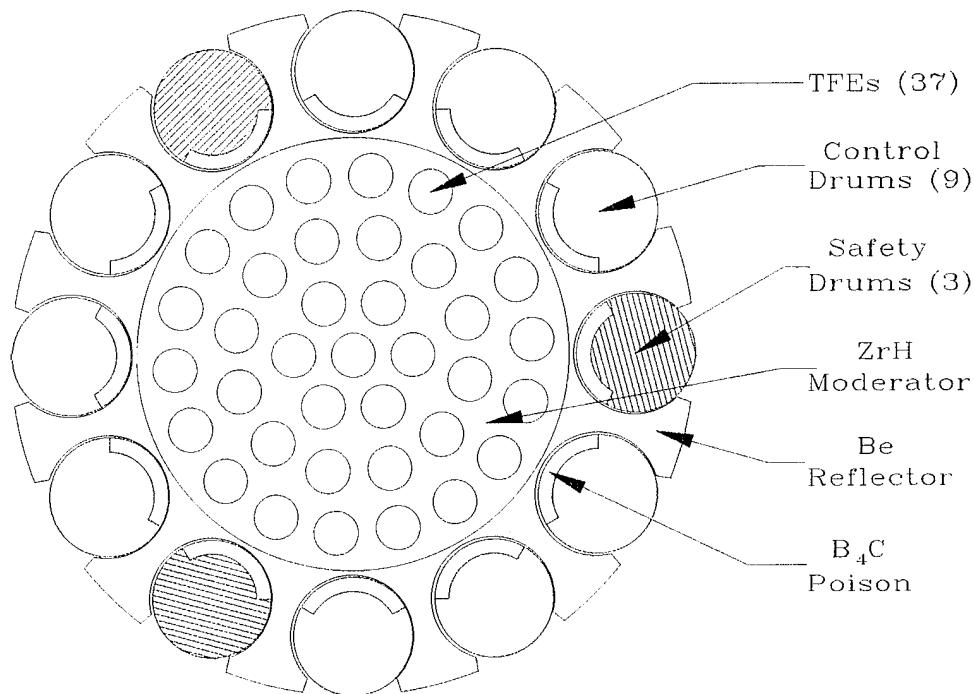


Figure 4-2. Cross-sectional View of the TOPAZ-II Reactor. From (Benke, 1994).

An axial beryllium (Be) and beryllia (BeO) reflector ring surrounds the reactors' power producing section. There are twelve Be control drums with boron-carbide (B₄C) poison plates. Nine of the drums provide control of the reactor after initial criticality. The three shaded safety drums (see Figure 4-1) ensure the reactor remains sub-critical until stationed in space. Once on station, the safety drums are rotated 180° outward to allow startup. Within seven hours after startup the motor drive for the safety drums is purposely rendered inoperable from the excessive heat of the reactor at full power operations. The remaining nine drums are rotated to varying degrees for controlling reactor power and are functional throughout the lifetime of the mission. (El-Genk and Xue, 1994)

B. TOPAZ-II THERMIONIC FUEL ELEMENT

The TOPAZ-II type TFEs are single-cell cylindrical thermionic converters. The TFE current pick-offs are located at each end of the emitter and collector. The emitter is monocrystalline molybdenum (Mo) with a 3% niobium (Nb) substrate. The emitter is coated with a 0.1 mm thick layer of tungsten to lower its emissivity (thus reducing radiation heat transfer from the emitter). The collector consists of polycrystalline Mo and is coated at its outside surface with a 0.15 mm sapphire insulation (Al_2O_3). The IEG of 0.45 mm is maintained with ceramic separators. Axial temperature expansions of the TFE components relative to each other are compensated for by four stainless steel expansion bellows. The collector is clad with stainless steel and blanketed with a small helium gap to transfer heat and provide insulation from the NaK coolant. (Ponomarev-Stepnoi, et al. 1991)

Figure 4-3 illustrates the difference between an earlier single-cell and the present multi-cell TFE design. Multi-cell TFEs provide significantly higher power and efficiency

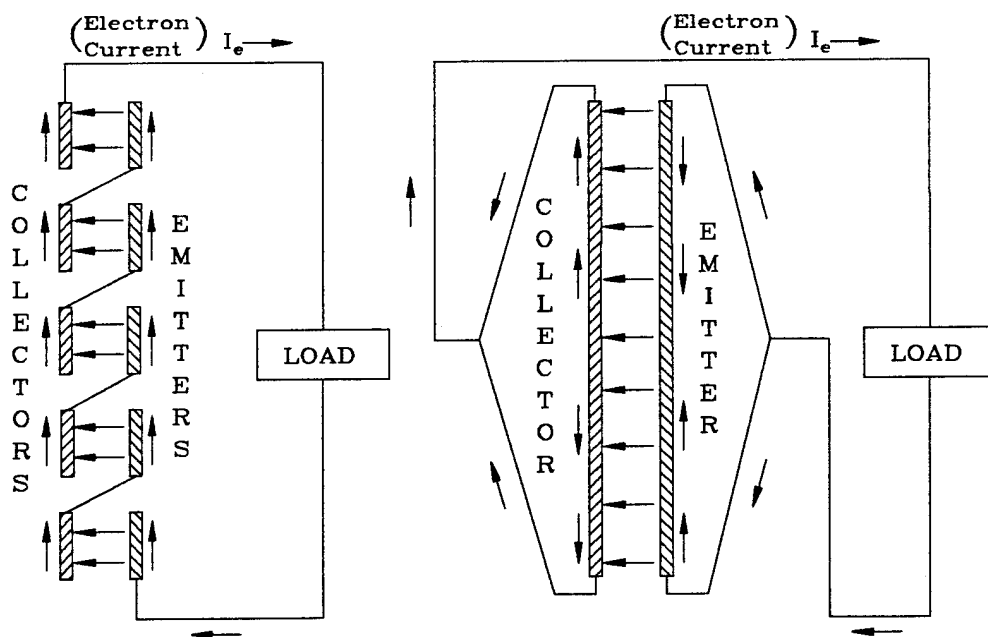


Figure 4-3. Simplified schematics for multi-cell and single-cell TFEs. From (Benke, 1994).

than the single-cell design (Paramonov and El-Genk, 1994).

Multi-cell TFEs are connected in series allowing for less voltage drop across the length of the converter. Ohmic loss in the single-cell TFE cause relatively large voltage drops along the electrodes. However, single-cell TFEs do have distinctive advantages over multi-cell designs. The open cavity in the fuel block of the TOPAZ-II TFE enables relatively simple construction of the fission product gas removal system without having to connect hardware to the interelectrode gap. Nuclear safety and radiation precautions are unnecessary in the manufacture and transportation phases. Multi-cell TFEs are constructed with the fuel in the system. The possibility for out-of-pile testing with electric heaters is one of the most desirable attributes of single-cell TFEs when compared to the multi-cell types. (Ponomarev-Stepnoi, 1991)

Power density in the reactor core varies both axially and radially. This causes differing operational performance for each of the thirty-seven TFEs in the core. Measuring the dissimilarity between the operation of the TFEs is presently indeterminate for numerous reasons. In the TOPAZ-II reactor, the TFEs are not electrically isolated from each other, but connected in series or parallel, which results in interaction of the output between TFEs. Individual temperature characteristics are difficult to determine since each TFE uses the same heat removal system. Thermionic energy conversion is greatly affected by cesium pressure in the IEG. Non-uniform power profiles in the TFEs require various cesium pressures to provide optimum thermionic conversion performance. A common cesium supply system is used precluding optimizing the output for each TFE in the system.

The TOPAZ-II single TFE test stand is provided to allow extensive testing of a single TFE without the interferences encountered in the overall reactor system. Thorough analysis of results obtained using the test stand are expected to support improved operation of the reactor system.

C. TOPAZ-II TFE TEST STAND

The TOPAZ-II TFE test stand comprises the apparatus for testing a single TFE within a vacuum chamber along with the associated vacuum, cesium, helium and cooling water systems located external to the vacuum chamber. Non-nuclear testing is performed using electrical tungsten heating elements (TISA heaters). The stand can also be used for thermophysical investigations of other materials and products associated with developing technological processes in the "electrovacuum industry" (Androsov, et al. 1991). The majority of the vacuum chamber is manufactured from Russian stainless steel type 12X18H10T. This type steel closely approximates American Iron and Steel Institute (AISI) standard 321. The heat transfer properties of AISI 321 stainless steel are used in the thermal model due to the better availability of information on this material.

An elaborate pumping system is used to provide vacuum conditions required for the subsystems in the test stand. The vacuum chamber is designed to be pumped out by two vacuum adsorption pumps and maintained at high vacuum using the combined magnetic discharge high vacuum ion pump. A turbomolecular pump is used to evacuate the helium cavities and a turbomolecular or magnetic discharge pump for the cesium system and TISA heater channel. The vacuum system provides oil-less pumping with no connection to atmosphere while operating. (Luchau, et al. 1994)

The cesium system is used to fill the cesium reservoir, purify the cesium, maintain the cesium reservoir temperature, prevent cesium ingress into other pumping systems and evacuate the TFE interelectrode gap. A separate reservoir is provided for cesium purification and for providing vapor to the IEG. Seventeen nickel-chromium alloy heaters and six molybdenum heaters are used to maintain the cesium in a gaseous state over the liquid in the reservoir. The reservoir temperature is maintained at the lowest temperature in the cesium system to prevent condensing cesium elsewhere in order to avoid pressure oscillations and significantly impacting on TFE electrical characteristics. The test stand can be operated with or without evacuation of the TFE IEG. (Androsov, 1991)

The cooling water system provides heat removal to all test stand components. The most important load on the system is the TFE working section. Other loads include valve electric drives, the transistor load bank, the cesium reservoirs and pumps (Androsov, 1991). A turbine type flow-meter is installed on the inlet to measure flow to within a 98% accuracy. K-type surface contact thermocouples are provided on the inlet and outlet water piping. Two outlet thermocouples are provided on the outlet because one of the pipes is in thermal contact with the test stand and the other is not. Data analyzed shows that both outlet thermocouples are in agreement. These measurements are essential for calculating the quantity of heat removed by the cooling water.

The stand utilizes an automatic control system, an automated data acquisition system and a variable electrical load bank. During the experiment for this research the data acquisition system consisted of three 80286 personal computers (PCs) with four megabytes of random access memory and one hundred and fifty megabytes of hard drive. The system was designed to operate two programs simultaneously, one for controlling the test stand and one for data acquisition. Data from both programs are stored on the server hard drive. The other two computers can be used by the operators. Normalizing and multiplexing equipment provides the interface between the test stand and the computers. (Luchau, et al. 1994)

The graphics displays were originally all in Russian for this experiment. The system was upgraded during 1994 to a 80486-66MHz processor and all displays are now in English. A fully automated temperature control has also been added to the cesium reservoir to improve accuracy since thermionic processes are so dependent on cesium pressure (as determined by the bulb temperature).

Figure 4-4 is a cross-sectional drawing of the TFE test stand. The upper and lower helium chambers provide helium to unregulated (helium pressure is not varied) gaps in the test section to enhance heat transfer across the gaps. Helium is also supplied to spaces in the TISA heater section. Cesium is provided via the lower helium chamber. Since the cesium lines are heated, temperatures of the lower helium chamber are greater than those

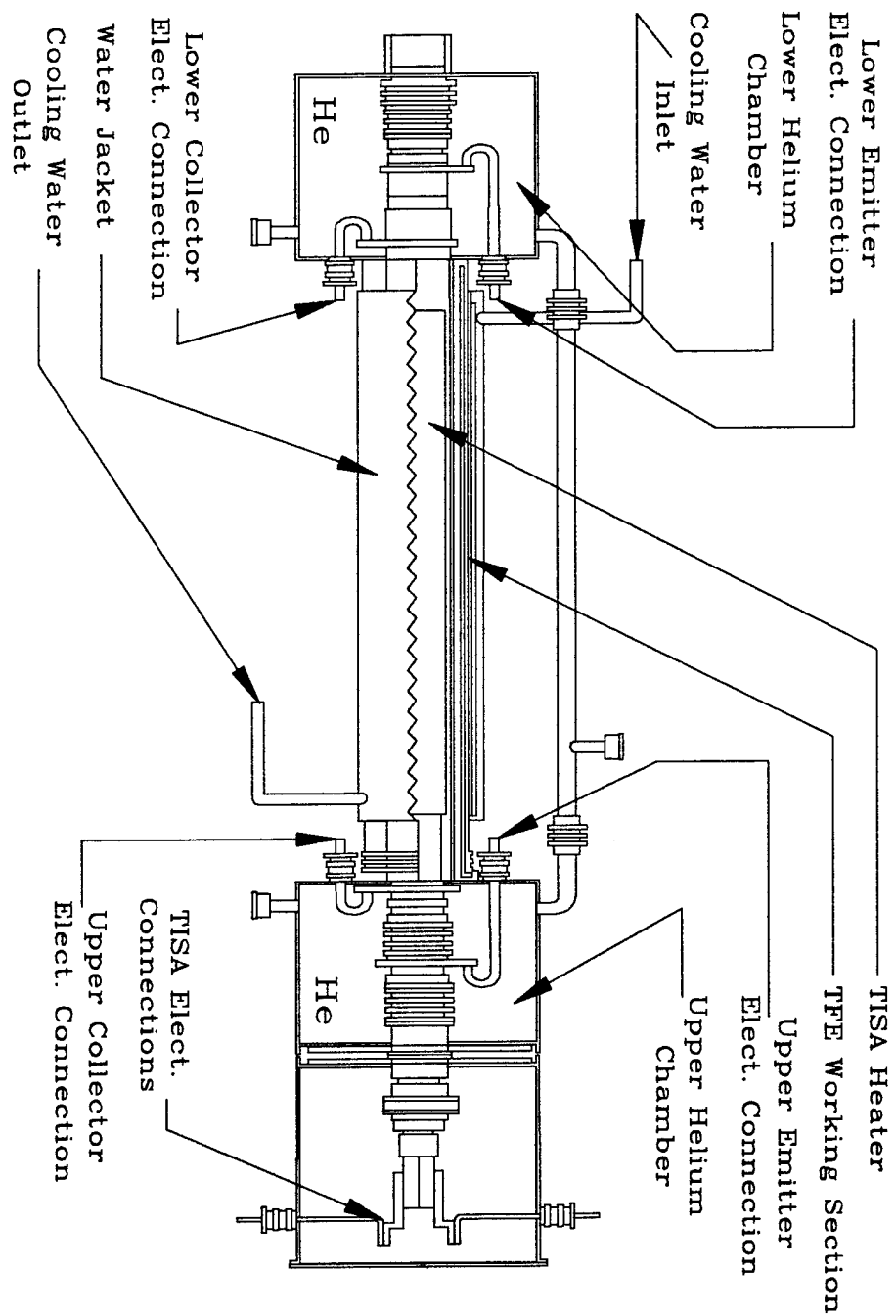


Figure 4-4. Cross-sectional view of the TOPAZ-II TFE test stand. After (Luchau, et al. 1994).

of the upper helium chamber when operating the test stand. The difference in temperature between the chambers affects the end losses for the thermal model described in the following chapter. Emitter and collector lead electrical connections are located in each helium chamber and TISA heater electrical connections are made in the section above the upper helium chamber. The working section cooling water jacket connections are also shown.

An axial cross-sectional view of the test stand working section (also called the heating core) is shown in Figure 4-5. Appendix B contains a comparable cross-section provided by the Russians. This figure shows the relative proportions of the various test section concentric cylinders. All of the dimensions are in millimeters. The diameter of the heating core is only 87.0 mm which corresponds to approximately 3.4 inches. Some of the smaller gaps are 0.05 mm wide. These tight tolerances indicate the difficulty involved in the manufacture of the test stand. The length of the emitter and collector is 375.0 mm and the TISA heater is 300.0 mm long. The cooling water jacket is 326.0 mm in length. The length to diameter (L/D) ratio of the working section is 4.31. A radial cut-away view of the test stand is shown in Figure 4-6 with an enlarged view of the test section from the collector sleeve inward provided in Figure 4-7.

The TFE and its associated TISA heater are fit into the collector sleeve tube of the test stand as shown in Figure 4-7. The TISA heater is constructed of a special tungsten heating element and flexible lobes that act as thermocompensators. The maximum supply voltage is 29 VAC with a maximum current of 170 A. The TISA heater can supply a maximum heating power to the working section of 4500 W (Wold, et al. 1994). The inner conductor of the TISA heater has a diameter of 6.5 mm and the outer conductor has a thickness of 0.4 mm with an outer diameter of 7.0 mm. The length of the heater is 300.0 mm making the heater 37.5 mm shorter at each end than the thermionic working section. This shorter length simulates the end effects associated with nuclear heating. Detailed discussions of the correlation of TISA heating to nuclear fuel heating are presented in El-Genk and Xue (1994). (Benke and Venable, 1995)

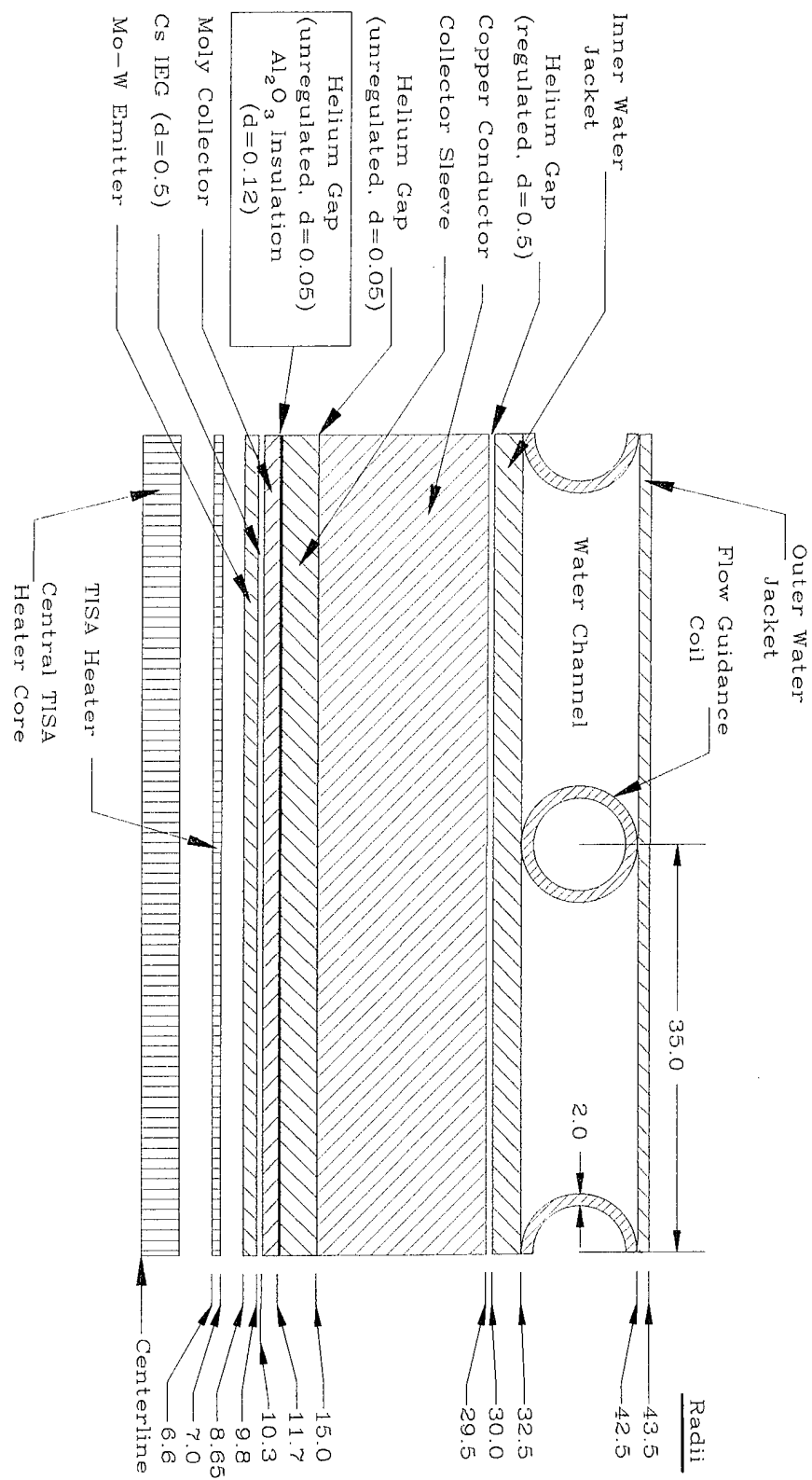


Figure 4-5. Cross-sectional view of a TOPAZ-II TFE in the test stand. From (Benke, 1994).

(all dimensions in mm)

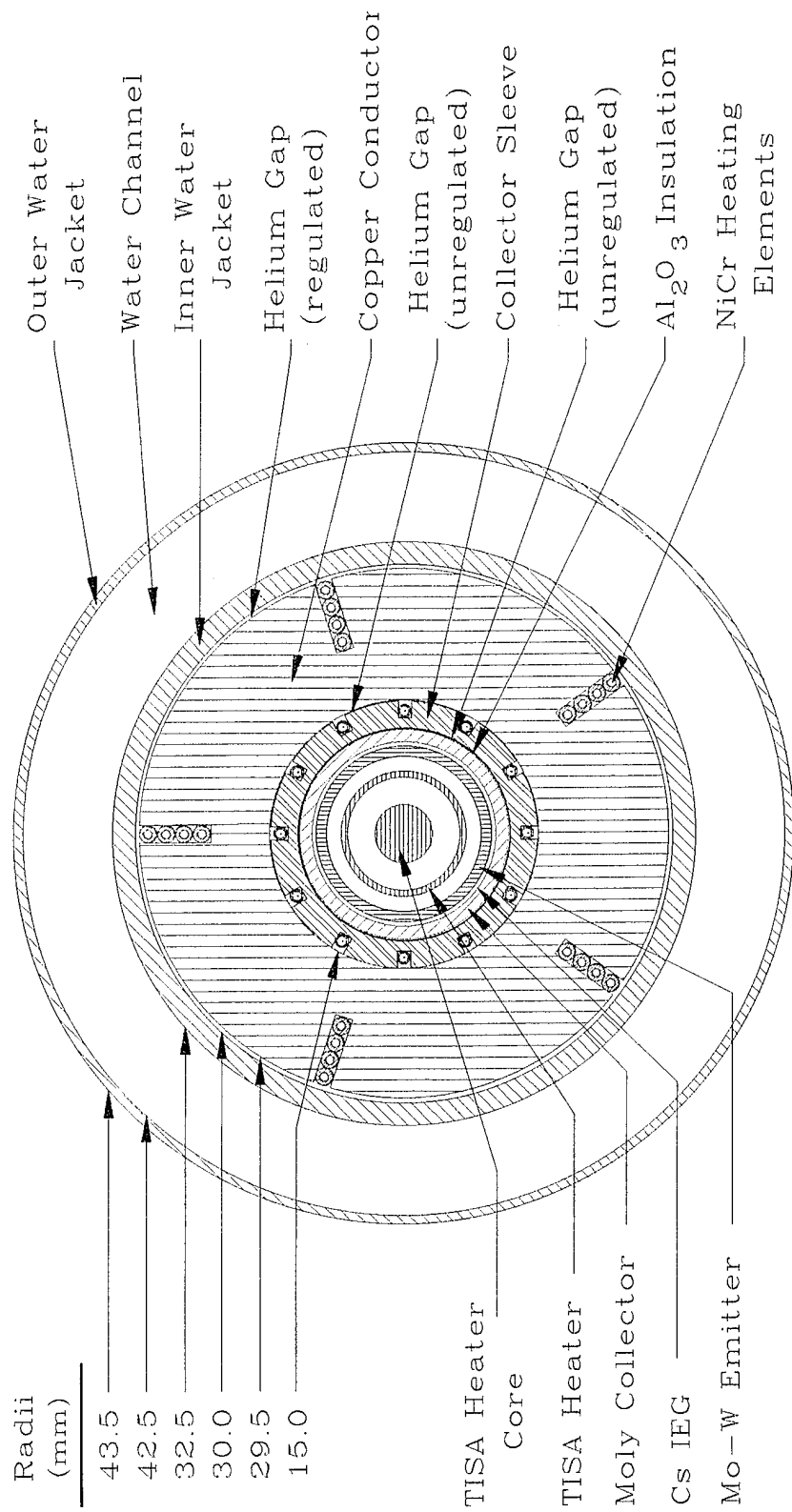


Figure 4-6. Radial cut-away view of a TOPAZ-II TFE in the test stand. From (Benke, 1994).

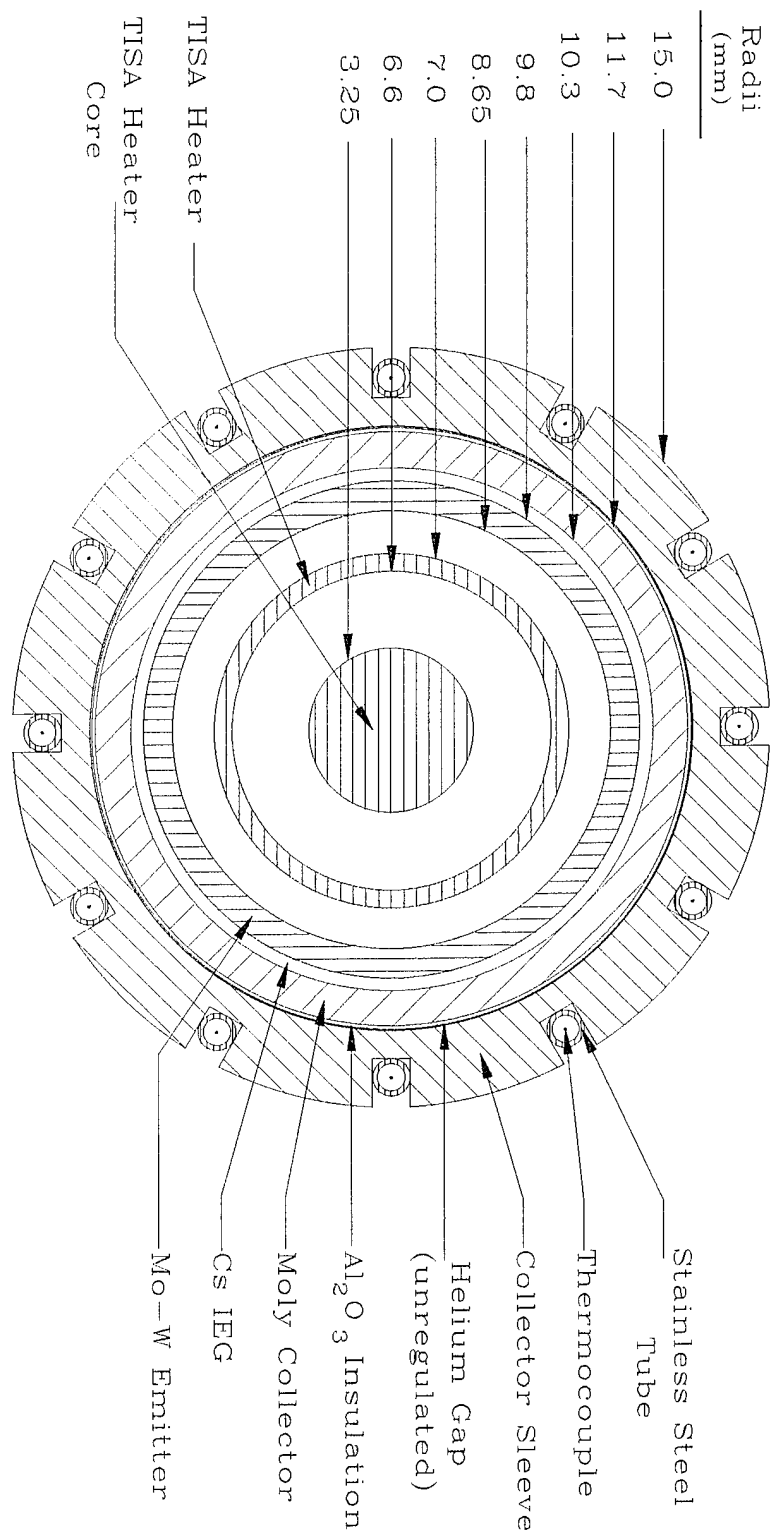


Figure 4-7. Radial cut-away detail of a TOPAZ-II TFE in the test stand. From (Benke, 1994).

A 0.05 mm gap separates the alumina insulator from the collector sleeve tube. This gap allows the TFE to be fit into the test rig and is filled with helium during normal operation. The helium is provided by the upper and lower helium chambers (see Figure 4-4). The helium pressure in this gap is unregulated and is normally in the 200 to 300 torr range. The collector sleeve tube is 3.0 mm thick with an outer diameter of 29.9 mm. It is constructed of Russian 1X18H10T stainless steel. The collector sleeve contains 12 evenly spaced, 2.0 mm deep slots in its outer surface that run the length of the collector sleeve. These slots in the collector sleeve contain the only thermocouples located in the interior of the test rig. The thermocouples are positioned in the collector sleeve at varying heights to provide indication of the axial temperature distribution along the working section. The thermocouple wires are packed in alumina inside of stainless steel tubes that are placed inside the slots. Another 0.05 mm helium gap separates the collector sleeve tube from the copper conductor. The unregulated helium in this gap is supplied from the upper and lower helium chambers at the same pressure as the gap separating the alumina insulator and collector sleeve tube. (Benke and Venable, 1995)

The copper conductor is 15.0 mm thick with an outside diameter of 60.0 mm. It is made of 99.99% pure copper and provides a high thermal conductivity to facilitate heat transfer radially outward to the cooling water. The outer surface contains five radially spaced slots that each contain four nichrome (NiCr) heating elements. These heaters are used for outgassing the rig prior to startup and are secured during normal operation. The heater wires are insulated with alumina and sheathed in stainless steel. A 0.5 mm gap separates the copper conductor from the inner cooling water jacket. This gap is filled with helium supplied from a source external to the test rig. The pressure of the helium is regulated in the band of 1 to 10 torr during normal operation to control the collector sleeve temperature by varying the thermal resistance of the gap. (Benke and Venable, 1995)

The cooling water jacket is made of Russian 1X18H10T stainless steel and has an inner wall thickness of 2.5 mm and an outer wall thickness of 1.0 mm. A coiled stainless

steel tube between the jacket walls provides a spiral flow path for the cooling water. The water flows from the bottom to the top of the water jacket around the outside of the coil in the cooling "channel" depicted in Figure 4-5. The coils are spaced by 35.0 mm and spiral approximately 6.5 times. Cooling water temperature is measured on the inlet and outlet piping exterior to the vacuum chamber using surface thermocouples. Cooling water flow rate is measured in the inlet piping using a turbine-type flowmeter located exterior to the vacuum chamber. (Benke and Venable, 1995)

V. TEST STAND THERMAL ANALYSIS

A thermal model of the TFE test stand is desired to provide necessary information about temperature distribution and limitations of the test stand. A better understanding of the operation of the TOPAZ-II reactor system may be provided by analyzing the performance of a single TFE. Comparisons of test stand temperature data to TOPAZ-II data can indicate how a single TFE's performance is affected by being placed in series or parallel with other TFEs. Heat dissipation is critical to the operation of the TOPAZ systems because TFE efficiencies are about five to seven percent; therefore, about 94% of the input power is waste heat. Limitations of the test stand can be modeled before subjecting the stand to overpower testing. Thorough understanding of the heat removal capability of the test stand can determine the stand's suitability for testing other TFEs or electrode materials. A brief discussion of the thermal model including a description of the model, areas of difficulty and limitations of the analysis will be presented here. A complete discussion together with computations concerning the thermal analysis can be found in Benke (1994).

A. THERMAL MODEL DESCRIPTION

A one-dimensional heat transfer analytical model has been used to develop the temperature profile radially through the TFE test stand. The extensive cross-sectional diagrams shown in Chapter 4 are designed to aid in the development of the model. A network method is used that accounts for conduction, radiation and forced convection heat transfer across the test stand.

The heating core assembly for the test stand extends from the TISA heater assembly to the cooling water jacket and is located in a vacuum chamber (see Figures 4-4 and 4-6). The basic design incorporates highly thermal conductive metals for ease of heat transfer out to the cooling water. Gaps in the test stand between sections contain helium to provide a heat transfer medium to the system since a vacuum is more heat transfer

inhibiting. Classification of the dimensions and material types in the test stand was done to enable determination of the proper heat transfer characteristics to be used.

Operating temperatures are taken on the collector sleeve tube and at the inlet and outlet piping of the cooling water system. The thermocouples and turbine-type flowmeter in the water system were added to support this work and are now a permanent tool used by the operators of the test stand. Collector sleeve tube thermocouples are located axially along the tube to give a temperature distribution along the length of the working section. Figure 5-1 indicates the location of the thermocouples along the collector sleeve. The length of the TISA heater is 30 centimeters. The thermionic working section that corresponds to the length of a TFE is substantially longer at 37.5 centimeters and the water jacket is 32.6 centimeters in length. These relative dimensions present a difficulty in determining the "end losses" or axial heat transfer in the test stand. A one-dimensional radial analysis cannot account for the end losses. Fortunately, the axial heat transfer is relatively small compared with the radial heat transfer. Since there is a 20% increase in cylinder length from the TISA heater length to the TFE working section length, the thermal resistance also increases by 20% (Benke, 1994). Across a single metal component this only results in a few degrees temperature difference, but the cumulative effect can lead to large calculational uncertainty (Benke, 1994). The 30 centimeter length is chosen for the model to provide a conservative estimate since this shorter length results in the highest end losses.

The network method is illustrated in Figure 5-2. The known temperatures are located at node 6 and node 12 in the figure. Node 6 corresponds to the collector sleeve temperature and is taken as an average of the axial thermocouple measurements along the collector sleeve. Node 12 is the water channel bulk temperature and is an average of the temperatures measured by the K-type surface contact thermocouples located on the inlet and outlet water piping. The heat carried away by the water corresponds to the heat lost in the system excluding end losses. With end losses, the calculation determining heat removal by the water should not be greater than the heat loss from the stand based on the

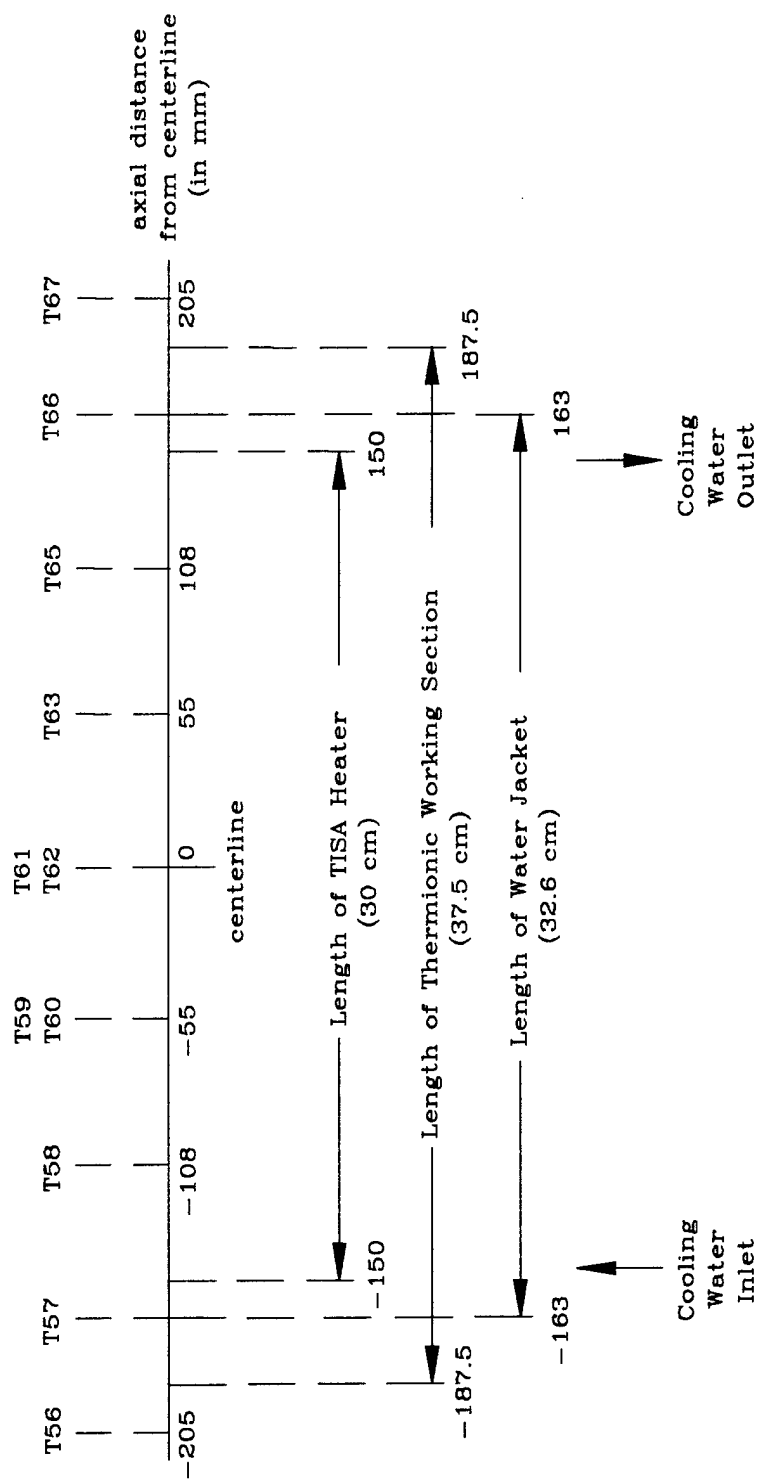


Figure 5-1. Axial location of the collector sleeve thermocouples. From (Benke, 1994).

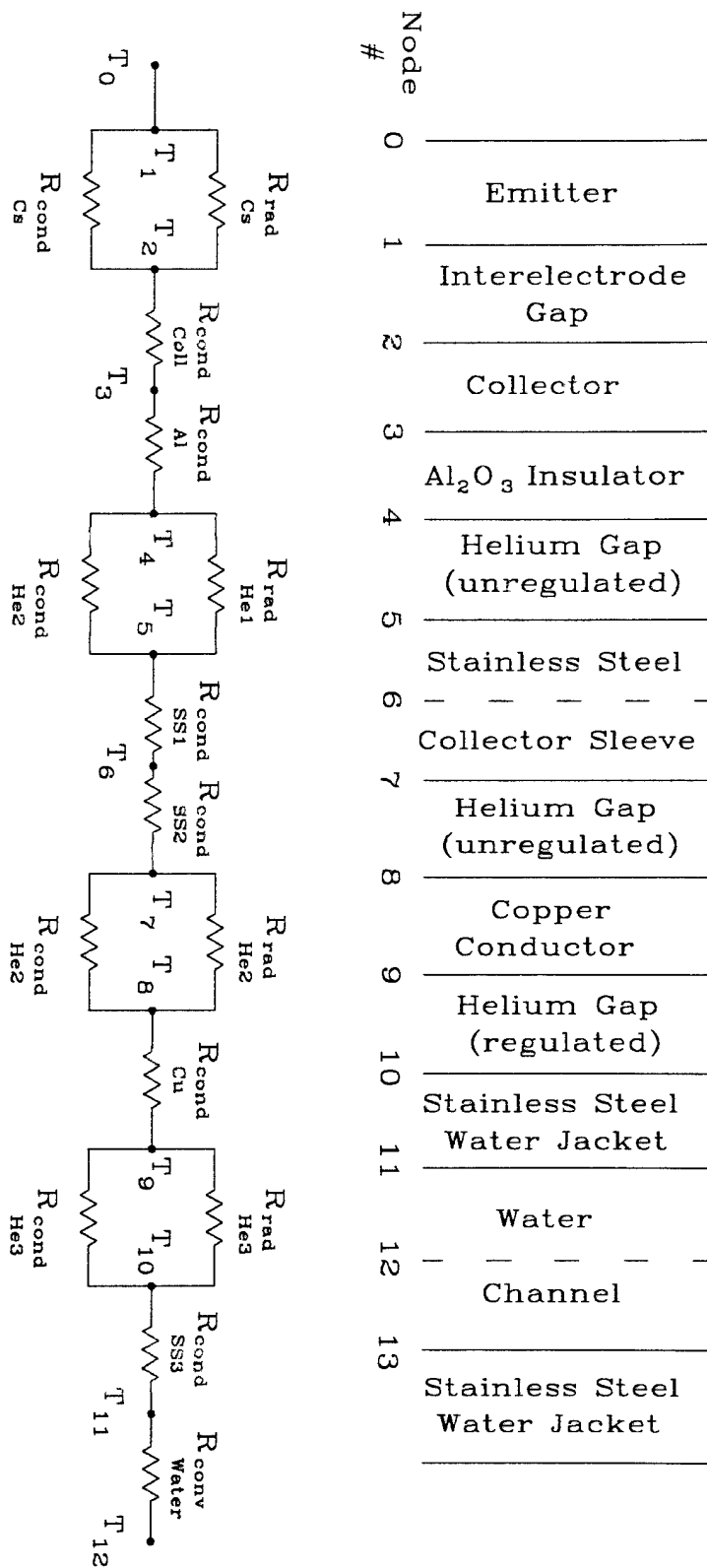


Figure 5-2. Thermal model resistance network.

difference between the TISA heater input power and the electrical power output of the TFE. The TISA heater input power is also called the "active zone" power by the Russians. It corresponds to the quantity of total TISA heater power that reaches the active zone (thermionic conversion section). Current and voltage applied to the TISA heater is measured and their product yields thermal input power. Lead losses then reduce the power that gets to the active zone. A factor of 88% is applied to the TISA heater power to account for the losses. This factor is used over all ranges of TISA heater operation. A constant loss factor can be used because there is a linear current-voltage relationship for the heater over its operating range. This correlation is documented by Figure 19 of Stepennov, *et al.* 1992. The heat loss from the stand can be represented by

$$Q_{\text{loss}} = P_{\text{az}} - P_{\text{out}} \quad (5.1)$$

where Q_{loss} is the heat lost from the test stand, P_{az} is the power supplied to the working section as described above and P_{out} is the output power of the TFE.

Measuring water flow and temperature of the cooling water provides a quick estimate of the heat transfer ability of the heating core since

$$Q = m' c_p (T_{\text{out}} - T_{\text{in}}) \quad (5.2)$$

where m' is the cooling water flow rate in kg/s, c_p the specific heat capacity of water, T_{out} and T_{in} the the cooling water inlet and outlet respectively in degrees K. This value yields the amount of heat removed by the water. Comparison of Q from Equation 5.2 to Q_{loss} indicates what portion of the unused power is transferred radially to the water. Differences are attributed to end losses and to instrument errors.

Heat transfer across the metal portions of the test section are solely due to conduction. The helium gaps have combined conduction and radiation heat transfer mechanisms. The water channel transfers heat through forced convection. Thermal conductivity variations as a function of temperature are well defined for the metal portions of the test stand. As mentioned before, AISI 321 stainless steel values are used for the Russian stainless steel in the test stand. Best fit polynomials for thermal conductivity of helium as a function of temperature are provided in Andrews and Biblarz (1981). The

radiation heat transfer in the helium gaps is negligible compared to the conduction heat transfer term. The network models the heat transfer mechanisms across the test stand as resistances (see Figure 5-2). There are three portions of the network that can be termed "critical" resistances, namely, the regulated helium gap, the cooling water channel and the interelectrode gap. They are critical because of the significant effect they have on heat transfer through the stand and, incidentally, also due to their difficulty of analysis.

B. CRITICAL RESISTANCES

1. Regulated Helium Gap

The two unregulated helium gaps are operated at a pressure of 200 to 300 torr. At these pressures the thermal conductivity of helium is independent of pressure, but still temperature dependent. The regulated helium gap is operated from 1 to 10 torr and controls the collector sleeve temperature. At a constant temperature, varying the helium pressure in the regulated helium gap changes the temperature of the collector sleeve. This change in collector sleeve temperature is due to the varying thermal conductivity of helium in the gap. This pressure dependence is a result of the helium being rarefied at the low pressures in the regulated gap. The mean-free-path for inter-atomic collisions is greater than the distance for atom collisions with the gap walls.

Helium in the unregulated gaps is at the continuum value for thermal conductivity. This means that the gap is filled with helium atoms such that the inter-atomic collisions dominate removing a pressure dependence for thermal conductivity. Reid *et al.*, 1977, determined that the continuum value was reached at 1 torr. Paul Agnew of the United Kingdom, currently working at the TOPAZ International Project performed a preliminary analysis of this pressure dependence in the test stand and found that approximately 5 torr of helium pressure results in a thermal conductivity at its continuum value. Agnew has completed a Monte Carlo calculation for the mean free paths to support his initial analysis. The results are within 2% of the previously reported conclusions. (Agnew, 1994)

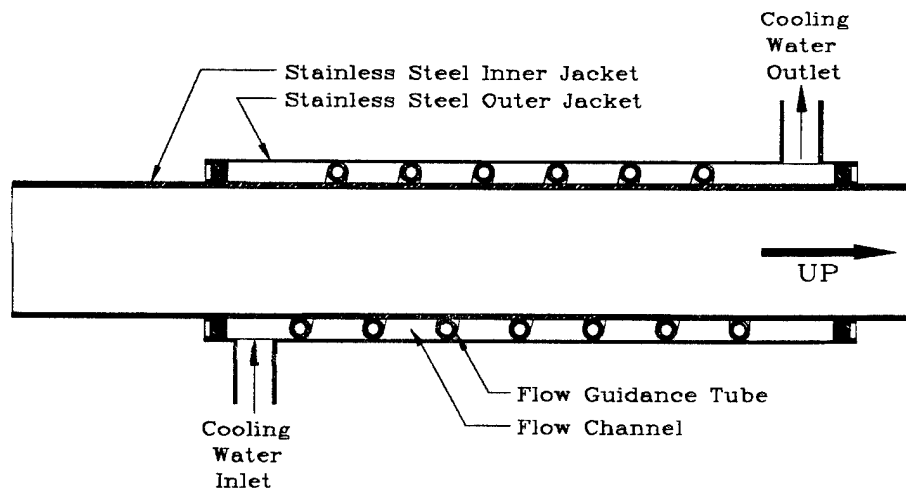
Empirical data taken for this experiment show that the thermal conductivity of helium is not at its continuum value up to the 10 torr range. Using continuum values from 5 torr and greater yielded unacceptably high channel wall temperatures that would indicate boiling in the water channel. Operating temperatures of the inlet and outlet cooling water and constant pressure of the water do not support boiling in the water channel. Empirical data showed channel wall temperatures consistent with the measured inlet and outlet water temperatures. Specific values and detailed calculations are provided in Benke, 1994. The difference between the empirical values and Agnew's calculations may be due to inconsistencies in the gap separations. The gap is 0.5 mm and it is difficult to maintain such a small spacing along the length of the working section. Another source of error is the accuracy of the helium pressure measurement that is ± 1 torr. Agnew also ignores the "sticking coefficient" which is an atoms' tendency to attach itself to a surface for a finite amount of time instead of bouncing off of the surface after impact.

2. Cooling Water Channel

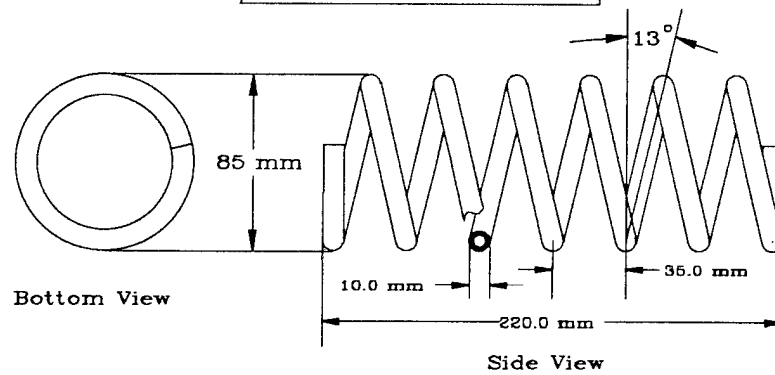
The convective heat transfer coefficient value is required to calculate the thermal resistance of the water channel. Low water flow rates and channel geometry make determination of the heat transfer coefficient difficult. Figure 5-3 provides detailed drawings of the water jacket. Note that water does not flow inside the hollowed out section of the flow guidance coil, but through the cross section that is almost rectangular shown in the bottom view of Figure 5-3. (Benke, 1994)

The Reynolds number calculated for the channel indicate that the flow is in the combined laminar flow regime. This flow regime is difficult to analyze with existing correlations. For this reason, two cases were chosen to bound the problem with an upper and lower limit for the convective heat transfer coefficient. The upper limit was chosen by the Dittus-Boelter correlation for fully developed turbulent flow and the lower by the Seider-Tate correlation for developing laminar flow. (Benke, 1994)

Flow Guidance Tube in the Water Jacket



Flow Guidance Tube



Flow Channel

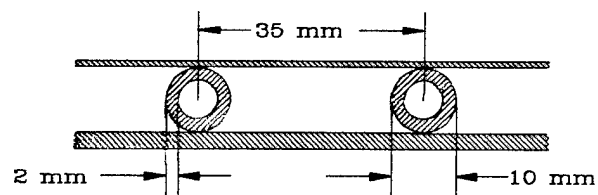


Figure 5-3. Cooling water jacket details. From (Benke, 1994).

Since the flow guidance coil is stainless steel and in thermal contact with the water channel walls that are also stainless steel, it is difficult to determine the surface area for heat transfer through the channel wall. The minimum heat transfer surface area is equal to the cylindrical surface area of the inner water jacket. The maximum surface area is the sum of the inner and outer water jacket surface areas and the total surface area of the flow guidance coil. (Benke, 1994)

3. Cesium Interelectrode Gap

The most formidable critical resistance in the network is the interelectrode gap. Conduction and radiation heat transfer through the IEG must be considered because the high emitter temperatures make radiation heat transfer significant. The thermal conductivity of the cesium in the gap depends on the emitter surface temperature, collector surface temperature, vapor pressure of the gas and the gap size (Paramonov and El-Genk, 1994). The plasma physics in the gap has to be modeled for both the ignited and unignited modes of operation. Accounting for transition from the obstructed region to the saturation region is also necessary. Determining the heat transfer characteristics in the IEG for all conditions of operation would provide the emitter temperature values during operation. This work has yet to be done. One method that could accomplish this goal is to couple this thermal model to the thermionic emission model created by Paramonov and El-Genk, (1994). Owing to the complexity of collisional effects in the plasma, they are neglected in this model (Paramonov and El-Genk, 1994).

C. TITAM COMPARISON

A Thermionic Transient Analysis Model (TITAM) of the TOPAZ-II space nuclear power system has been designed by Paramonov and El-Genk at the Institute for Space Nuclear Power Studies at the University of New Mexico. TITAM provides thermal performance data for the entire reactor and individual TFEs. TITAM is used to check the accuracy of the thermal model.

The common point that allows comparison of TITAM to this thermal model is the NaK coolant temperature and the collector sleeve temperature. The radial distance of the collector sleeve thermocouples from the centerline in the test stand is the same as radial distance of the NaK coolant in the TOPAZ-II reactor. This was a design consideration to allow comparison of test stand data to reactor data. The collector sleeve temperature is maintained at a constant temperature with the regulated helium gap to approximate NaK coolant temperatures. NaK temperatures are relatively constant at nominal operation due to the coolants high heat capacity.

TITAM is used in the single TFE mode and a one-to-one comparison is done to check the accuracy of this model. Required inputs to TITAM are thermal input power which is equal to active zone power (P_{az}), NaK inlet temperature which is entered as average collector sleeve temperature and NaK coolant flow rate which is input as a nominal value. Table 5-1 shows a typical output of this method.

Parameter	TITAM Output	Thermal Analysis Results
Thermal Power to TFE (W)	3,003	3,003
Emitter Surface Temperature (K)	1,835.57	-
Collector Surface Temperature (K)	765.71	763.93
Insulator Temperature (K)	763.75	761.88
Coolant Average Temperature (K)	727.58	726.83

Table 5-1. Comparison of TITAM output to Thermal Analysis Results.

After (Benke, 1994)

Thermal analysis results are supported by TITAM calculations. There is a difference in coolant average temperature because TITAM calculated a temperature based on the

average coolant temperature input as 726.83 K. The empty box in the table reemphasizes that this model does not calculate emitter surface temperature due to the difficulty of modeling the cesium IEG.

VI. SINGLE TFE ELECTRICAL CHARACTERISTICS

Data taken for the thermal modeling of the test stand were used to investigate the electrical characteristics of a single TOPAZ-II TFE without interferences found in the reactor system over a wide operating range. Of particular interest were data taken at low thermal input powers. Low thermal input powers correspond to converter operation in the unignited mode and had not been explored heretofore. Standard operating procedures for the TOPAZ-II reactor prescribe nominal power levels that result in ignited mode operation only.

A. EXPERIMENT DESCRIPTION

Thermal input power levels for the TOPAZ-II reactor are 115 kWt (kilowatt-thermal) nominally and 135 kWt maximum. These power levels correspond to 3.11 kWt and 3.65 kWt on average for each of the 37 TFEs in the reactor. Uneven radial power distribution in the reactor however, leads to differing input powers between the TFEs in the reactor system. The range of power levels used in the single TFE test stand to investigate the low power operation of the TFEs was chosen based upon the assumption that all TFEs in the reactor system operate at the same thermal input power level.

Data were taken from 1.0 kWt to 3.6 kWt TISA heater input power at intervals of 200 W. Cesium pressure was varied for each power level and current voltage sweeps were taken at each cesium pressure for the given power level. The significance of varying cesium pressure can be seen in Figure 6-1. The three curves shown in Figure 6-1 illustrate how disparate the electrical output power of a thermionic converter can be for a given thermal input power when cesium pressure is varied. Note that as cesium pressure changed from 0.4 torr to 1.0 torr, electrical output increased, but subsequently decreased as cesium pressure was raised to 1.3 torr. The performance of the TFE from low to high cesium pressure can be generalized to the case shown in Figure 6-1, but the exact values of cesium pressure for which electrical output power is a maximum, for a given thermal

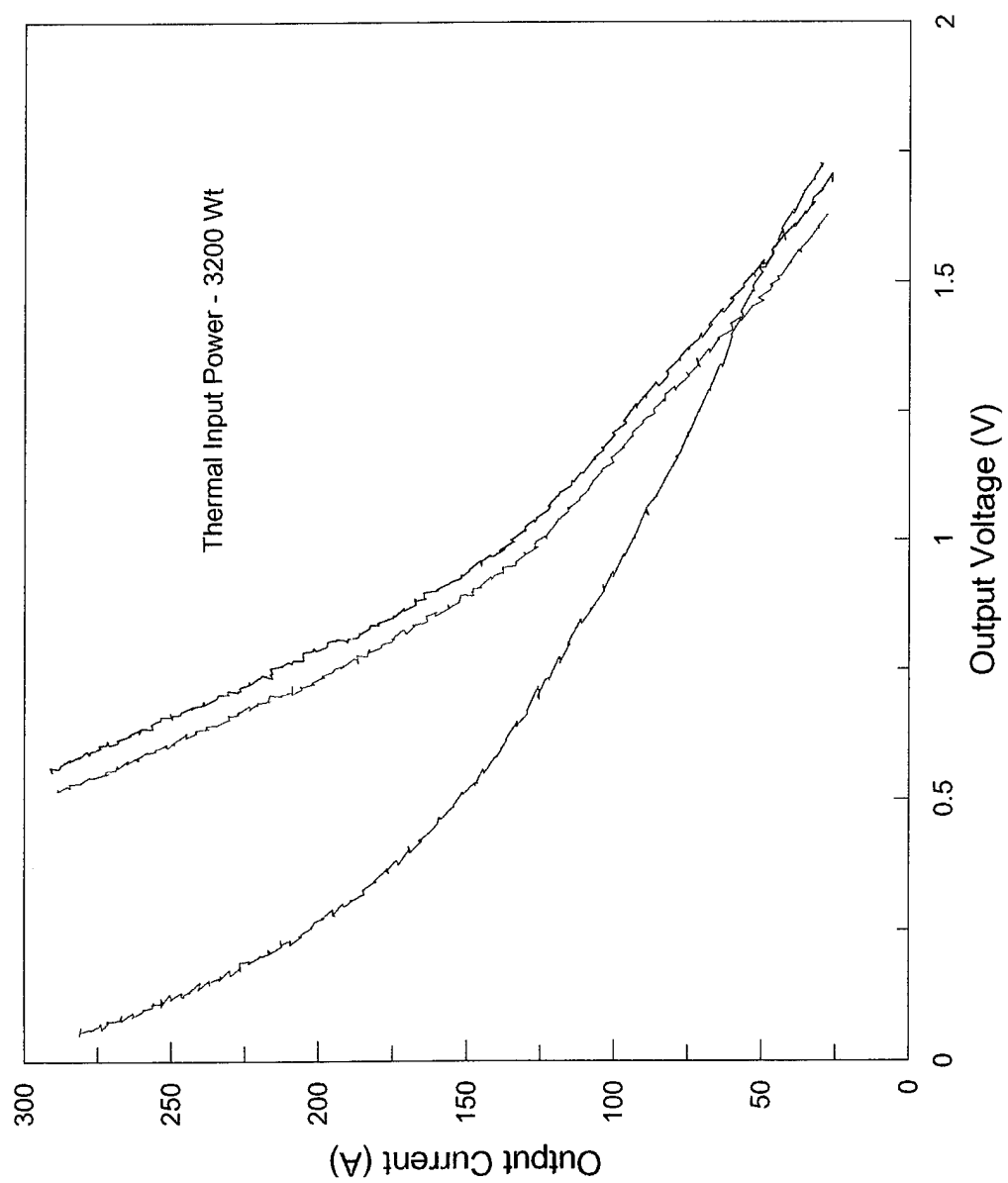


Figure 6-1. I-V sweep variation with cesium pressure.

input power, are not constant with changing power levels. Optimization of cesium pressure over the range of power levels must be done to determine maximum TFE efficiencies.

B. CESIUM PRESSURE OPTIMIZATION

A cesium pressure that is too low for a given thermal input power may result in inadequate adsorption of cesium onto the electrode surfaces. This prevents the emitter work function from reaching its optimum value. Impact ionization of cesium atoms may also be lower than desirable, thus preventing beneficial space charge neutralization. The 0.4 torr curve in Figure 6-1 is an example of this case.

If cesium pressure is too high, there can be excess cesium ions in the IEG that inhibit electron flow because of increased collisions. This too could lower the electrical output of the converter. The 1.3 torr curve in Figure 6-1 indicates operation with cesium pressure too high for the given thermal input power.

To better categorize TFE operation in the test stand over the power ranges chosen for the experiment conducted at TIP, a method for determining an optimum cesium pressure was employed. For each power level, cesium pressure was incremented by 0.1 torr over a range of about ten cesium pressures. Current-voltage (I-V) sweeps were conducted at each cesium pressure once steady state conditions had been established. Approximately 30 minutes are needed to reach steady state after a TISA heater power change and 45 minutes after a cesium pressure change. The cesium pressure change was done manually with a vernier adjustment to the cesium reservoir heater. Automation of this system has markedly lowered the time to steady state for a cesium pressure change.

The raw data that comprised the sweeps were put in spreadsheets to enhance the analytical process. The maximum output powers of the I-V sweeps were obtained from their spreadsheet and plotted against cesium pressure. Results are shown in Figure 6-2. As discussed above, there is a region of high inefficiency at low cesium pressures then

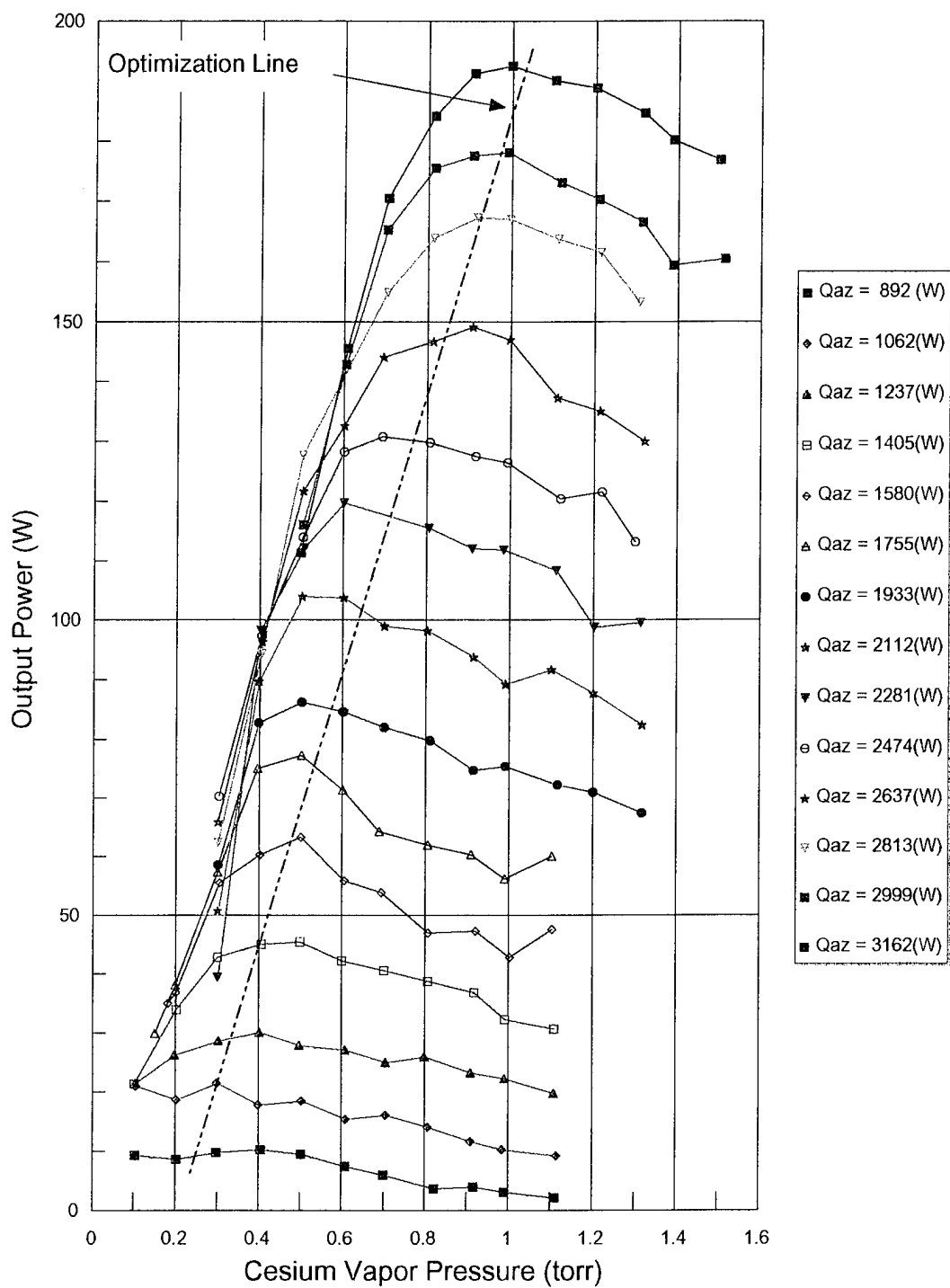


Figure 6-2. Cesium pressure optimization curves.

output power and efficiency reach a maximum and again decrease at higher cesium pressure. At the lower input power levels, performance is less sensitive to changes in cesium pressure.

Continued data analysis is referred to the optimum cesium pressures illustrated in Figure 6-2. Since it is impractical to choose a specific cesium pressure for each thermal input power level, the data are grouped into four different categories. The optimum cesium pressures chosen for the given input power levels were:

From 892 Wt to 1405 Wt 0.4 torr

From 1580 Wt to 2112 Wt 0.5 torr

From 2281 Wt to 2637 Wt 0.8 torr

From 2813 Wt to 3162 Wt 1.0 torr

The dashed line in Figure 6-2 labeled the "optimization line" is a straight line approximation to the optimum output power attainable over the range of thermal input powers shown on the figure. This curve is useful because it gives a relationship between optimum electrical output versus cesium pressure. Equation 6-1 represents the optimization line in Figure 6-2.

$$\text{Maximum output power (W)} \cong [260 P_{cs} (\text{torr}) - 68] \quad (6-1)$$

C. CURRENT-VOLTAGE CHARACTERISTICS

The test stand uses a transistor load bank to vary the load resistance seen by the TFE. An external current source is used to drive the TFE. This test circuit setup is shown in Figure 6-3. (Wyant, 1995)

The external current supply is needed to drive the TFE over a range of resistive loads to generate I-V sweeps. Curves generated using this test setup are similar to the one shown in Figure 6-4. This curve is a general representation of a single TOPAZ-II TFE operating in the ignited mode. The obstructed region is a low current region with relatively high output voltages. As current is increased, more cesium ionization is needed

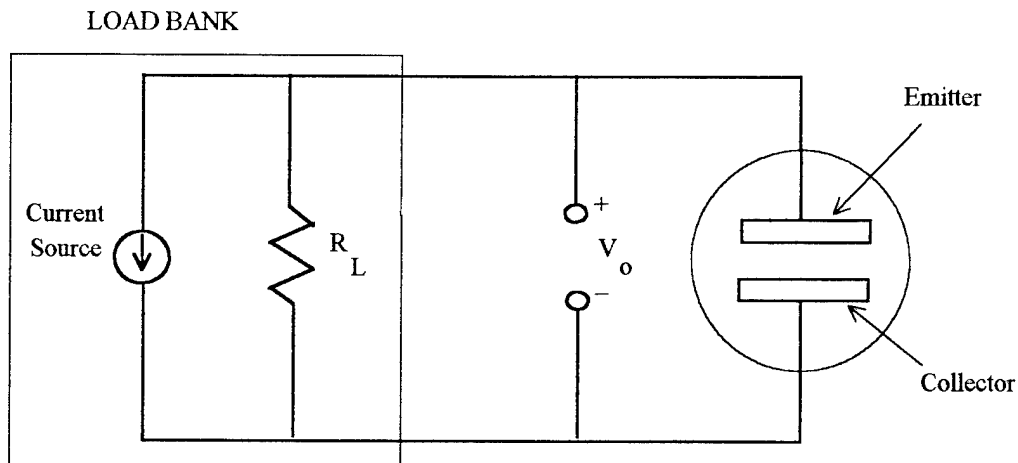


Figure 6-3. Single TFE test circuit. From (Wyant, 1995).

in the IEG and the potential drop across the emitter increases. With the collector work function relatively constant, an increase in the potential drop across the emitter corresponds to a decrease in the output voltage of the converter. This effect can be seen in the saturation region. If current continues to increase, the potential drop across the emitter will continue to rise and the output voltage will approach zero.

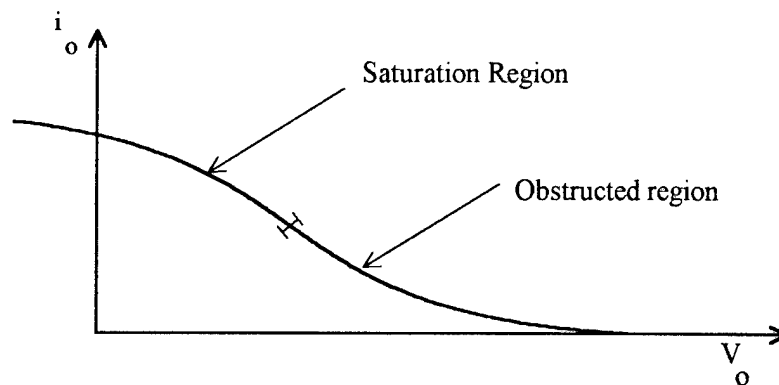


Figure 6-4. Test circuit current-voltage sweep. From (Wyant, 1995).

Figure 6-4 shows the output voltage crossing the zero axis and becoming negative. If an external current source were not being used in the test circuit this negative output voltage would not occur since the TFE would no longer be a generator of power, but a

consumer of power. Figures 6-5 through 6-8 show the I-V sweeps for the power levels investigated in this experiment. The sweeps shown in these figures represent the optimized cesium pressures discussed in the previous section. A complete set of I-V upsweeps taken during the experiment can be found in Appendix B.

Figures' 6-5 through 6-8 are arranged from the lowest thermal input power to the highest. The curves are labeled with the active zone power levels, Q_{az} , that are 88% of the TISA heater input power as described in Chapter 3. The I-V sweeps greater than 2112 W of power follow the form shown in the test circuit diagram, Figure 6-4, but curves below this input power have an additional feature. These lower power levels show the unignited mode of operation. In some cases the curves clearly show the ignition point that delineates the shift from the unignited to ignited mode of converter operation. The ignition point and operating regions are annotated on the 1580 W curve of Figure 6-6.

The ignition point is not clearly represented on all the I-V sweeps below 2112 W of input power. The ignition point is missing on some of the plots because of the method used for data acquisition. Each I-V sweep requires thirteen to fifteen minutes to complete and a data point is taken every three seconds. If ignition occurs at a time when data is not being collected it will be missed since ignition occurs rapidly, not unlike a spark.

As thermal input power is increased the I-V sweeps show that output current and voltage increase. At active zone power levels greater than approximately 2112 W (TISA heater power of 2400 W), the TFE no longer operates in the unignited mode. Active zone power levels below approximately 1405 W (TISA heater power of 1600 W) do not generate favorable power outputs in the unignited region.

All the I-V sweeps shown are "upsweeps" which means that they are started at low current and high voltage and the transistor load bank resistance is changed to increase current and create the "set" of operating points that represent the curves shown. The capability exists in the test circuit to then perform a "downsweep" by reversing the process. Downsweeps are interesting because the ignition point found at low thermal input powers when doing an upswing is not found in any downsweep. In going from

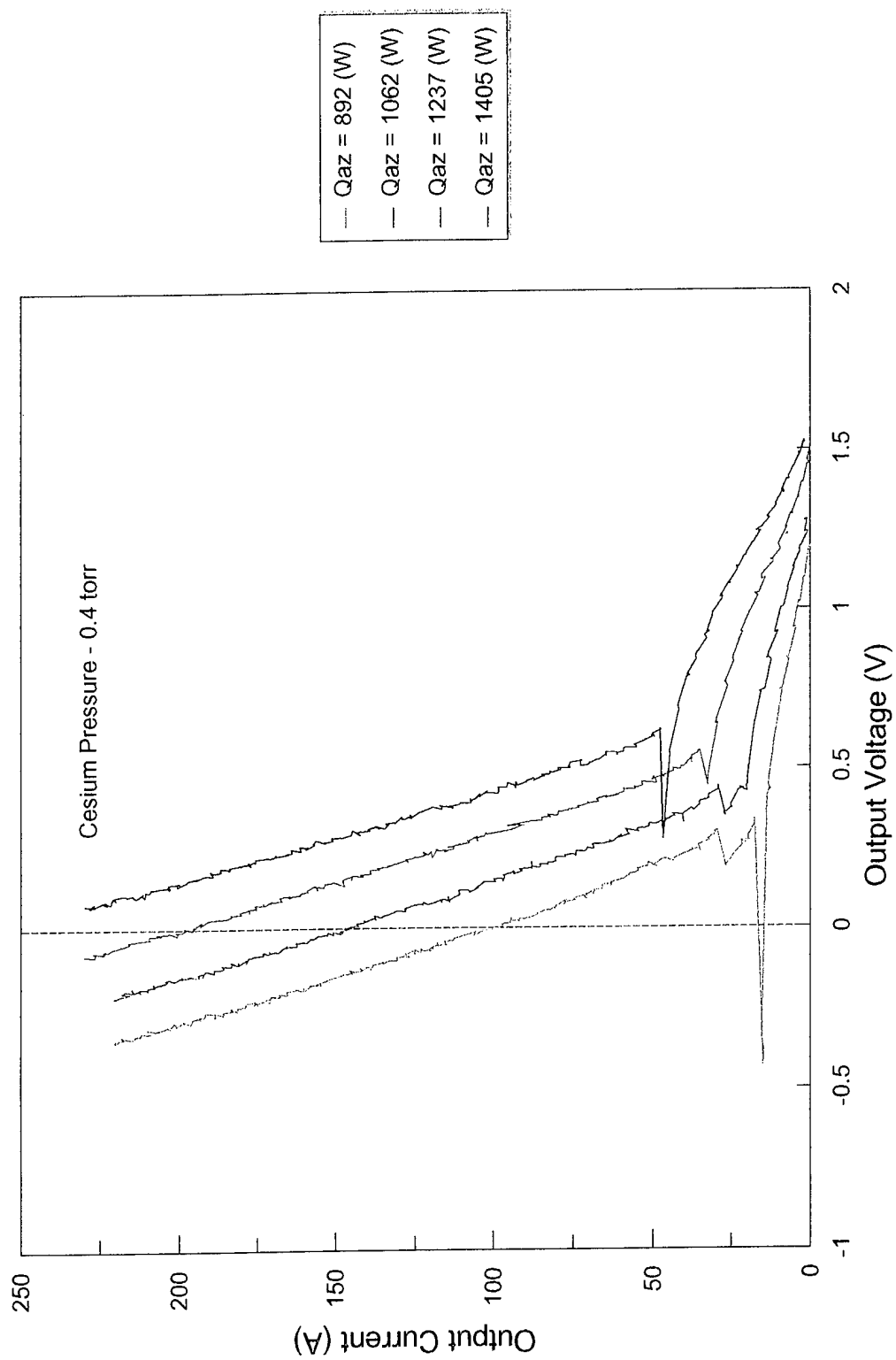


Figure 6-5. Optimum cesium pressure current-voltage sweeps.

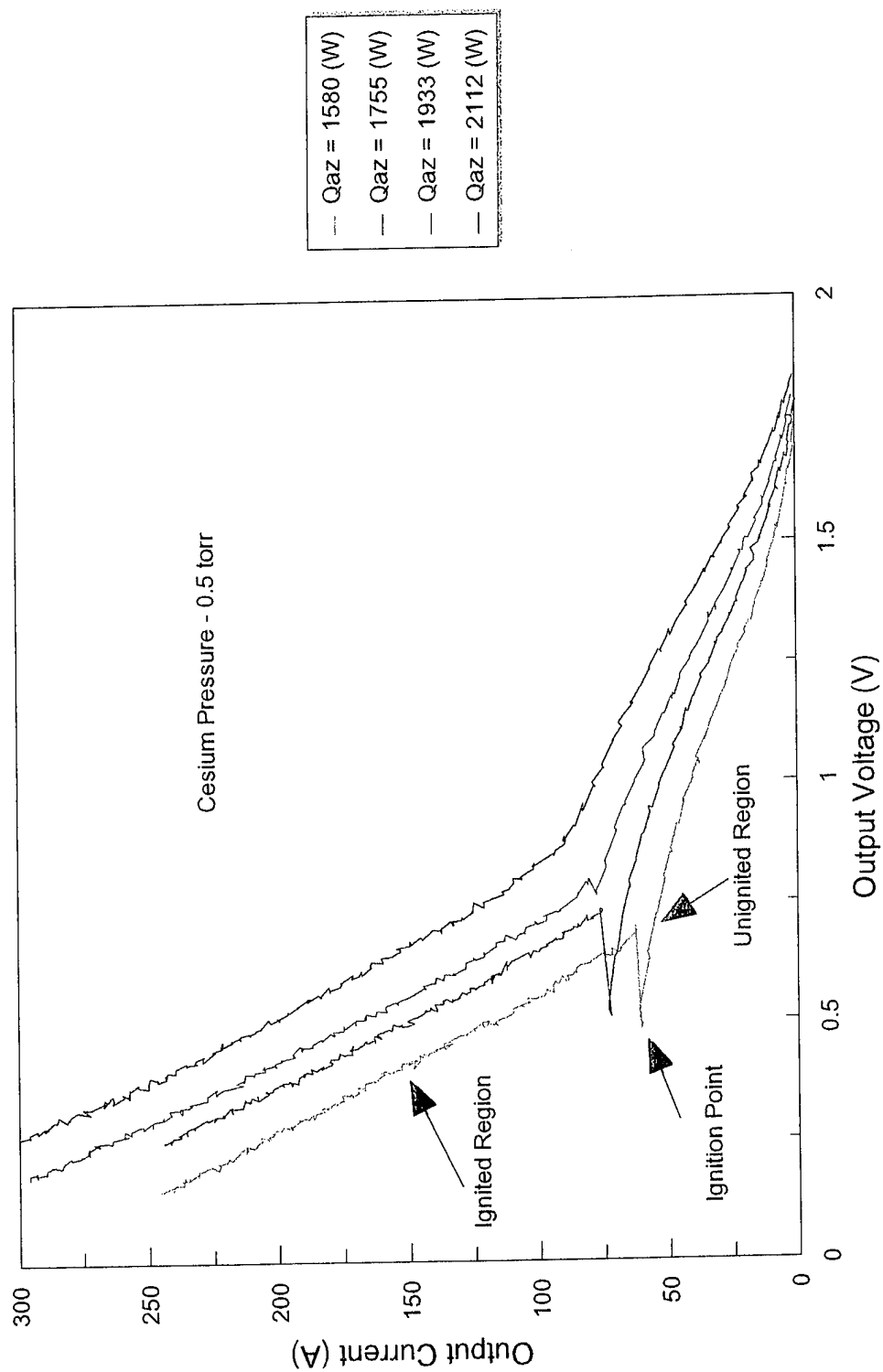


Figure 6-6. Optimum cesium pressure current-voltage sweeps.

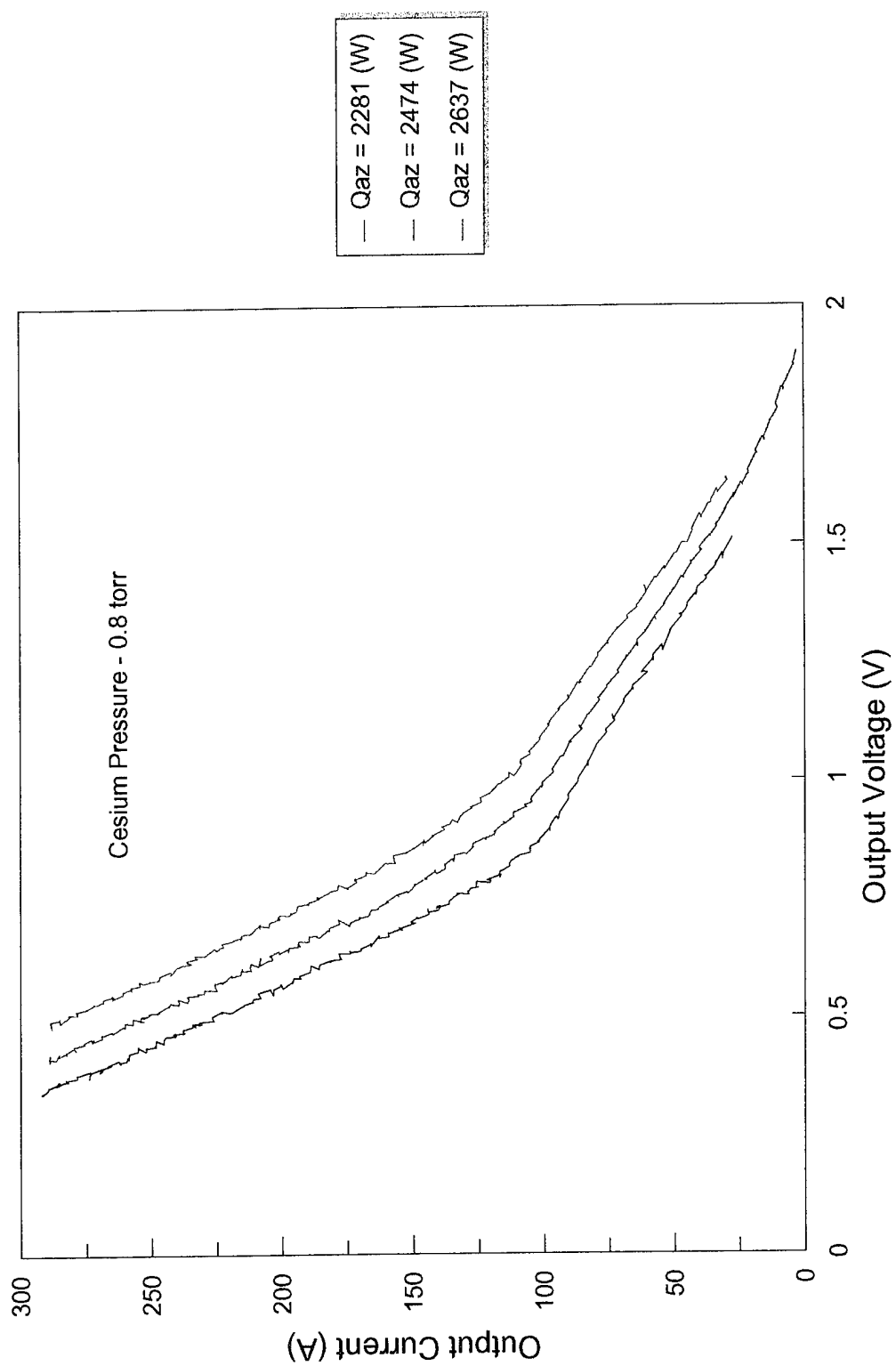


Figure 6-7. Optimum cesium pressure current-voltage sweeps.

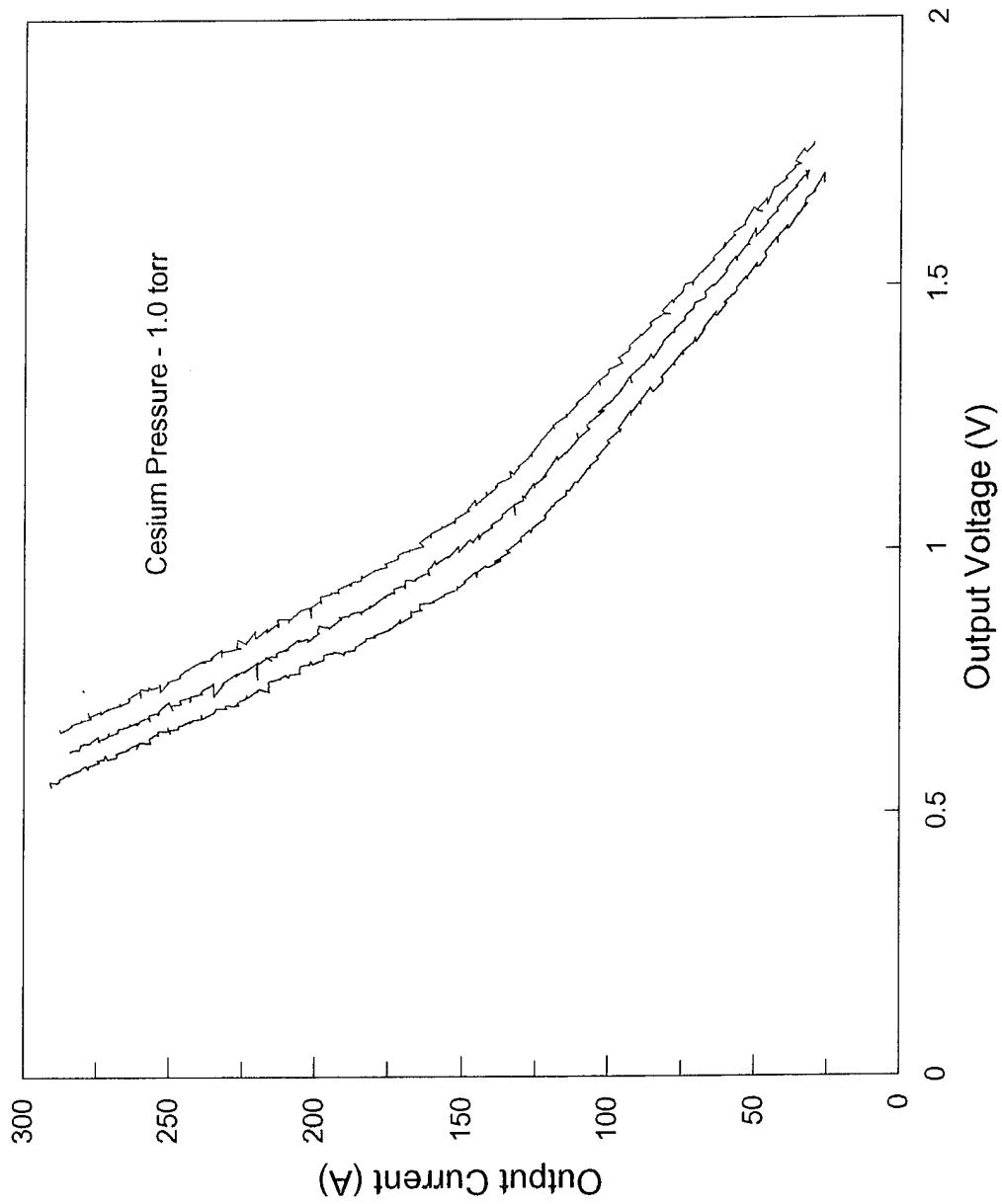


Figure 6-8. Optimum cesium pressure current-voltage sweeps.

ignited back to unignited operation, a voltage step does not transpire as it does in the upsweep when the plasma ignites (volume ionization of the plasma begins).

A major concern of this work was to evaluate TFE output in the unignited mode of operation so upsweeps at all power levels were used because the unignited region may be displayed on the plot of the upsweep.

Another characteristic attributable to downsweeps in the TFE test stand is that they are always lower in current and voltage than the corresponding upsweep. This results from the relatively long duration required to complete an upsweep. The time involved in the upsweep affects electron cooling. Electron cooling of the emitter is caused by the energy flux associated with electrons flowing from the emitter into the IEG (Anonymous, 1971). The longer an upsweep takes, the more electron cooling transpires. As output current increases this effect is compounded.

D. TFE OPERATING POINT

The choice of the operating point of a TFE at a given power and cesium pressure is based on output voltage and current desired. Since the electrical power producing section of TOPAZ-II is connected in series, all the TFEs operate at the same current, thus desired output current is a criterion for selecting the TFE's operating point. Bus voltage is a limiting parameter for any space electrical power system.

Figures 6-9 through 6-12 illustrate how electrical power output varies with current. The graphs reflect operation at optimum cesium pressures as determined previously. These curves can be used to aid in selection of an operating point for the TFEs. As input power is increased, the value of current corresponding to the maximum output power of the TFE occurs at higher levels. At lower input power levels, the TFE electrical output is more sensitive to changes in operating current than at higher input power levels.

The pronounced dip in the curves at powers below 2112W active zone power are representative of ignition. The dips in the current curves at higher power levels appear to be ignition points, but the I-V sweeps do not substantiate this observation.

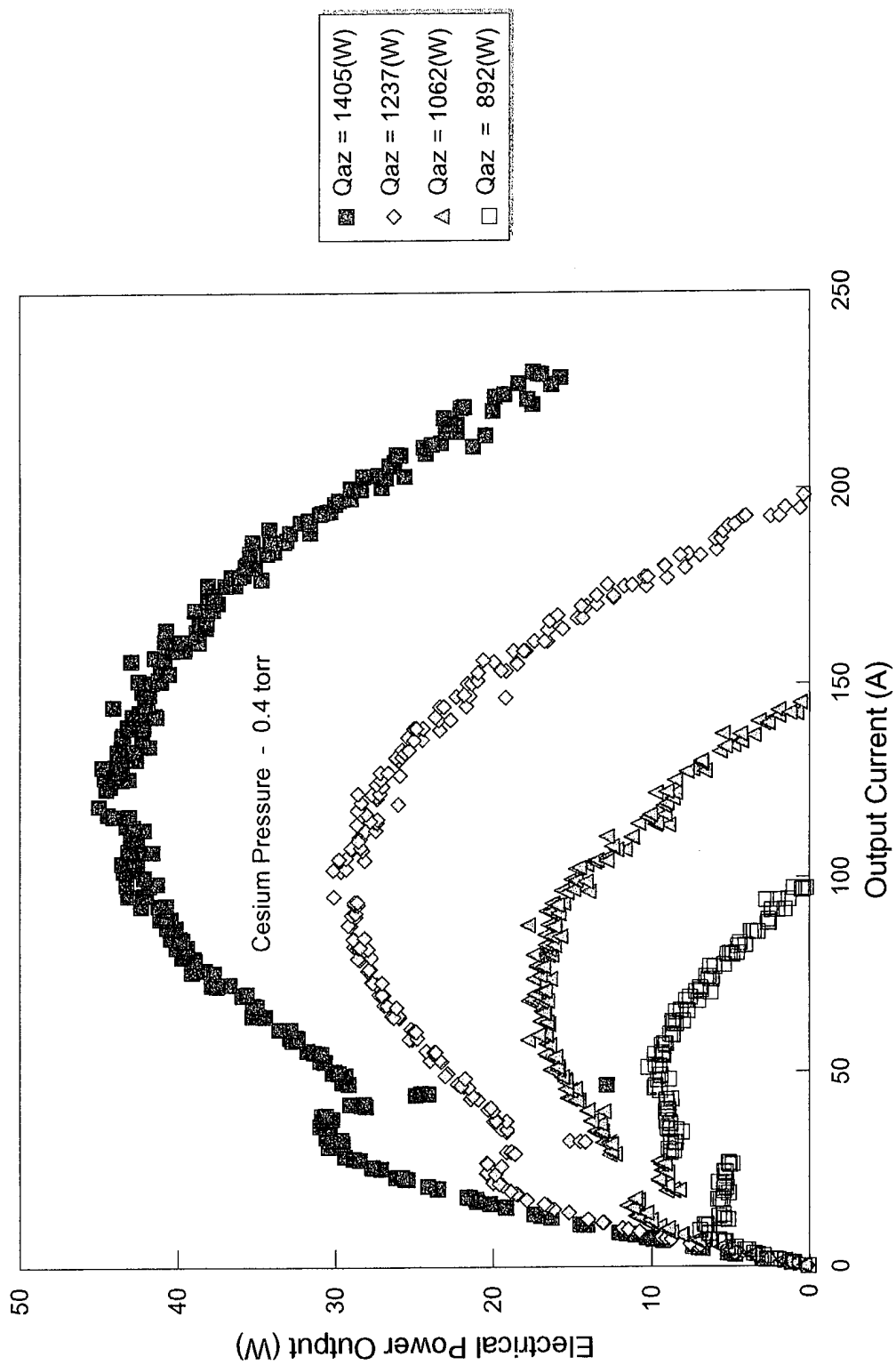


Figure 6-9. Electrical output power variation with current.

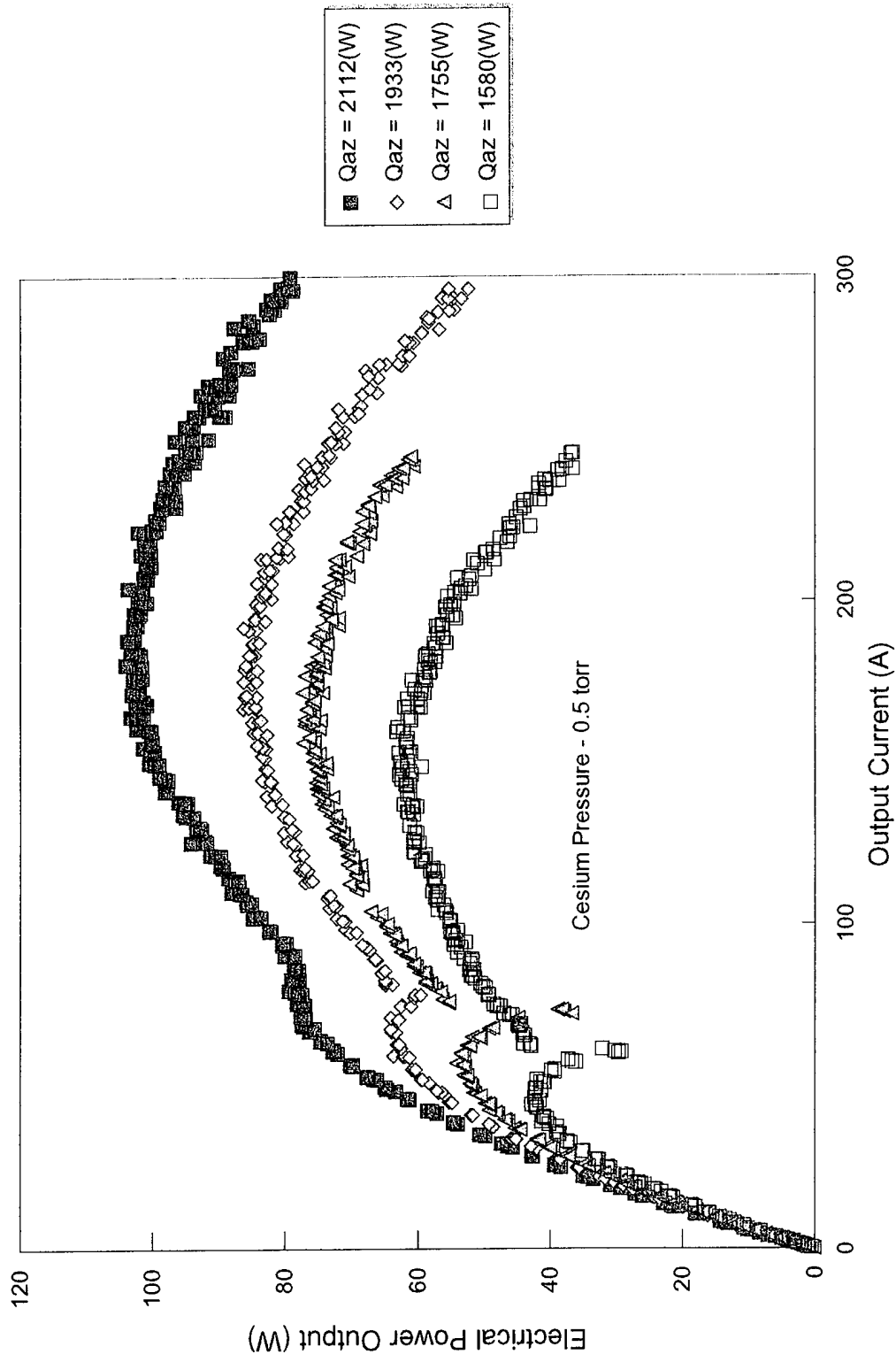


Figure 6-10. Electrical output power variation with current.

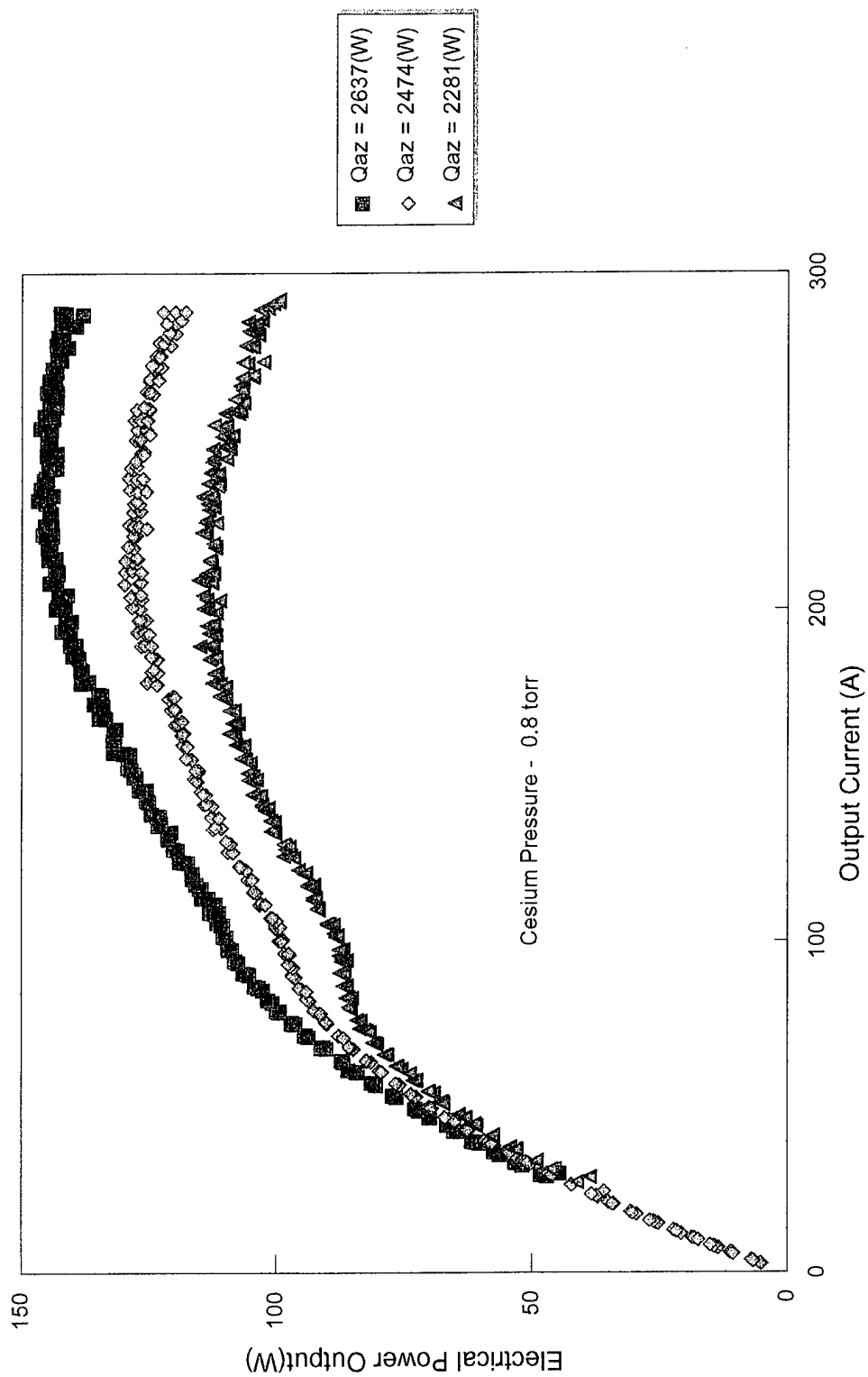


Figure 6-11. Electrical output power variation with current.

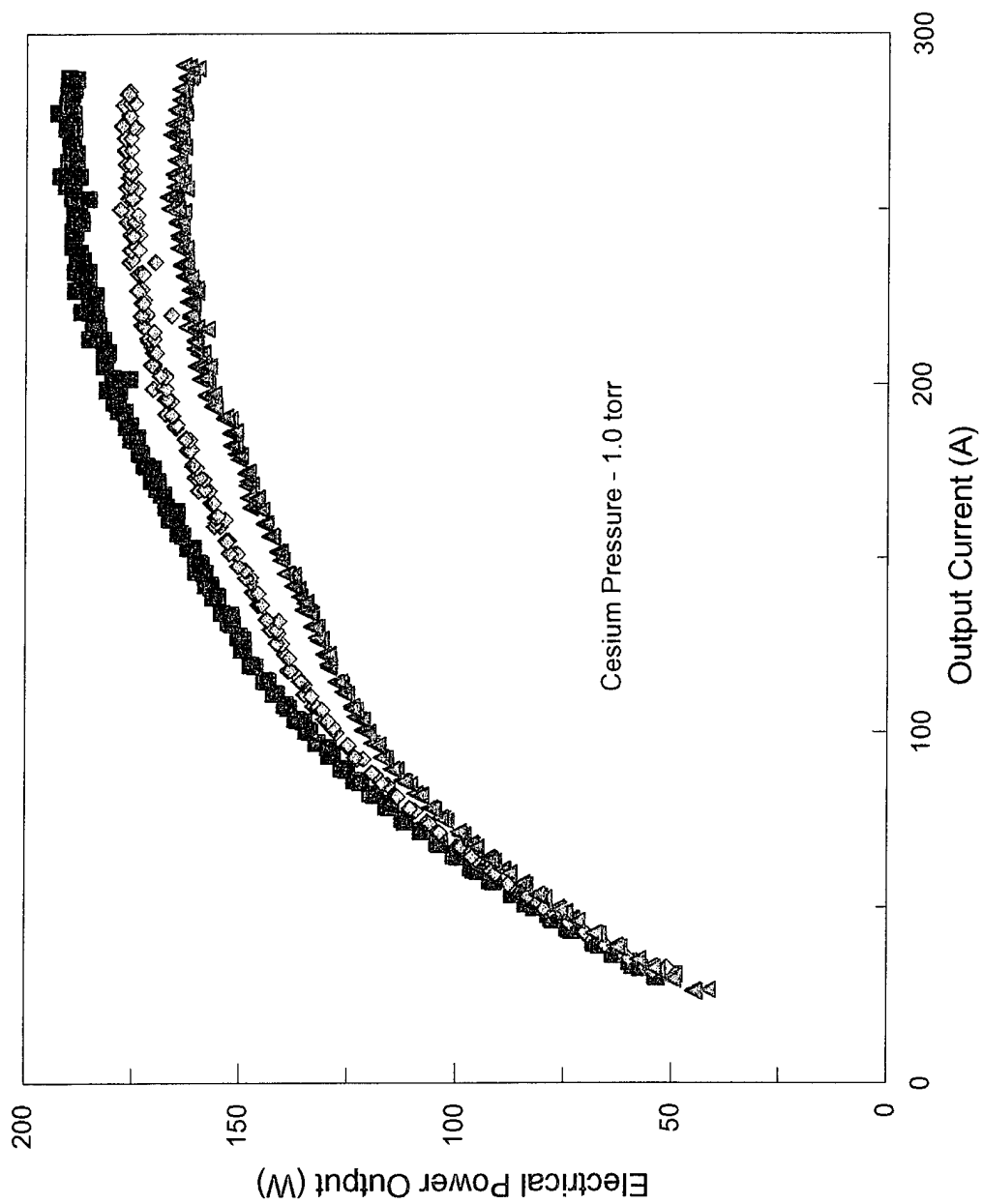


Figure 6-12. Electrical output power variation with current.

The presence of the small dip in the current curves above 2112 W results in an ambiguity between the I-V curves (Figures 6-6 and 6-7) and current curves (Figures 6-10 and 6-11) that cannot be resolved with the collected data (if resolution of this situation is desired it can be resolved at the TIP lab facilities). It is possible to set up an oscilloscope that gives an almost instantaneous image of the I-V curve. Conditions can be closely matched to the initial experimental conditions and the oscilloscope measurement may resolve the issue.

Consideration must be given to the load resistance and power distribution when choosing an operating point for the TFEs. At the very low operating voltages of the TFEs, high currents coupled with small load resistances can quickly cause unacceptable output voltage losses.

E. TEST STAND RESULTS APPLIED TO THE REACTOR SYSTEM

Results from the single TFE test stand indicate that useful power for the reactor system may be generated at substantially lower thermal input powers than the nominal 3.11 kWt presently used for reactor operations. Comparing the data from the test stand to the reactor system is not a straightforward process. The interaction between the TFEs in the reactor system and the difference in thermal losses of TFEs in the reactor is difficult to determine.

Thermal input power as low as 1.58 kWt yields 40 W of electrical power in the single TFE test stand at 0.8 V and 50 A (see Figure 6-6). This operating point occurs in the unignited region of thermionic emission. If the 34 electrical power generating TFEs were all at 1.58 kWt thermal input and 0.5 torr cesium pressure, the reactor could generate 1.36 kWe (kilowatt-electric) at 28 volts. As discussed previously, the uneven radial power distribution would preclude this ideal case.

Given a nominal reactor thermal input power per TFE (P_m) in the reactor, the relative power densities in the reactor vary from $1.19P_m$ at the center of the reactor to $0.89P_m$ near the outer ring of the reactor as shown in Figure 6-13.

Using the relative power densities from Figure 6-13, the previous analysis may be modified to account for power density differences between TFEs in the TOPAZ-II reactor system.

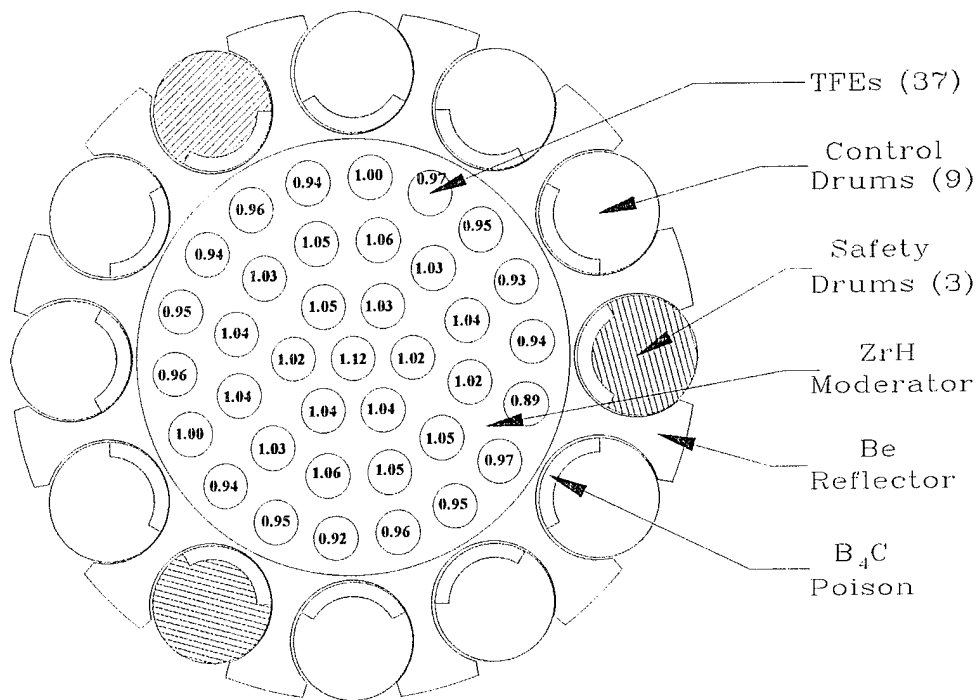


Figure 6-13. Relative TFE power densities in the TOPAZ-II reactor. After (Benke, 1994).

Considering the center TFE as the 0-ring and the other TFEs as the 1-ring, 2-ring and 3-ring respectively in Figure 6-13, the average electrical power per TFE in a ring can be found for a given thermal input power by averaging the relative power densities in the ring.

Assuming 1.58 kWt yields 40 We (watts-electrical), see Figure 6-6, the average electrical output for the TFE rings in the reactor is as follows:

$$0\text{-ring} = 44.8 \text{ We}$$

$$1\text{-ring} = 41.3 \text{ We}$$

$$2\text{-ring} = 41.7 \text{ We}$$

$$3\text{-ring} = 38.0 \text{ We}$$

Electrical output power for the reactor, P_{out} , can now be calculated as,

$$P_{\text{out}} = [44.8 + 6(41.3) + 12(41.7) + 15(38.0)] = \underline{1.36 \text{ kWe}}$$

Note that the 3-ring used 15 TFEs in the calculation for P_{out} because 3 of the 18 TFEs in the outer ring are connected in parallel and power the electromagnetic NaK coolant pump. Output voltages for the TFEs in this case vary from 0.76 V to 0.90 V producing approximately 27 V total output voltage.

Recall that the previous estimate, based solely on the output of the single TFE in the test stand, was 1.36 kWe at 28 V for the reactor system. This shows that the power density distribution is relatively constant for the reactor system. The greatest variation from nominal power density is 12%, and most of the TFEs range from 3% to 6%.

An assumption is made that the 0-ring TFE is operating at a thermal input power 12% greater than the nominal 1.58 kWt input power. This corresponds to 1.77 kWt input power to the 0-ring TFE. Since this is the highest TFE output power in the core, if the 0-ring TFE is operating in the unignited region all the other TFEs in the reactor will be also. Referring to the 1.755 kWt curve in Figure 6-6, the 50 A operating point occurs in the unignited region. As a first approximation, these results indicate that the TOPAZ-II reactor system can generate useful power with all TFEs in the unignited region at low current.

To more accurately determine TOPAZ-II reactor performance at the low power levels investigated in this thesis, actual system tests on the reactor are necessary. A low

power test of the reactor system was conducted in April of 1994 at the TIP facility. The purpose of this test was to investigate the low thermal power region of operation, the so called "housekeeping" mode, to determine if this mode of operation could provide enough power for necessary communications and control functions of a spacecraft. (Taylor, 1995).

The reactor was started up and operated at 75 to 95 kWt input power for several days. These power levels are not active zone power levels, but power to the electrical TISA heaters. Cesium pressure was optimized at various power levels over the 75 to 95 kWt input power range. Cesium pressure was set at the average value of the optimized pressures, 0.6 torr, to simulate space conditions. TOPAZ-II is designed so that once cesium pressure is set on orbit it cannot be changed. Several days after operation in this mode power level was reduced with the intention of taking current-voltage comparisons at 70, 65, 60, 55, 50 and 45 kWt input power. (Taylor, 1995)

The radiator outlet temperature was to be maintained above 648 K during the experiment. This limitation is necessary to ensure proper operation of the cesium supply system. If cesium is not maintained in its normal range, 648 K to 873 K, the cesium pressure set on the system will not be the same in the IEGs of the system TFEs. Also, condensation and flashing to vapor in the cesium system piping may cause instabilities that result in fluctuations of the reactor's electrical output. The 648 K cesium temperature limit was reached at a TISA heater power level of 71.6 kWt. This corresponds to an active zone power of 63 kW. After reaching this limit the reactor was successfully returned to the nominal thermal input power range. (Taylor, 1995)

The active zone input power levels and output electric power are plotted in Taylor, 1995. The resulting curve is nearly linear at the low input power end of the experiment. The curve was extrapolated to give an estimated electrical output for lower thermal power than was attainable due to the cesium temperature limit. An electrical output power level of 1 kWe was chosen as a baseline for the "housekeeping" mode. This power level allowed for 300 We for the reactor control unit, 200 We for the NaK coolant

electromagnetic pump and 500 We for command, communications and other spacecraft system loads. (Taylor, 1995)

The extrapolated curve indicated that the active zone thermal power input required for a 1 kWe output would be 58 kWt (Taylor, 1995). The previous example for the single TFE test stand data indicated that 1.58 kWt input power produced 40 We output power at an operating current of 50 A. If all 37 TFEs in the reactor, including the 3 pump TFEs, were operating at this input power, the total input power level would be 58.5 kWt. The expected output for the reactor system based on the previous approximations however, would be 1.48 kWe. This is a 48 % increase over the extrapolated value determined in the April, 1995 reactor system low power tests.

This large difference may be caused by losses in the electrical output from unequal load resistances between the TFE test stand and the reactor system. Further testing of the reactor system and comparison with the data presented in this thesis may be used to find a relationship between the experimental results of the test stand and the reactor system.

VII. SUMMARY CONCLUSIONS AND RECOMMENDATIONS

The TOPAZ-II single TFE test stand is an important tool for understanding the operation of a TOPAZ-II TFE. Output of the TOPAZ-II reactor system does not provide information on the performance of individual TFEs making the TFE test stand invaluable in understanding the thermionic process that is occurring in the TOPAZ-II reactor. A thermal model of the test stand and an analysis of the electrical characteristics of a TFE in the test stand over a wide operating range enhances this understanding.

Benke's thermal model led to the development of extensive cross-sectional diagrams of the TFE test stand. These cross-sections represent an improvement to the Russian diagrams previously available to TIP (see Appendix A). These new drawings are presently used by TIP personnel and have been verified as correct by the Russian engineers who provided the TFE test stand. The thermal model has been validated with the University of New Mexico Space Nuclear Power Institute's computer code (TITAM). This model provides the temperature profile across the thermionic working section of the test stand from the TFE's collector to the heat removing water channel. The emitter temperature is not provided by this model because the complex plasma physics in the IEG (that varies depending on which mode of operation the TFE is in) has not been analyzed.

Optimum cesium pressures change depending on the thermal input power level. As thermal input power is increased, optimum cesium pressure is also increased. Current-voltage (I-V) sweeps and current versus optimum electrical output power curves are provided in Chapter 6. There is an ambiguity in these curves regarding the ignition point of the converter. This ambiguity arises from the data acquisition system that takes data every three seconds on average. Ignition (commencement of volume ionization in the TFE) occurs rapidly and three second intervals for data acquisition can miss this event. I-V sweeps are generated by changing the load resistance to the TFE. If the load is varied rapidly, a more accurate representation of the I-V sweep can be obtained by using an

oscilloscope. This would give a better representation of the ignition point. A complete set of upsweeps taken during the experiment is given in Appendix B.

Electrical characteristics of the single TFE showed that useful output power can be generated at power levels considerably lower than the present operating power for TOPAZ-II TFEs. Table 7-1 indicates the efficiencies of a TOPAZ-II TFE over the thermal input powers investigated. Efficiency increases with higher thermal input power and starts to level off to a maximum of about 7 %. Efficiencies notwithstanding, once the reactor is fueled, operation at lower input power presents some distinct advantages.

Active Zone Power (W)	Output Power (W)	Efficiency (%)
892	10.23	1.15
1,062	17.8	1.68
1,237	30.13	2.44
1,405	45	3.2
1,580	63.25	4.01
1,755	77.28	4.4
1,933	86.26	4.46
2,112	103.97	4.92
2,281	115.44	5.06
2,474	129.87	5.25
2,637	146.75	5.57
2,813	167.06	5.94
2,999	178.16	5.94
3,162	192.46	6.09

Table 7-1. Maximum TFE efficiencies.

One of the limiting factors in the lifetime of a TOPAZ-II space nuclear power system is fuel swelling. Fuel swelling of too great an extent could cause the emitter to physically touch the collector causing a TFE to short out and no longer provide output. Lower power operation limits fuel swelling and would alleviate this concern. Another

advantage of low power operations is lower temperatures in the core. These lower temperatures would limit thermal stresses on reactor subsystems and would reduce the infrared signature of the spacecraft.

Taylor (1995) discusses a low power experiment for the TOPAZ-II reactor system that indicates some limitations concerning operation at low powers. The radiator temperature must be maintained at greater than 648 K to prevent cesium from condensing in the supply lines. Condensation of cesium and subsequent flashing of cesium to vapor causes pressure changes that lead to output power fluctuations. This limit was reached during the experiment before the reactor thermal input power could be lowered to the target value needed to supply output of 1 kWe. (Taylor, 1995)

Another situation of concern is the electromagnetic (EM) NaK coolant pump current supply. Current to the EM pump is supplied by three TFEs in parallel when the system is operating in space. The low power experiment conducted on the TOPAZ-II system include a "makeup" current supply provided by an auxiliary system that provided a constant source to the EM pump. A more realistic test would be to raise reactor power to a level that provides ample power to the EM pump with its three TFEs, and then to lower reactor power to the point that the EM pump no longer provides adequate coolant flow. (Taylor, 1995)

Besides the previously discussed concerns with operation at lower powers, operation of the reactor system in the unignited mode presents another unique concern. The voltage transient that is experienced by the TFE in going from the unignited to ignited region of operation may cause damage to the thin stainless steel expansion bellows provided for thermal expansion of the TFE in the reactor core (Mulder and El-Genk, 1994). For this reason, normal operation of the TOPAZ-II system requires the system to be brought up to nominal operating temperature with helium in the IEG (this precludes volume ionization in the gap) and then to displace the helium with cesium vapor (Mulder and El-Genk, 1994). In this manner, there will not be a voltage transient in the TFE. It seems that this problem can be avoided by using the same method and then lowering

power until the TFE is in the unignited mode since the transient does not occur when this is done. However, once reactor power was raised again the transient would occur. A solution to this problem could be the ability to switch between helium and cesium vapor during operation.

The purpose of this research was to explore the usefulness of a TOPAZ-II TFE at low powers. Useful power is available in the ignited mode at low power levels and even at levels corresponding to unignited thermionic converter operations. Subsystem redesign would be needed to take advantage of this useful power. Specifically, subsystems include but are not restricted to, the coolant pumping system, electrical power distribution system and cesium supply system. The coolant pumping system is needed to provide adequate heating of the coolant to prevent freezing and the electrical power distribution system would need to be operable at various currents since the optimum load current varies with thermal input power level as shown in Chapter 6. The cesium supply system would have to be more dynamic to allow for various cesium pressures. Presently the cesium pressure is set when on orbit and cannot be changed. These changes cannot be applied to TOPAZ-II, but may be valuable for design of a new thermionic space nuclear power system.

Direct energy conversion methods are still being pursued and continue to be important energy transformation techniques for future systems. In addition to Rasor Associates Inc., ThermoElectron Corporation (TECO), founded in 1957 by Dr. George Hatsopolous, commercializes thermionic energy conversion technologies. Today, TECO is a Fortune 500 company, traded on the New York Stock Exchange with 1993 revenues of \$1.2B. While thermoelectric and thermionic energy conversion have not been directly commercialized they have provided the base for other technologies based on energy conversion, energy conservation and high temperature materials. Some of these technologies developed by TECO include, the left ventricular assist device (LVAD) that is a temporary device that a heart patient could use until a heart transplant could be performed, instruments to measure nitrogen oxides in car emissions, improved thermal

insulation for use in the high vacuum environment of space and thermoelectric cooling devices to cool diode lasers used in fiber optic communications. (Scoville and Masters, 1995)

Wright Laboratory's Aerospace Power Division at Wright Patterson Air Force Base, Ohio has demonstrated principal developments in single-cell TFE design, improved emitters, simplified passive cesium reservoirs, diamond film coated collector electrodes, dual gases in the IEG and a PC based space nuclear power system design code. Loral company has developed an out-of-core thermionic converter with an efficiency as high as 14%. (Donovan and Lamp, 1994)

The Russians are developing a 40 kWe space nuclear power system with a design lifetime of 10 years using an improved single-cell TFE. The system is called the "SPACE-R" reactor system and the TFE has passed preliminary hot vacuum tests and is prepared for power testing with electric heaters. (Nikolaev, et al. 1995)

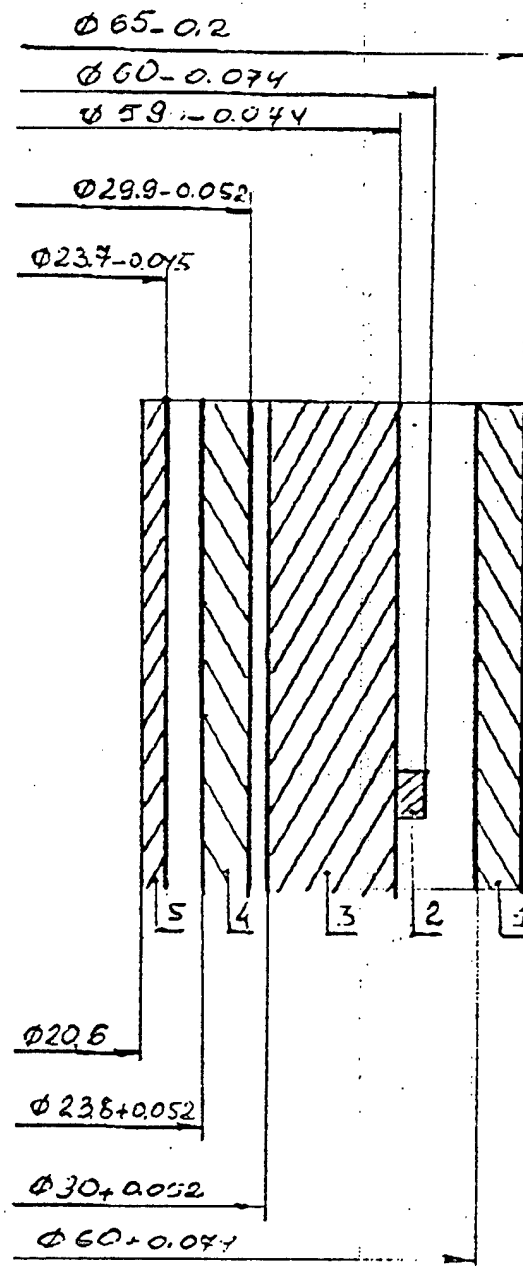
The complete elimination of space nuclear power systems technology in progress will hinder capabilities in planetary science. There are five concepts that illustrate the benefit to science research of high power sources in space ranging from 15 to 30 kWe. They are higher data rates (Mbps) to increase the quantity of science data, increased signal-to-noise ratios resulting in increased instrument sensitivity and better science, increased mission opportunities and flexibility and the use of science instruments that may only be practical when high power is available. (Harris, 1995)

Nuclear power in space is the only practical source for many space missions that are envisioned in the future. To stop all research in the area of space nuclear power will set the space program back considerably. Budget constraints that effect everybody are not conducive to continued efforts in the area of space nuclear power. Therefore, individuals concerned with the advancement of these technologies need to find ways to increase efficiency and productivity despite shrinking resources. The Topaz International Program is an example of how efforts in the area of space nuclear power should be approached. The program is a testament to international cooperation and represents a significant

savings in manufacturing and development costs to the U.S. The TOPAZ-II system is the only fully developed space nuclear power system and knowledge from its operation should have the widest dissemination possible to the space power community. TOPAZ-II provides unique opportunities for testing that companies in the U.S. should take complete advantage of to further space nuclear power systems knowledge for future uses.

APPENDIX A. TEST STAND RUSSIAN CROSS-SECTION

A Russian cross-section for the test stand is presented here to illustrate the need for development of detailed cross-sections as shown in Chapter 4. Figure 4-5 is a comparable axial cross-section created to aid in producing the thermal model that supports this work. A more precise drawing of the test stand working section was needed since thermal analysis is strongly dependent on material properties, component sizes and spacing between components.



- 1.-техл. Труба ;
- 2.-дистанционатор
тепловода ;
- 3.-тепловод из
меди ;
- 4.-несущая
труба ;
- 5.-коллекторный
пакет .

1. tube
2. heat conductor
spacer
3. copper heat
conductor
4. bearing tube
5. collector system

Рис 1. Расчетная схема системы теплоброса
с медным теплопроводом.

Fig. 1. Calculational diagram of thermal release system
with copper heat conductor

APPENDIX B. CURRENT-VOLTAGE SWEEPS

Current-voltage (I-V) upsweeps taken during the experiment are provided here beyond those presented as Figures 6-5 to 6-8. The sweeps are arranged by cesium pressure, starting with 0.4 torr and going to 1.5 torr at 0.1 torr increments. Although data were taken from 0.1 torr through 1.5 torr cesium pressure, the curves generated below 0.4 torr are not useful. This fact is illustrated in the cesium pressure optimization graph (Figure 6-2) in Chapter 6. The last two figures contain two curves each because I-V sweeps at cesium pressures of 1.4 and 1.5 torr were only done at the highest two power levels investigated. It was not necessary to run I-V sweeps at the lower power levels for these cesium pressures because the optimum pressure for those powers were already established at lower cesium pressures (see Figure 6-2).

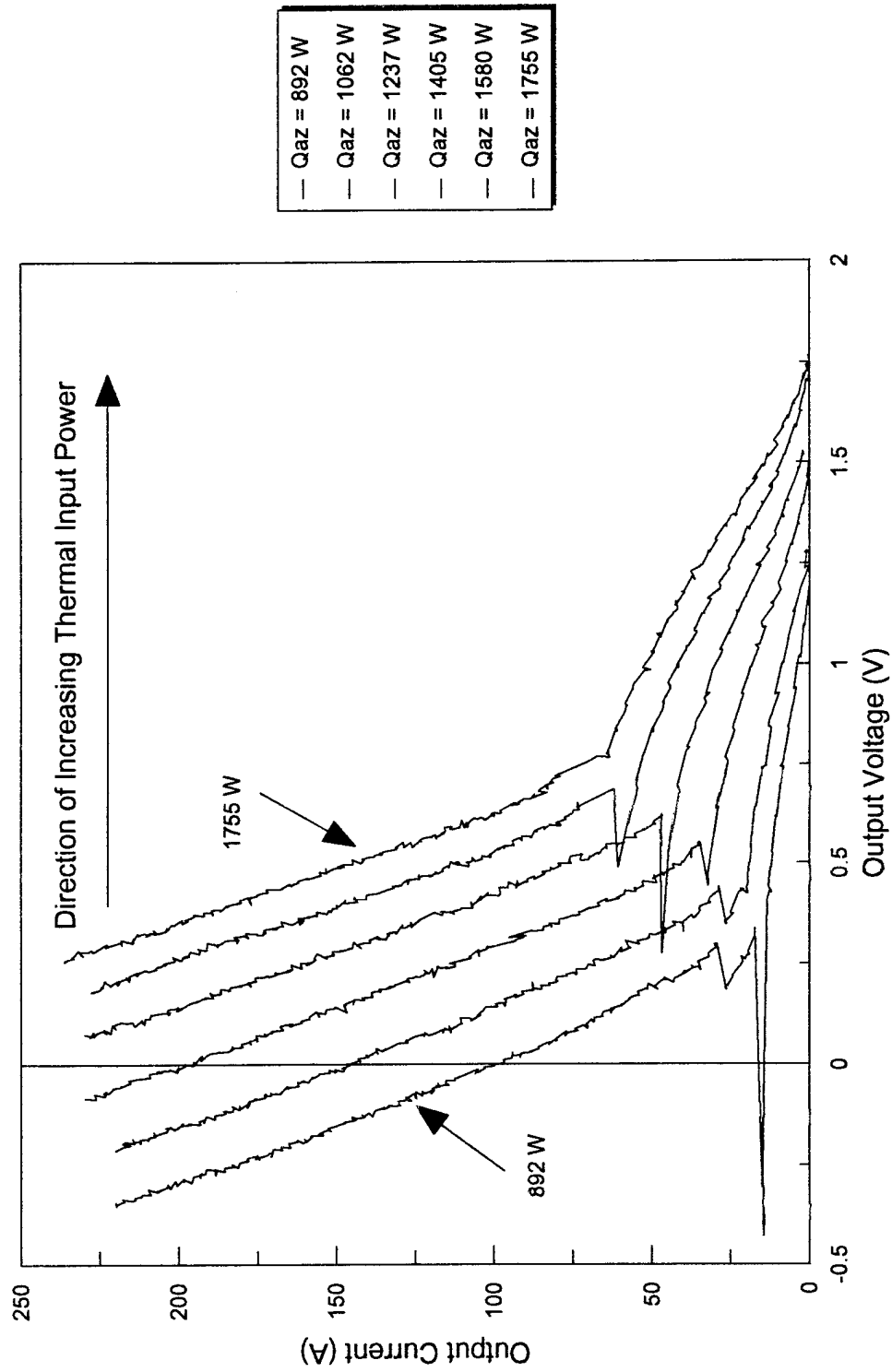
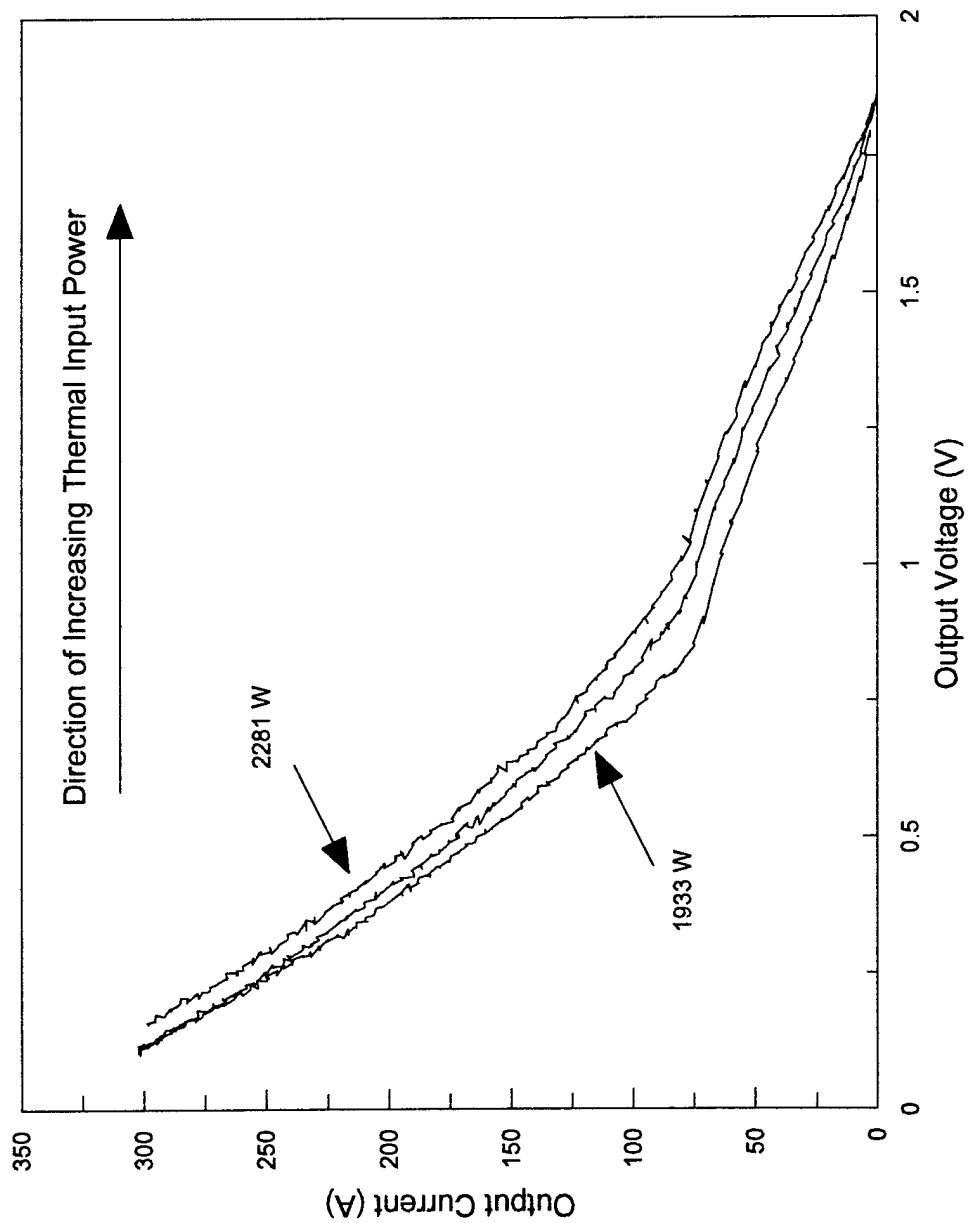


Figure B-1. Current-Voltage sweeps at 0.4 torr cesium pressure.



— Qaz = 1933 W
 — Qaz = 2112 W
 — Qaz = 2281 W

Figure B-2. Current-Voltage sweeps at 0.4 torr cesium pressure.

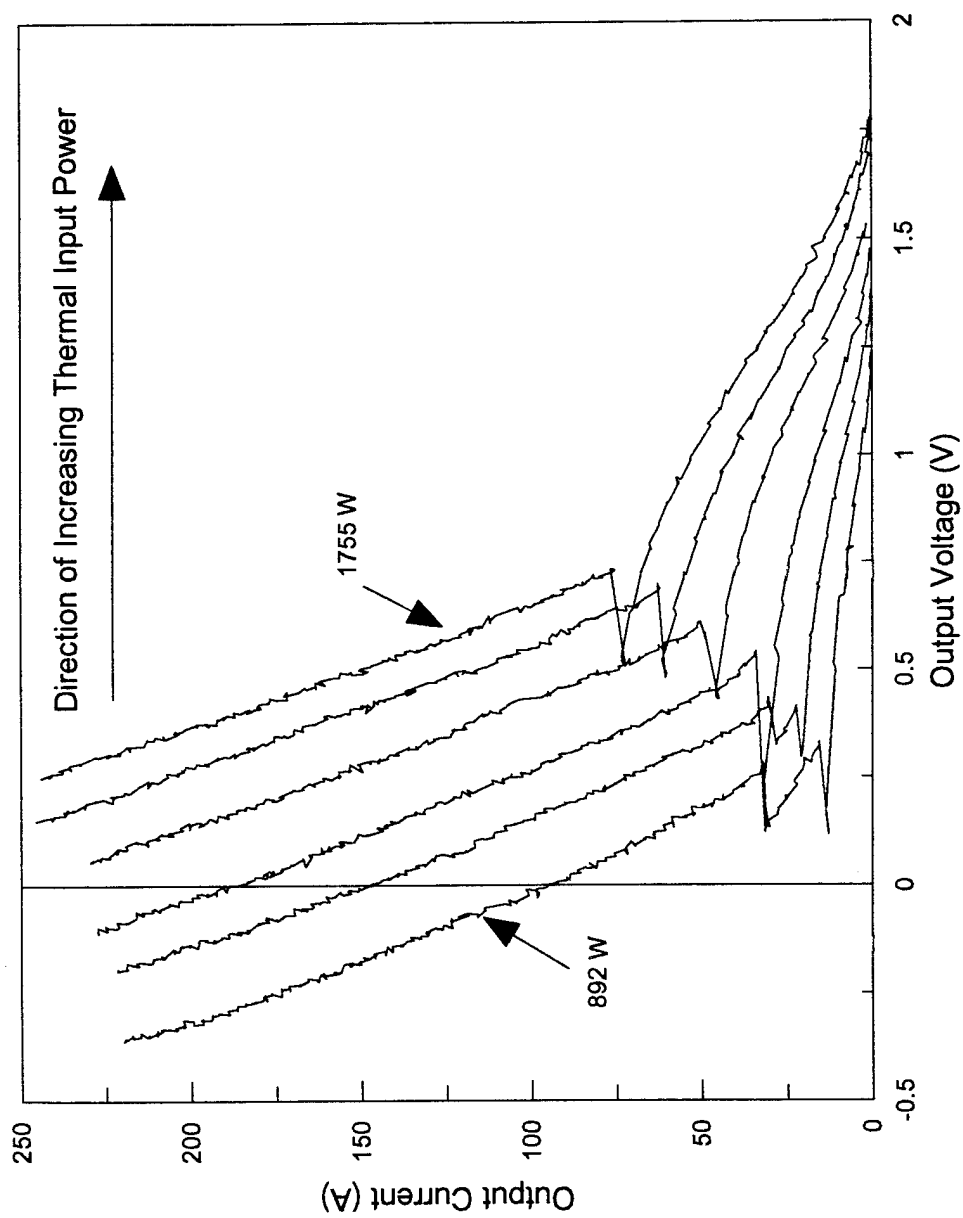


Figure B-3. Current-Voltage sweeps at 0.5 torr cesium pressure.

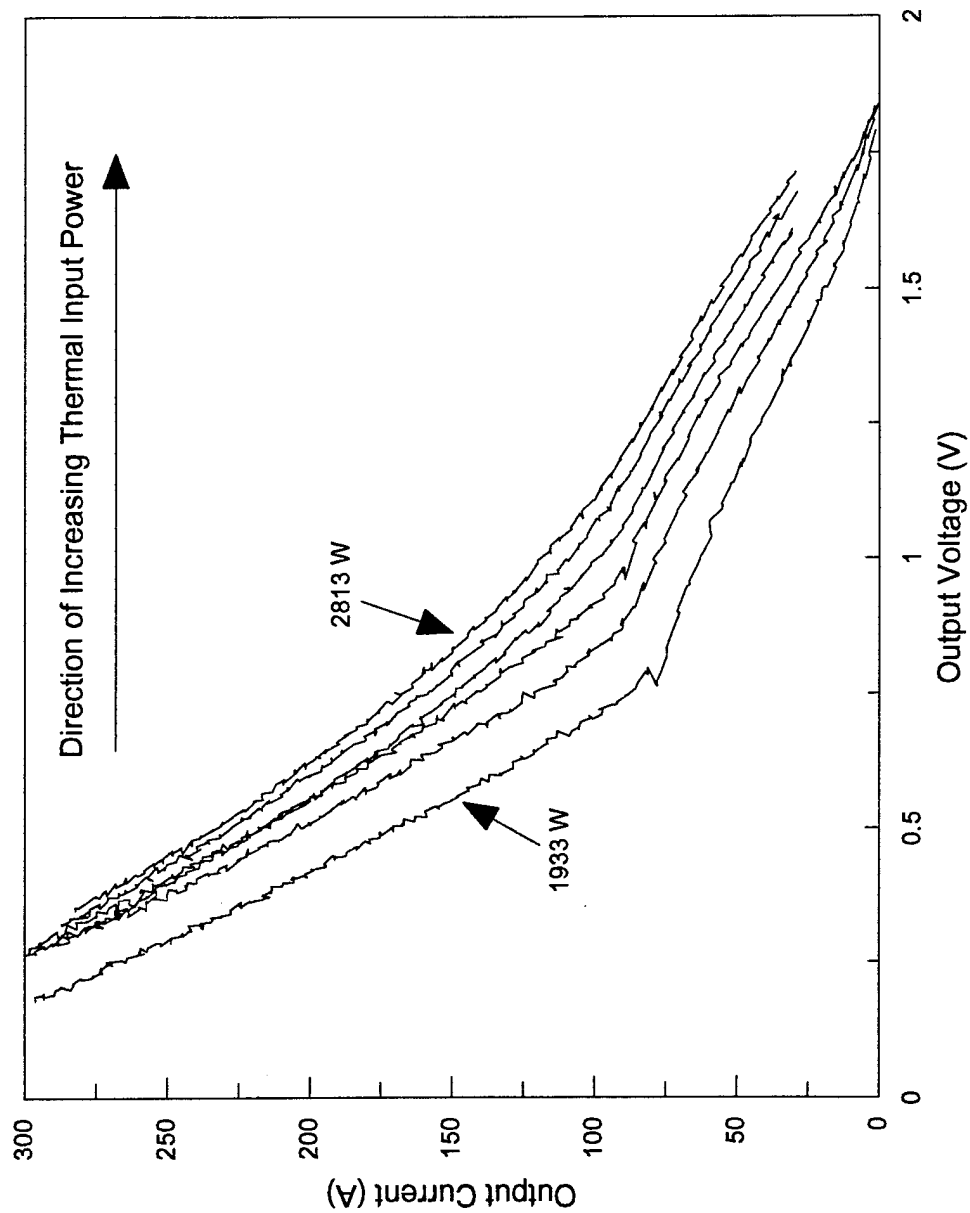


Figure B-4. Current-Voltage sweeps at 0.5 torr cesium pressure.

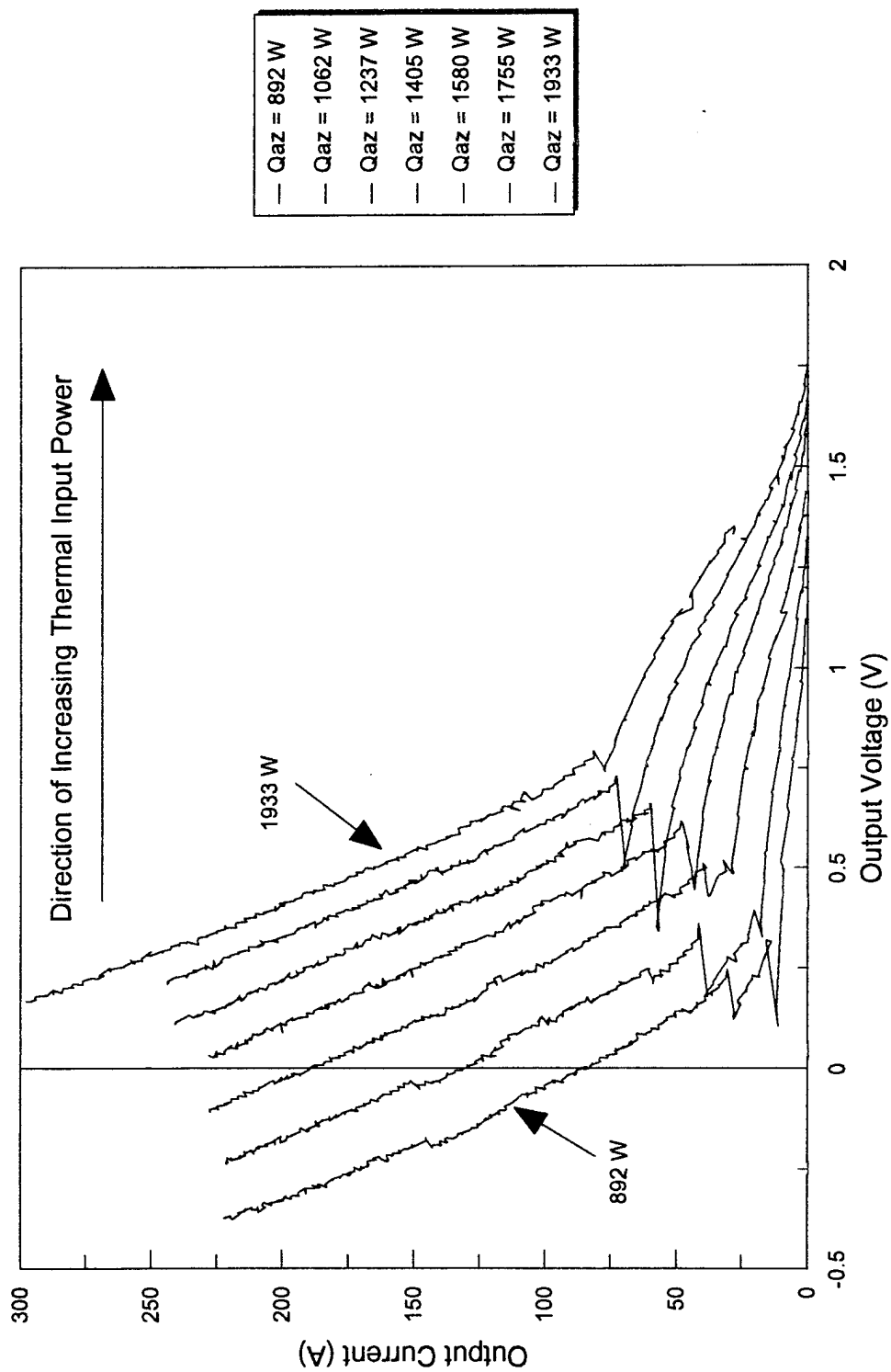


Figure B-5. Current-Voltage sweeps at 0.6 torr cesium pressure.

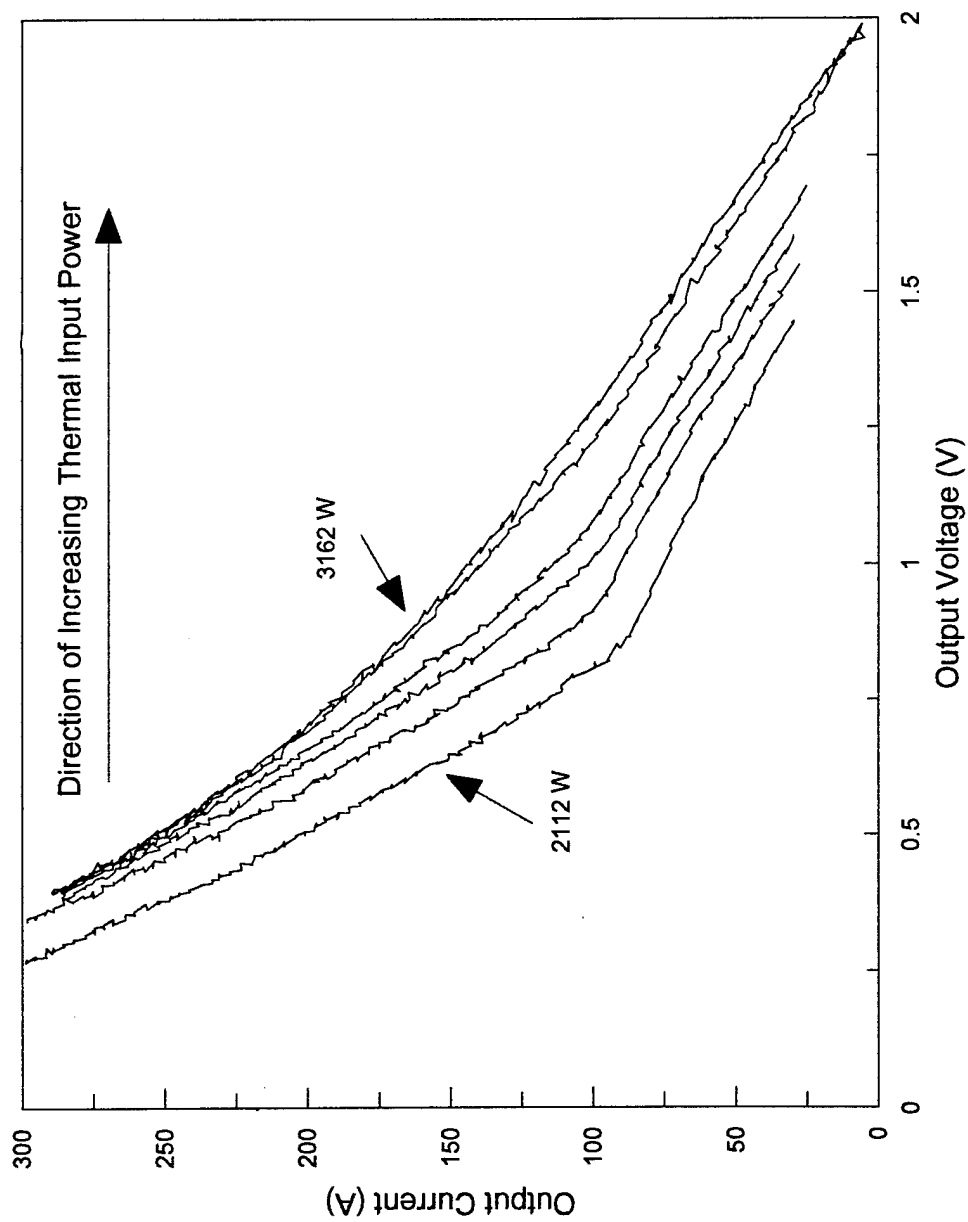


Figure B-6. Current-Voltage sweeps at 0.6 torr cesium pressure.

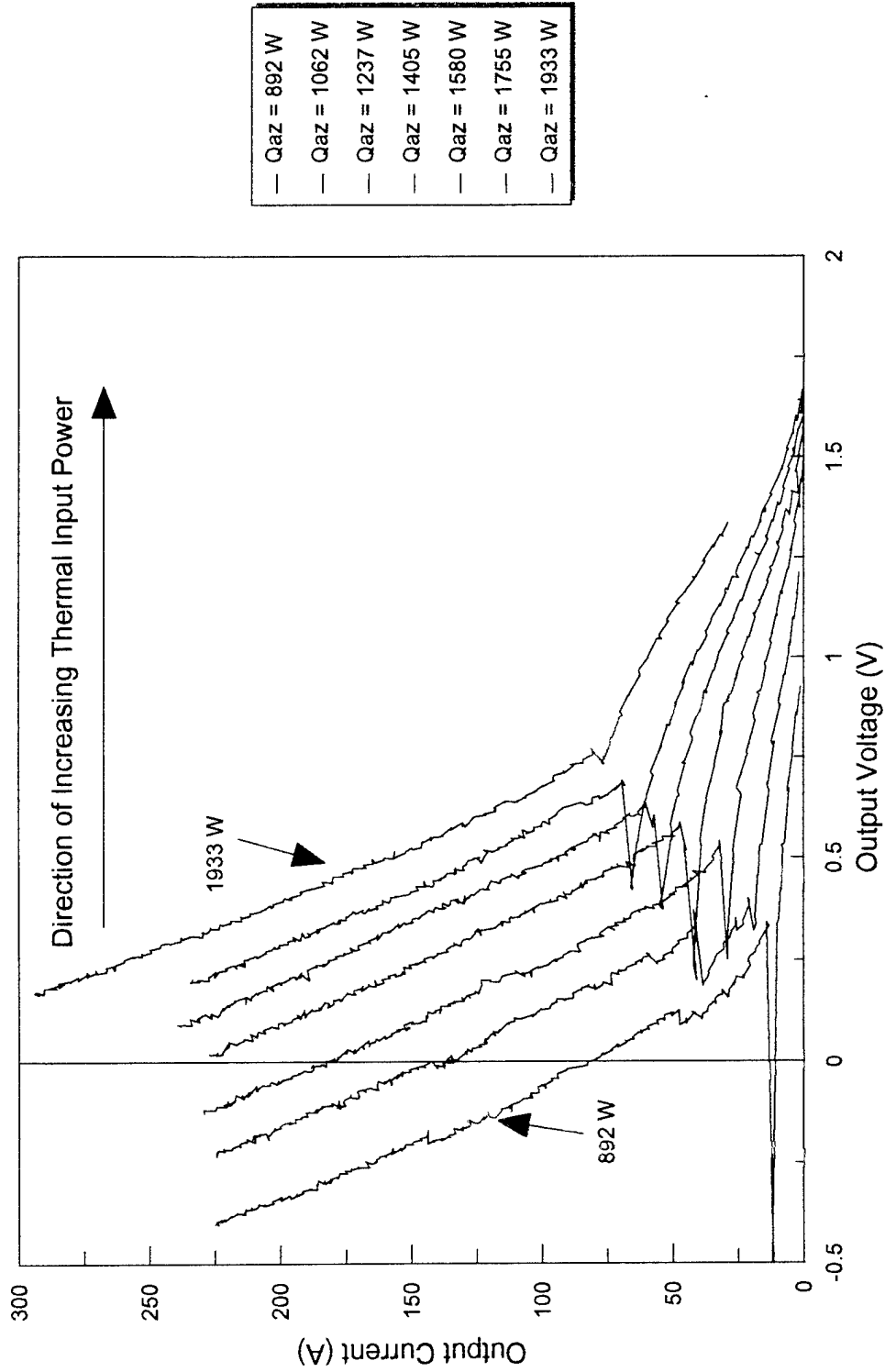


Figure B-7. Current-Voltage sweeps at 0.7 torr cesium pressure.

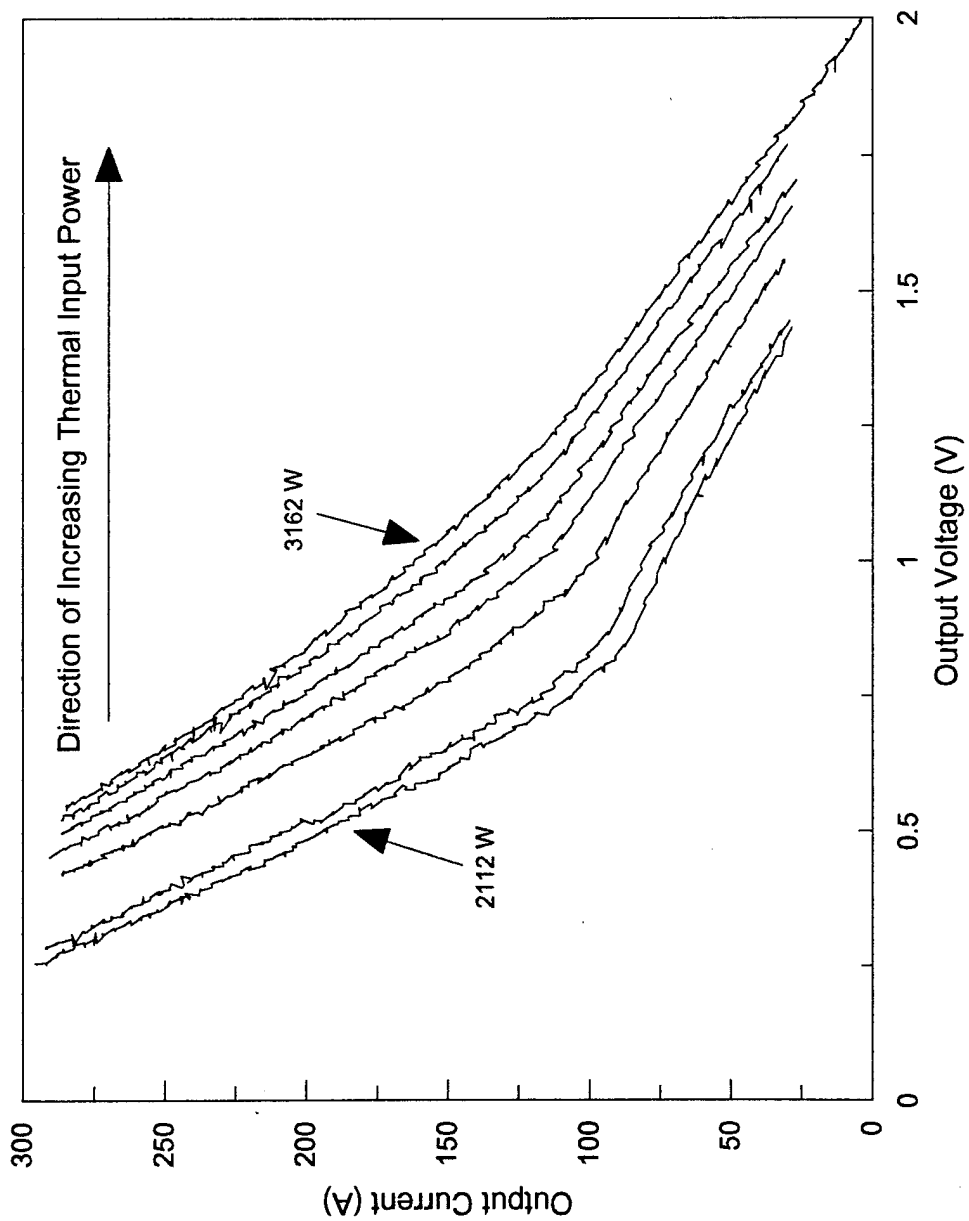


Figure B-8. Current-Voltage sweeps at 0.7 torr cesium pressure.

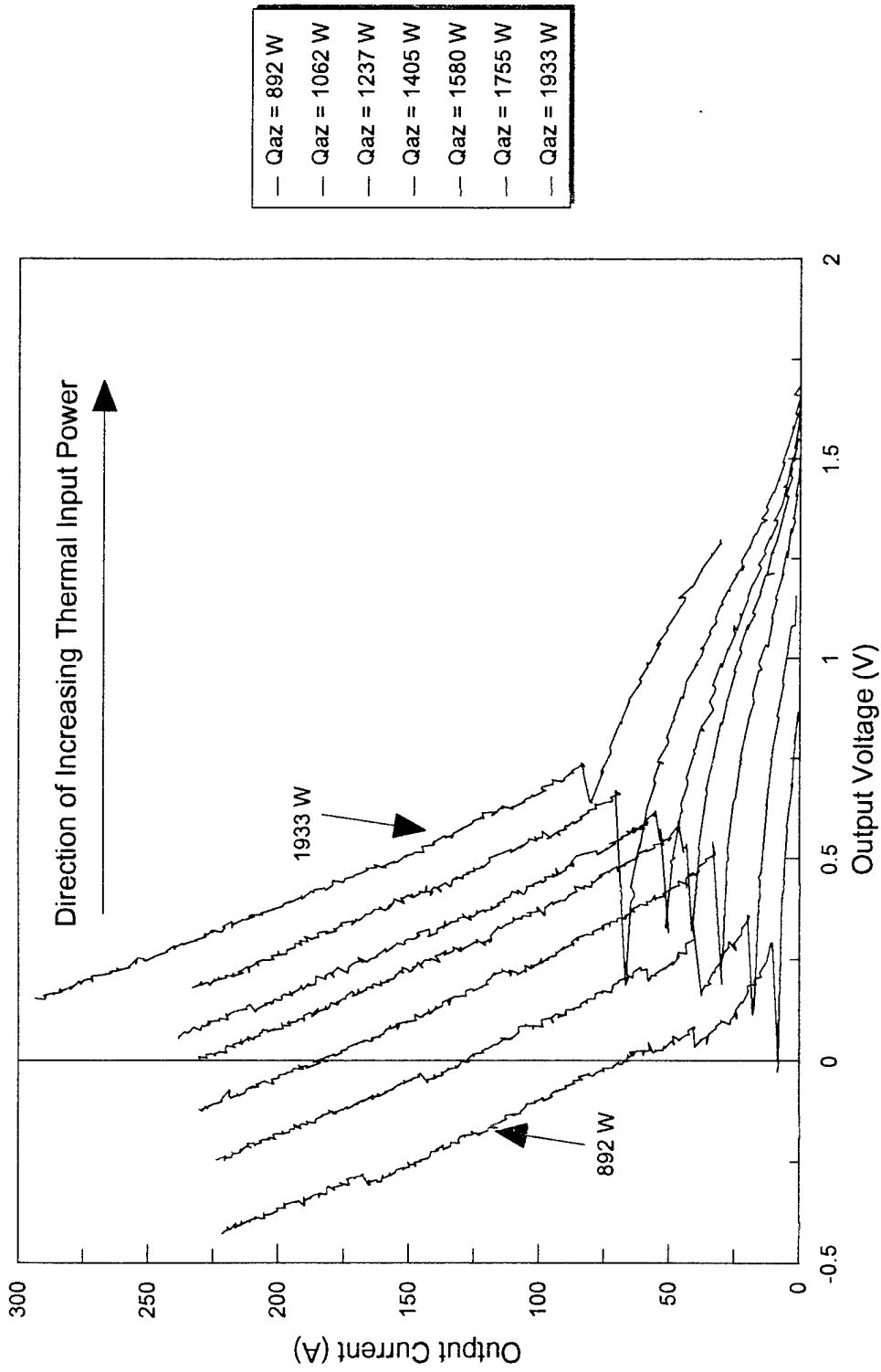


Figure B-9. Current-Voltage sweeps at 0.8 torr cesium pressure.

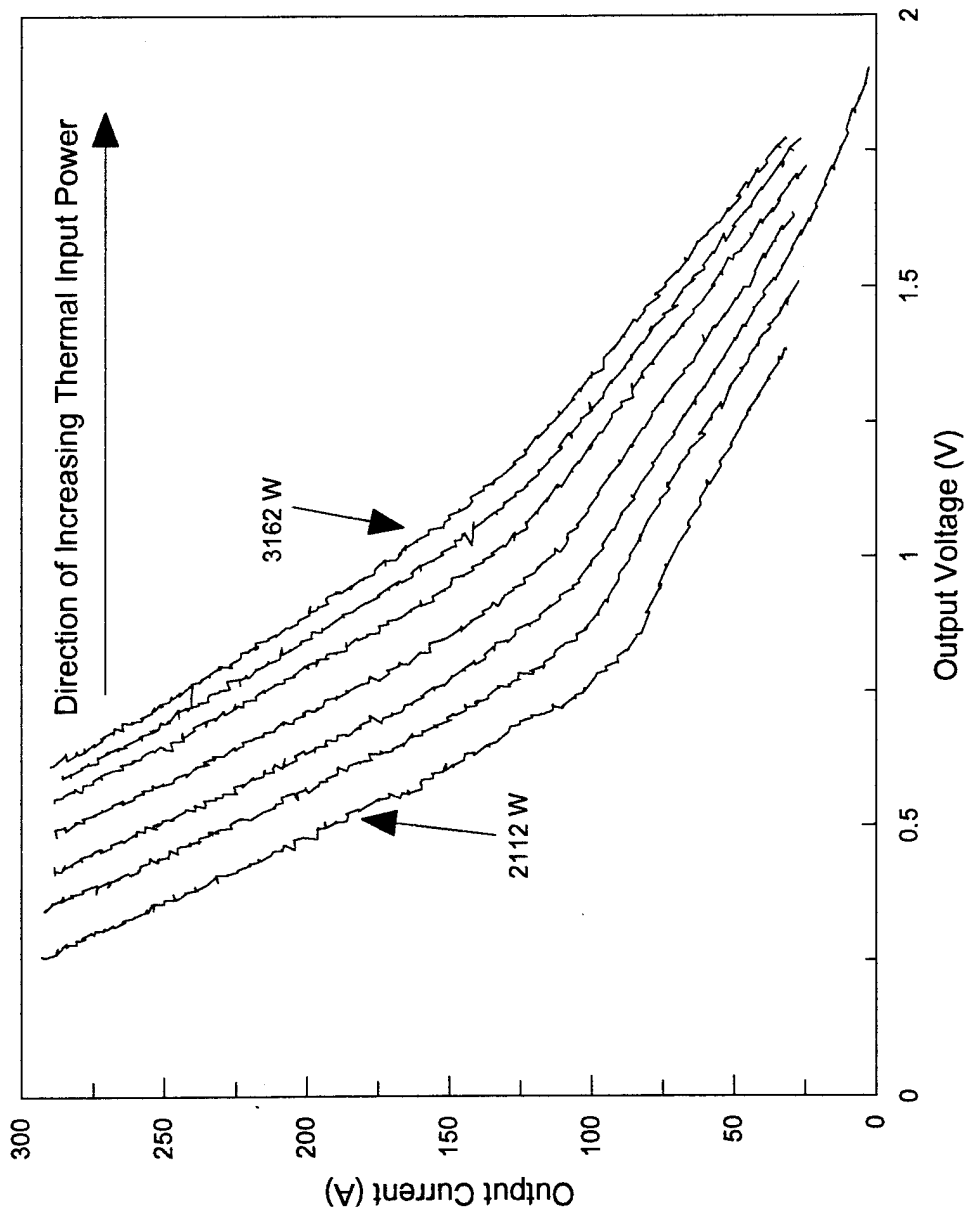


Figure B-10. Current-Voltage sweeps at 0.8 torr cesium pressure.

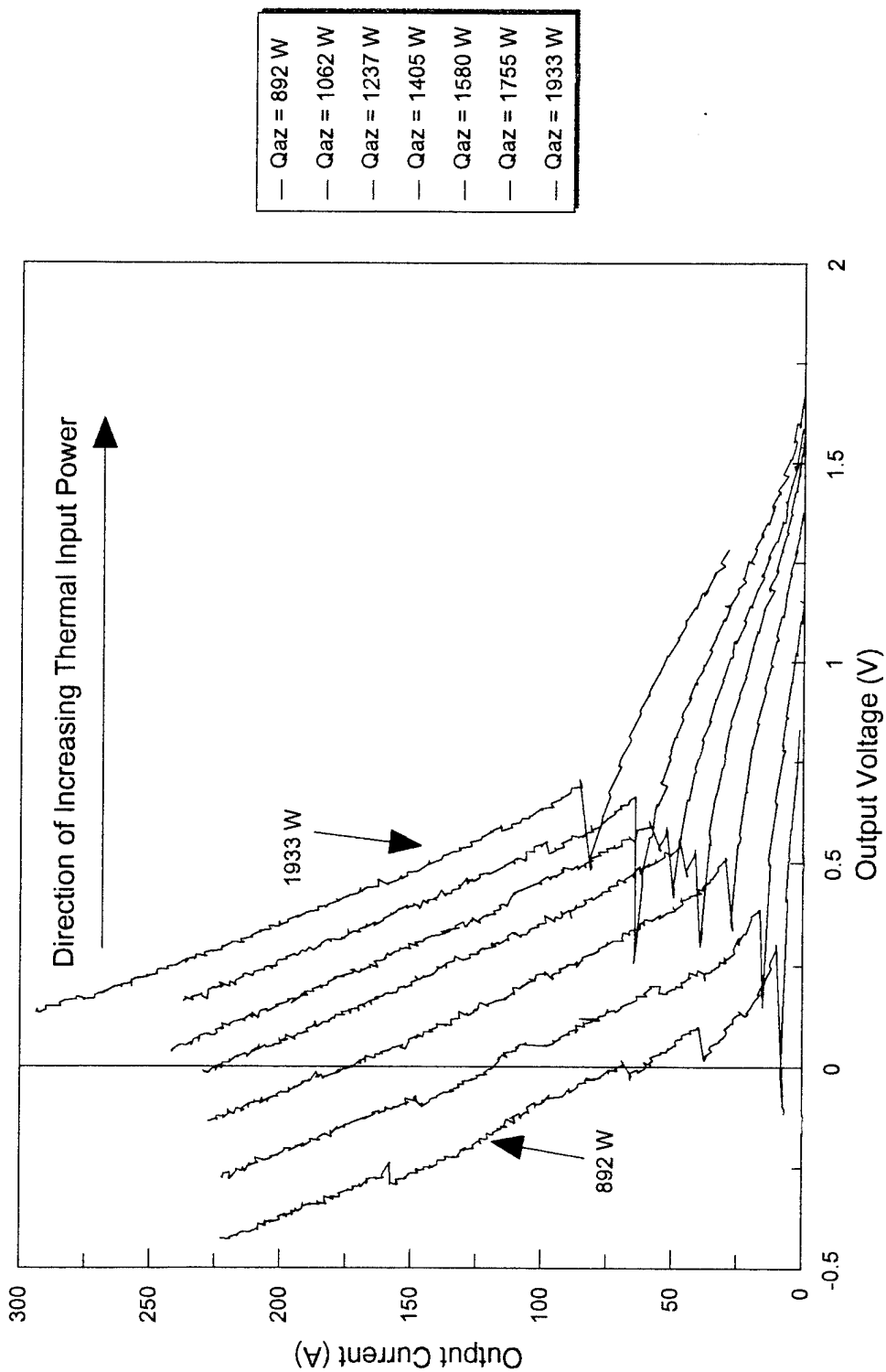


Figure B-11. Current-Voltage sweeps at 0.9 torr cesium pressure.

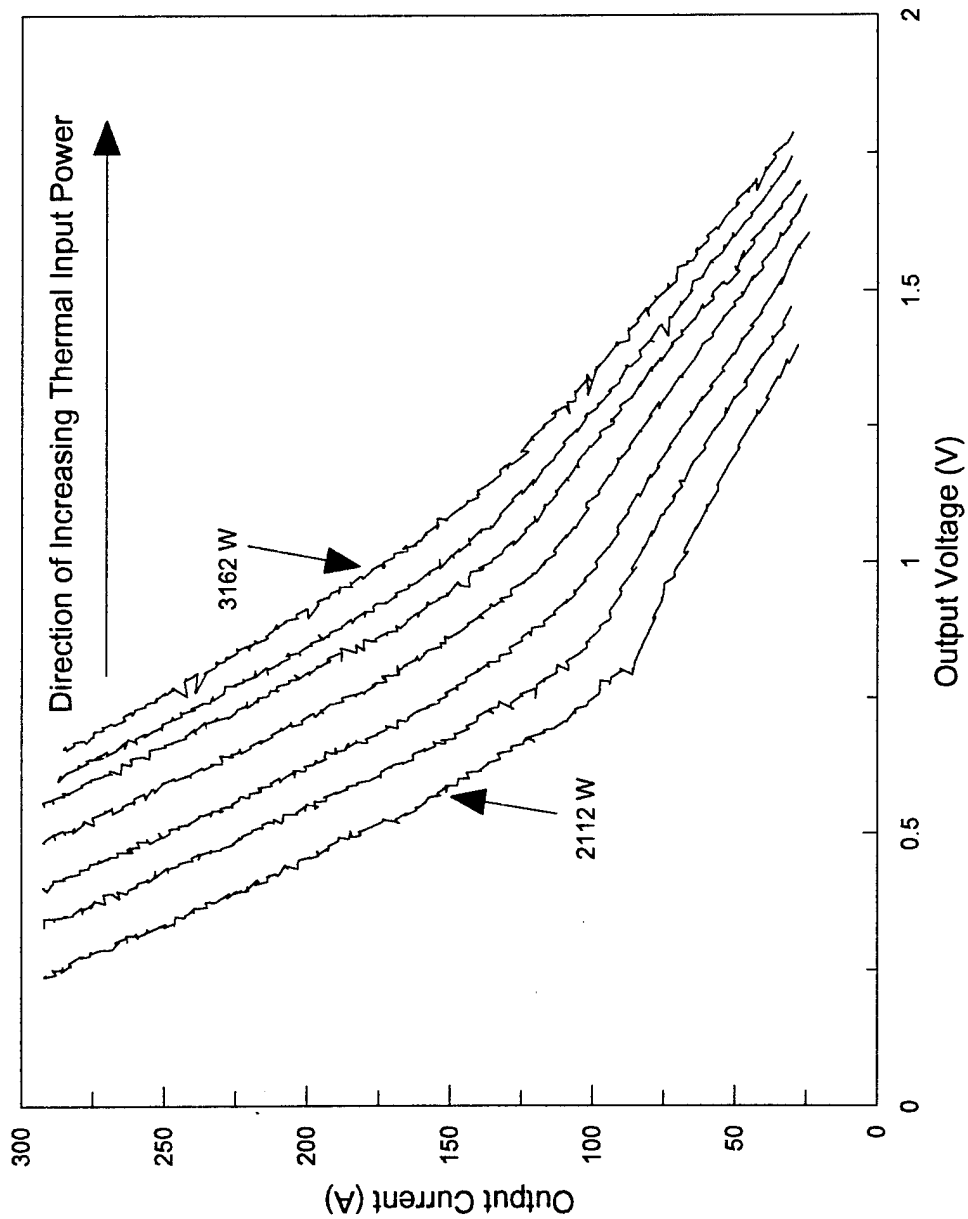


Figure B-12. Current-Voltage sweeps at 0.9 torr cesium pressure.

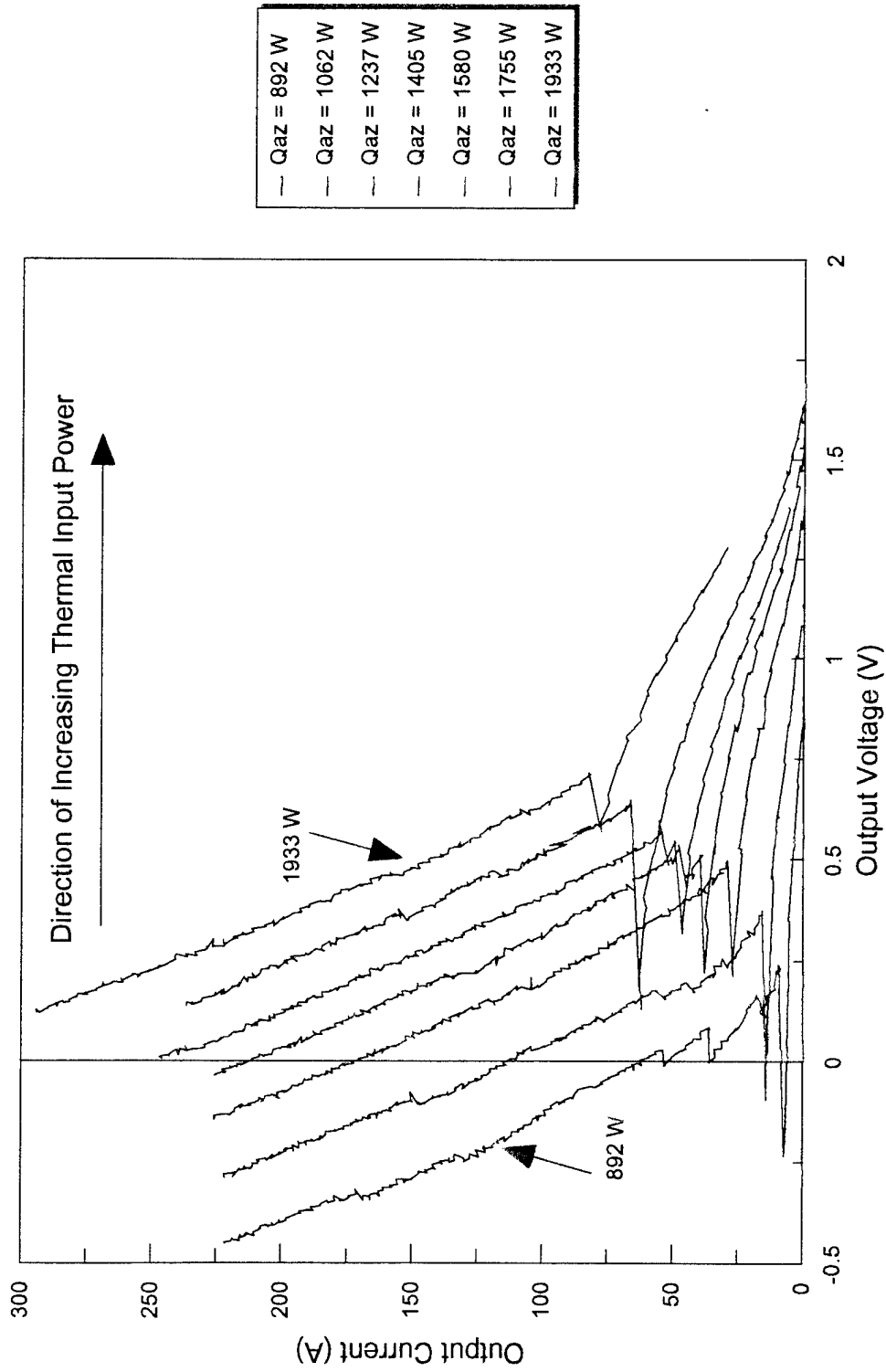


Figure B-13. Current-Voltage sweeps at 1.0 torr cesium pressure.

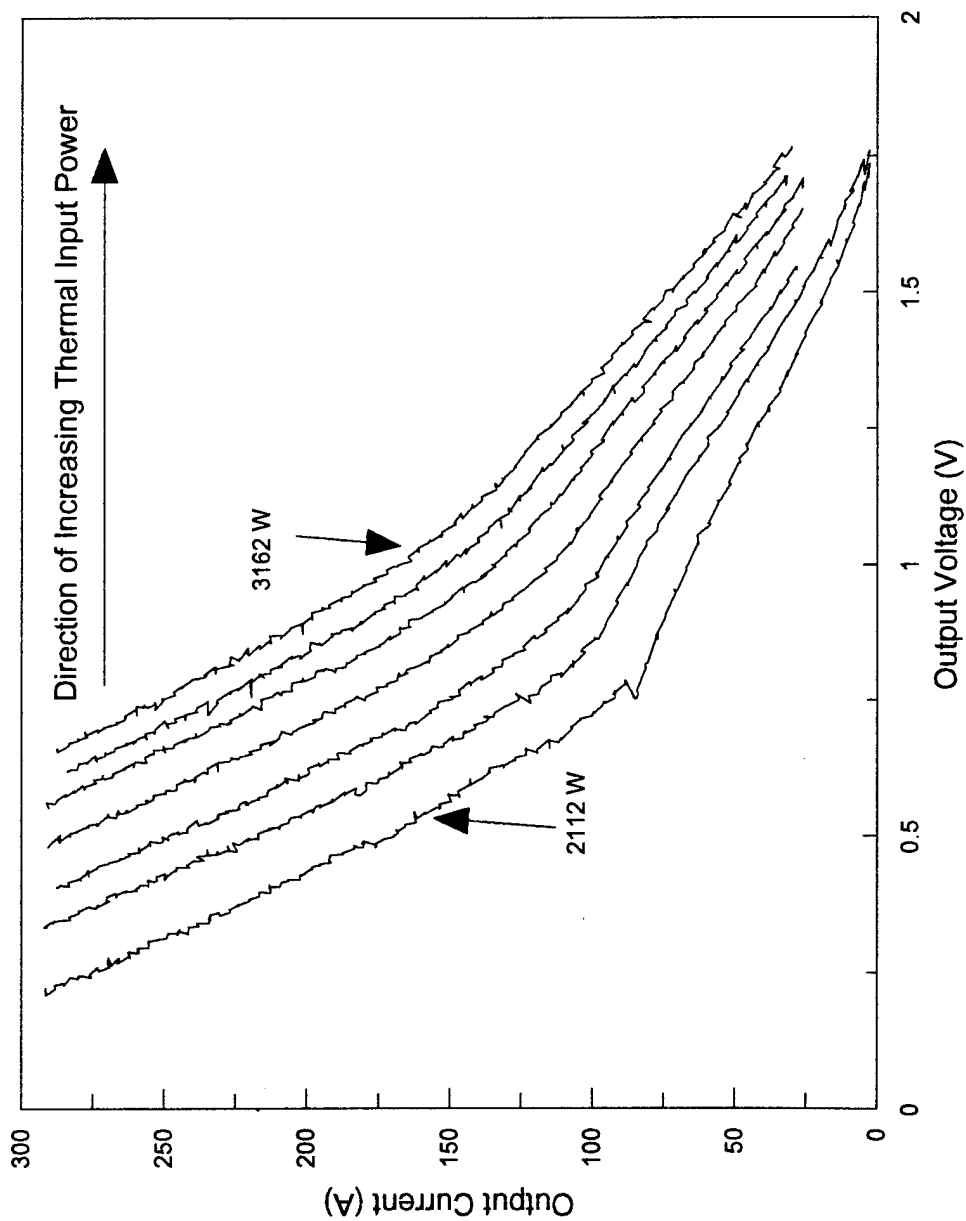
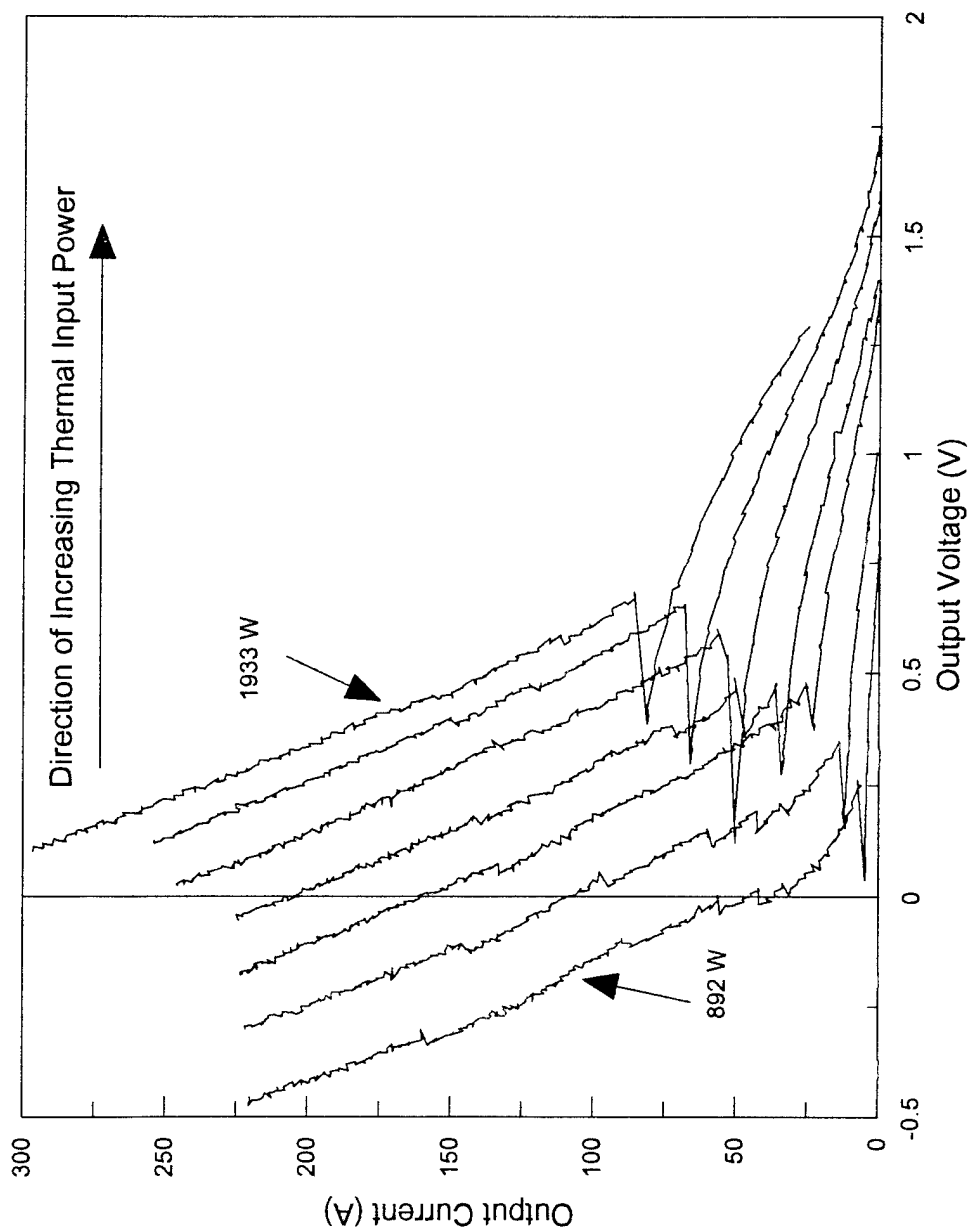
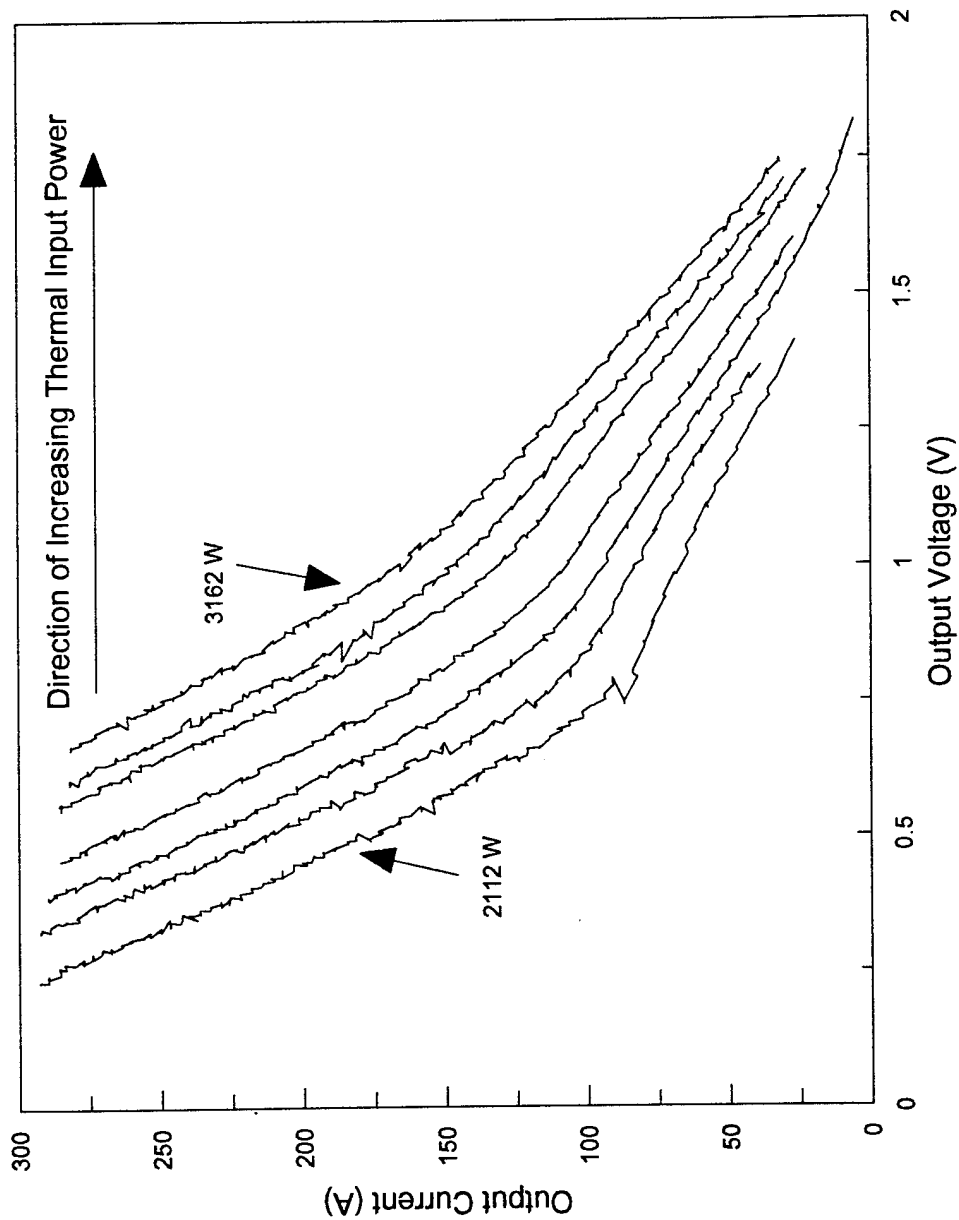


Figure B-14. Current-Voltage sweeps at 1.0 torr cesium pressure.



—	Qaz = 892 W
—	Qaz = 1062 W
—	Qaz = 1237 W
—	Qaz = 1405 W
—	Qaz = 1580 W
—	Qaz = 1755 W
—	Qaz = 1933 W

Figure B-15. Current-Voltage sweeps at 1.1 torr cesium pressure.



—	Qaz = 2112 W
—	Qaz = 2281 W
—	Qaz = 2474 W
—	Qaz = 2813 W
—	Qaz = 2637 W
—	Qaz = 2999 W
—	Qaz = 3162 W

Figure B-16. Current-Voltage sweeps at 1.1 torr cesium pressure.

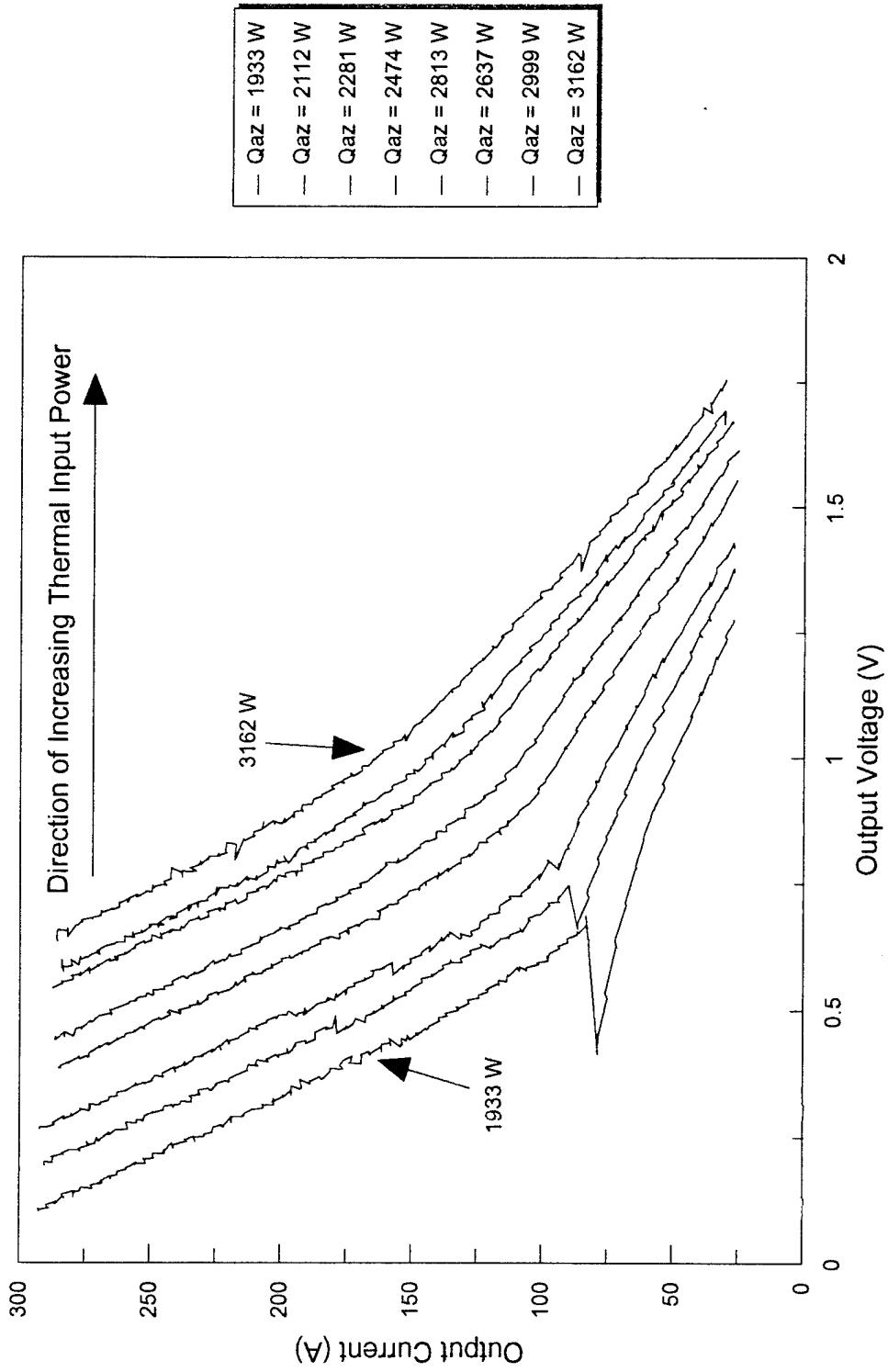


Figure B-17. Current-Voltage sweeps at 1.2 torr cesium pressure.

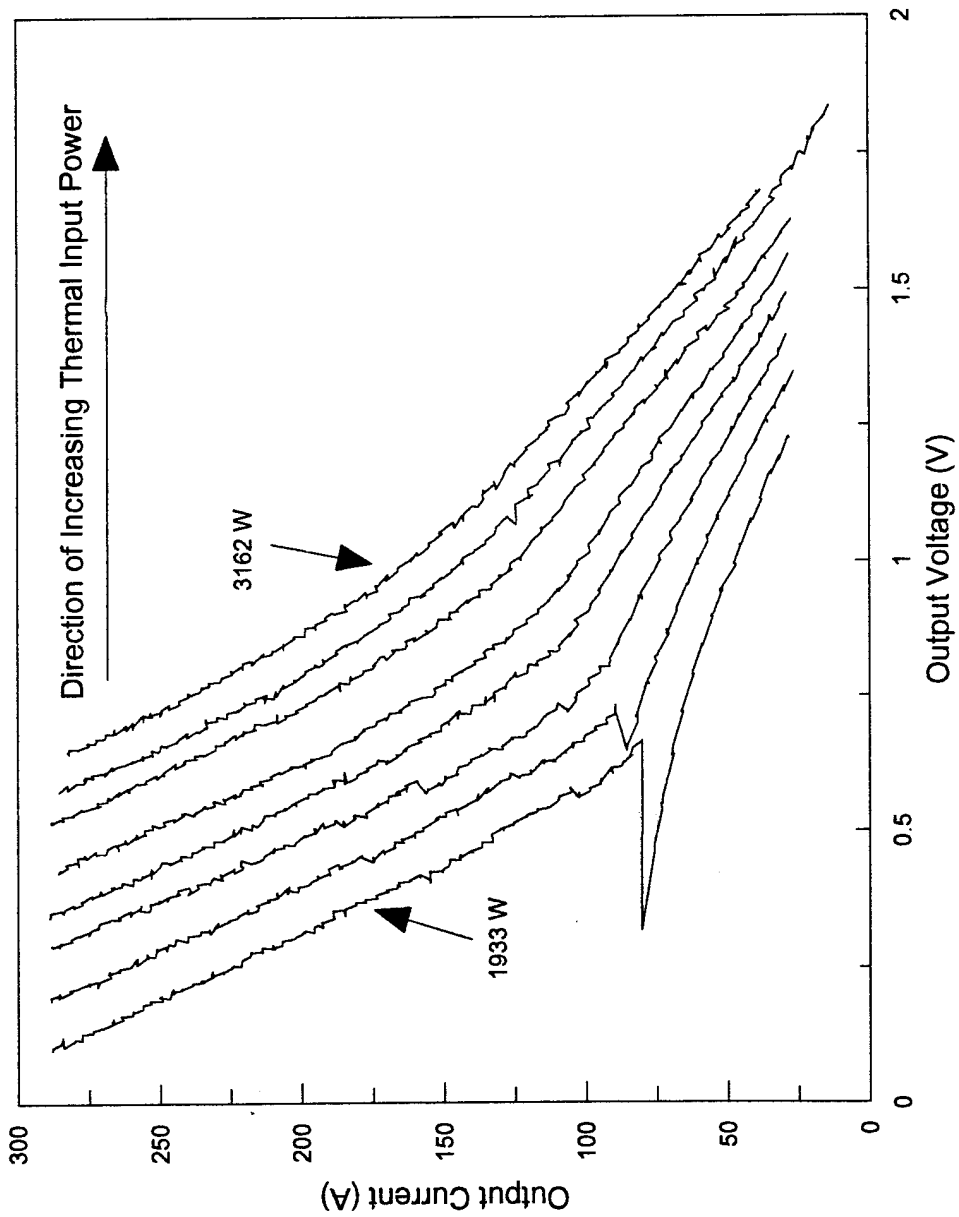


Figure B-18. Current-Voltage sweeps at 1.3 torr cesium pressure.

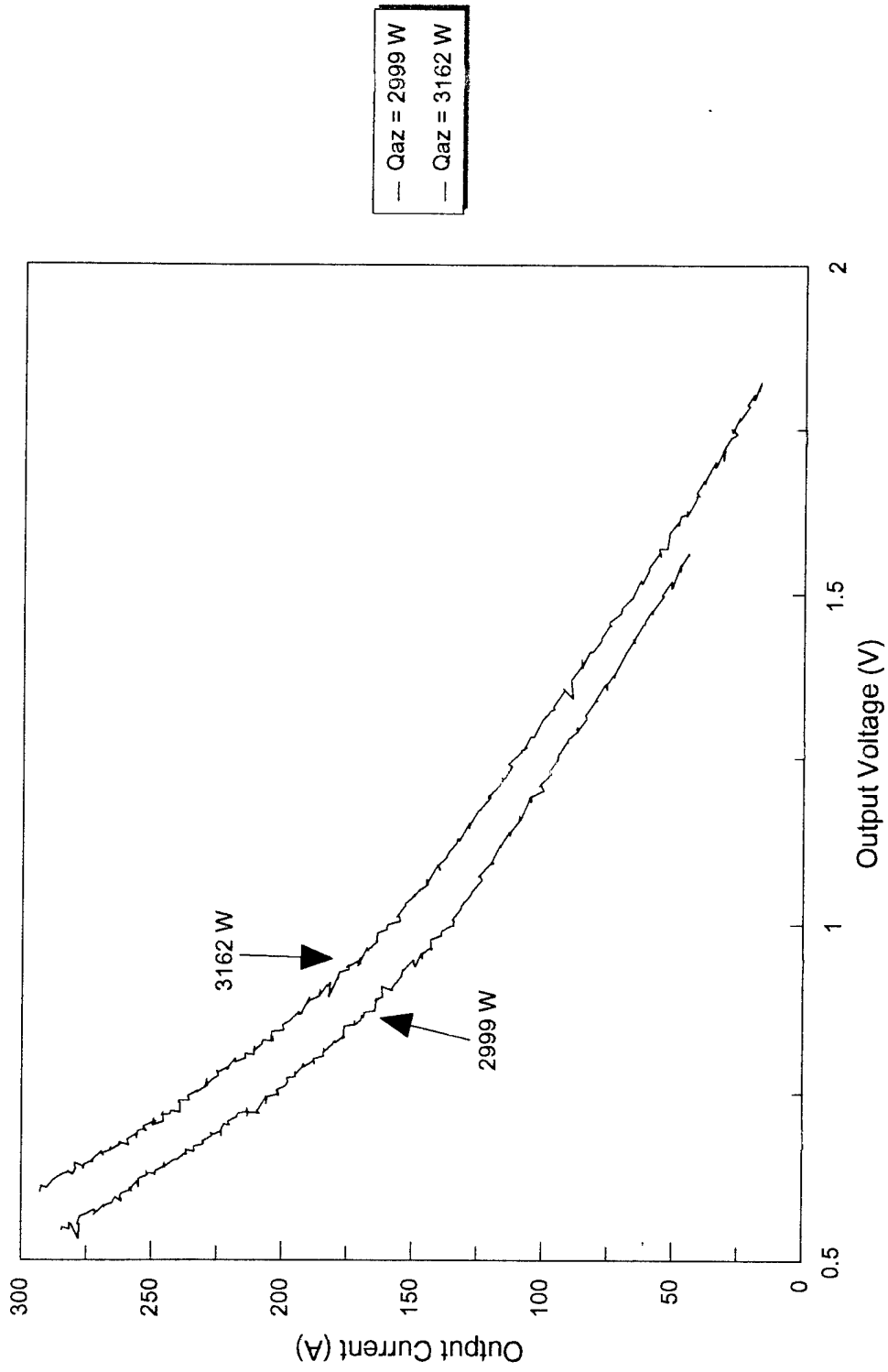


Figure B-19. Current-Voltage sweeps at 1.4 torr cesium pressure.

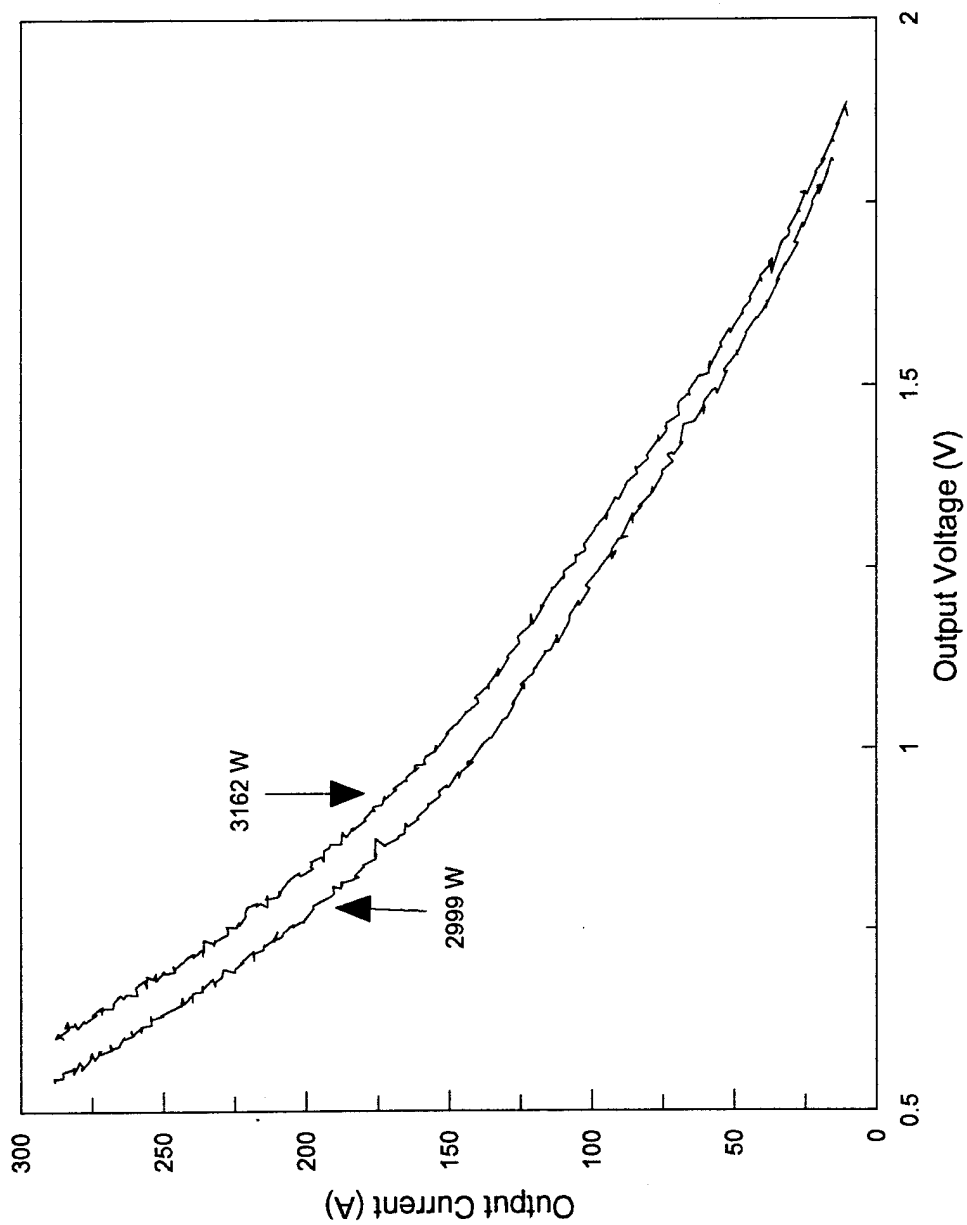


Figure B-20. Current-Voltage sweeps at 1.5 torr cesium pressure.

LIST OF REFERENCES

- Agnew, P. (1994) Personal Communication, NMERI, Albugquerque, NM, August 1994.
- Agnew, P. (1994) Personal Communication, NMERI, Albugquerque, NM, December 1994.
- Andrews, J. R. and O. Biblarz (1981) "Temperature Dependence of Gas Properties in Polynomial Form," NPS67-81-001, Naval Postgraduate School, Monterey, CA.
- Androsov, V. et al. (1991) "Description and Operating Instruction of the 'Rig'," JV Inertek, Moscow, USSR.
- Angrist, S. W. (1965) *Direct Energy Conversion*, Allyn and Bacon, Inc., Boston, MA.
- Anonymous (1971) "Glossary of Terms and Symbols in Thermionic Conversion," Joint European Nuclear Energy Agency - International Atomic Energy Association Liaison Group on Therminic Electrical Power Generation.
- Baksht, F. G. et al. (1973) *Thermionic Converters and Low Temperature Plasma*, Moyzhes and Pikus, eds., Academy of Science, Moscow, USSR.
- Benke, S. M. (1994) "Operational Testing and Thermal Modeling of a TOPAZ-II Single-Cell thermionic Fuel Element Test Stand," Naval Postgraduate School, Monterey, CA.
- Biblarz, O. (1995) Personal Communication, Naval Postgraduate School, Monterey, CA, February, 1995.
- Donovan, B. D. and T. R. Lamp (1994) "Thermionic Technology Programs at Wright Laboratory," AIAA-94-4141-CP, American Institute of Aeronautics and Astronautics, Inc., Washington D.C.
- El-Genk, M. S. and H. Xue (1994) "Simulation of Fission Heated Thermionic Fuel Elements Using Uniform Electrical Heating," in *Proc. 11th Symposium on Space Nuclear Power and Propulsion*, CONF-940101, M. S. El-Genk, ed., American Institute of Physics, New York, AIP Conference Proc. No. 301, 1: 287-295.
- Harris, H. M. (1995) "Science Opportunities Through Nuclear Power in Space," in *Proc. 12th Symposium on Space Nuclear Power and Propulsion*, CONF-950110, M. S. El-Genk, ed., American Institute of Physics, New York, AIP Conference Proc. No. 324, 1: 161-168.

- Hatsopoulos, G. N. and E. P. Gyftopoulos (1973) *Thermionic Energy Conversion Volume I: Processes and Devices*, Massachusetts Institute of Technology Press, Cambridge, MA.
- Luchau, D. W. et al. (1993) "Thermionic Fuel Element Test Rig: Testing of Single Cell Thermionic Fuel Element Technology," in *Proc. 11th Symposium on Space Nuclear Power and Propulsion*, CONF-940101, M. S. El-Genk, ed., American Institute of Physics, New York, AIP Conference Proc. No. 301, 2: 1031-1036.
- Mondt, J. F. (1994) "SP-100 Power Program," in *Proc. 11th Symposium on Space Nuclear Power and Propulsion*, CONF-940101, M. S. El-Genk, ed., American Institute of Physics, New York, AIP Conference Proc. No. 301, 1: 143-155.
- Mulder, D. and M. S. El-Genk (1994) Personal Communication, NMERI, Albuquerque, NM, March 1994.
- Nikolaev, Y. V. et al. (1995) "A Single-Cell TFE Mock-Up of the Thermionic Nuclear Power System 'Space-R' " in *Proc. 12th Symposium on Space Nuclear Power and Propulsion*, CONF-950110, M. S. El-Genk, ed., American Institute of Physics, New York, AIP Conference Proc. No. 324, 2: 815-820.
- Paramonov, D. V. and M. S. El-Genk (1994) "Steady-State and Transient Analyses of the TOPAZ-II Space Nuclear Power System," UNM-ISONPS-3-1994, Institute for Space Nuclear Power Studies, University of New Mexico, NM.
- Ponomarev-Stepnoi, N. N. et al. (1991) "Thermionic Fuel Element of Power Plant TOPAZ-2," JV Inertek, Moscow, USSR.
- Rasor, N. S. and C. Warner (1964), *J. Appl. Phys.*, 35: 2589.
- Rasor, N. S. (1991) "Thermionic Energy Conversion Plasmas," in *IEEE Transactions on Plasma Science*, 19 (6): 1191-1208.
- Reid, R. C., J. M. Prausnitz, and T. K. Sherwood (1977) *The Properties of Gases and Liquids*, McGraw-Hill Book Company, New York, NY.
- Rosa, R. J., C. H. Krueger, and S. Shioda (1991) "Plasmas in MHD Power Generation," in *IEEE Transactions on Plasma Science*, 19 (6): 1180-1190.

- Schmidt, G. L., F. Thome, B. Ogloblin, and V. Sinkevich (1994) "TOPAZ-II Non-Nuclear Qualification Test Program," in *Proc. 11th Symposium on Space Nuclear Power and Propulsion*, CONF-940101, M. S. El-Genk, ed., American Institute of Physics, New York, AIP Conference Proc. No. 301, 3: 1185-1192.
- Scoville, A. N. and R. Masters (1995) "Thermoelectron Corporation: From Space Power to Fortune 500," in *Proc. 12th Symposium on Space Nuclear Power and Propulsion*, CONF-950110, M. S. El-Genk, ed., American Institute of Physics, New York, AIP Conference Proc. No. 324, 2: 663-668.
- Stepennov, B. et al. (1992) "Control Test of Power Plant TOPAZ-II Single-Cell TFE at the 'Rig'," JV Inertek, Moscow, USSR.
- Taylor, J. M., Jr. (1995) "Experimental Results of Low Power Operation of the TOPAZ-II Space Nuclear Power System," in *Proc. 12th Symposium on Space Nuclear Power and Propulsion*, CONF-950110, M. S. El-Genk, ed., American Institute of Physics, New York, AIP Conference Proc. No. 324, 2: 693-697.
- Voss, S. S. (1994) "TOPAZ II Design Evolution," in *Proc. 11th Symposium on Space Nuclear Power and Propulsion*, CONF-940101, M. S. El-Genk, ed., American Institute of Physics, New York, AIP Conference Proc. No. 301, 2: 791-802.
- Wyant, F. J. (1995) Personal Communication, NMERI, Albuquerque, NM, February 1995.

INITIAL DISTRIBUTION LIST

1. Defense Technical Information Center 2
 Cameron Station
 Alexandria, Virginia 22304-6145

2. Library, Code 52 2
 Naval Postgraduate School
 Monterey, California 93943-5101

3. Chairman 1
 Department of Aeronautics and Astronautics, Code AA
 Naval Postgraduate School
 Monterey, California 93943-5106

4. Chairman, Code SP 1
 Space Systems Academic Group
 Naval Postgraduate School
 Monterey, California 93943-5101

5. Professor Oscar Biblarz 2
 Department of Aeronautics and Astronautics, Code AA/Bi
 Naval Postgraduate School
 Monterey, California 93943-5106

6. Professor Sandra L. Scrivener 1
 Department of Aeronautics and Astronautics, Code AA/Ss
 Naval Postgraduate School
 Monterey, California 93943-5106

7. Captain Thompson 1
 Office of the Chief of Naval Operations
 Code N63, Room 4E679 The Pentagon
 Washington, DC 20350-2000

8. TOPAZ International Program 2
 Attn: Frank Thome
 Frank Wyant
 901 University Blvd, S.E.
 Albuquerque, New Mexico 87106

9. Professor Mohamed S. El-Genk 1
Chemical and Nuclear Engineering Department
University of New Mexico
Albuquerque, New Mexico 87137-1341
10. Captain Doug Dell, USAF 1
Phillips Laboratory
VTP
Kirkland AFB, New Mexico 87117-5776
11. Lieutenant Commander J. Richard Venable, USN 3
140 Benton Court
Stevensville, Maryland 21666
12. Lieutenant Steven M. Benke, USN 1
205 St. Louis Ave.
Fulton, Missouri 65251